2016

Measurement Of Non-Covalent Aromatic Interactions Using Molecular Balances

Jung wun Hwang
University of South Carolina

MEASUREMENT OF NON-COVALENT AROMATIC INTERACTIONS USING MOLECULAR BALANCES

by

Jung wun Hwang

Bachelor of Science
Chung-Ang University, 2009

Master of Science
Tennessee Technological University, 2011

Submitted in Partial Fulfillment of the Requirements

For the Degree of Doctor of Philosophy in

Chemistry

College of Arts and Sciences

University of South Carolina

2016

Accepted by:

Ken D. Shimizu, Major Professor

John J. Lavigne, Committee Member

Daniel L. Reger, Committee Member

Andreas Heyden, Committee Member

Paul Allen Miller, Vice Provost and Interim Dean of Graduate Studies

DEDICATION

To my parents

ACKNOWLEDGEMENTS

I would like to thank my advisor Dr. Ken D. Shimizu for his support and encouragement during the course of the research. I also like to thank our current and previous group members for being great coworkers and friends. Also, I greatly appreciate the help from our department staff at the NMR and X-ray facilities and the advice from my committee members. Last but not least, I would like to thank my family for their unconditional love and support.

ABSTRACT

Non-covalent aromatic interactions govern many of the unique structures and properties of biological and synthetic molecules. Despite the importance of these interactions, their weak nature makes it challenging to study the interactions. To accurately measure weak non-covalent aromatic interactions in solution, we have designed molecular torsion balances that provide a quantitative measure of non-covalent intramolecular interaction strengths. First, we investigated the importance of electrostatic interactions in aromatic interactions. Substituent effects were strongly correlated with electrostatic Hammett parameters. In addition, the substituent effects were additive and showed significant direct substituent-arene interactions that support the recent direct substituent effect model. Next, the studies of dispersion interactions were carried out by introducing various sized arenes, alkyl groups, and heteroatoms. First, dispersion contributions in organic solution were found to be minimal. Second, the interaction surface distances played a more important role than the size of the alkyl groups.[3] Lastly, larger changes in the interaction strengths were observed in the sulfur-arene versus the oxygen-arene interactions, presumably due to greater dispersion and steric interaction from sulfur atoms.

TABLE OF CONTENTS

LIST OF TABLES

LIST OF FIGURES

CHAPTER 1

INTRODUCTION

Non-covalent aromatic interactions govern supramolecular the structures and properties of biomolecules[1] and synthetic molecular devices.[2] Despite the importance of these interactions, their weak nature makes it challenging to quantitatively and qualitatively study contributions of individual components of the interactions. To accurately measure weak non-covalent aromatic interactions in solution, model systems that can form desirable non-covalent interactions of interest need to be designed and studied, and strategies to measure the magnitude of their interactions need to be developed. Most experimental studies have used unimolecular or bimolecular model systems. Unimolecular systems contain two interacting units within a common molecular framework, and their intramolecular interactions are measured using thermodynamic or kinetic approaches based on conformational equilibria or rotational barriers. Bimolecular model systems place the interacting units on separate molecules. Due to the weak nature of most non-covalent interactions, bimolecular complex formation is usually assisted by additional secondary non-covalent interactions such as hydrogen-bonds. Differences in the thermodynamic stability of the bimolecular complexes provide a measure of the strengths of intermolecular interactions. Thus, association constants are measured to quantify the strength of the non-covalent interactions of most bimolecular systems.

Since our research has mainly focused on the design and measurement of the non-covalent interactions of aromatic rings, previous model systems designed to study non-

covalent aromatic interactions will be briefly discussed in this chapter. Specifically, unimolecular and bimolecular model system studies that examined the substituent effects of arene-arene face-to-face and edge-to-face interactions and direct substituent-arene interactions will be highlighted.

1.1 Arene-arene interactions

Studies of substituent effects in arene-arene interactions have been primarily focused on verifying the significance of electrostatic interactions in arene-arene interactions. One of the earliest studies by Cozzi and Seigel developed unimolecular models in the early 1990's to examine the substituent effects of aromatic stacking interactions.[3] 1,8-Diarylnaphthalene derivatives with a series of electron-donating or electron-withdrawing substituents were prepared, and their rotational barriers were measured via NMR line-shape analysis (Figure 1.1 a). Higher rotational barriers were attributed to the stabilization of the ground state by enhanced stacking interactions between the two phenyl rings. With an electron-donating substituent, the rotational barrier became lower. Conversely, with an electron-withdrawing substituent, the rotational barrier was higher. Thus, the substituents were hypothesized to polarize the attached phenyl ring leading to a strengthening or weakening of the electrostatic component of the aromatic stacking interaction. Later, another series of 1,8-diarylnaphthalene derivatives were tested, in which a pentafluorophenyl and substituted phenyl rings formed intramolecular aromatic stacking interactions (Figure 1.1 b).[4] The substituent effects showed the opposite trend, as electron-donating substituents raised the rotational barrier. This was also attributed to variations in the same electrostatic term of the aromatic stacking interaction. However, in this case, the reversed quadrupole moment

of the pentafluorophenyl ring led to the opposite electrostatic substituent trend. Later, Cozzi and Siegel designed other unimolecular models such as 1,8-diarylbiphenylenes[5] and polycyclic diol and dione compounds[6] in which significance of electrostatic contributions in the substituent effects was consistently observed.

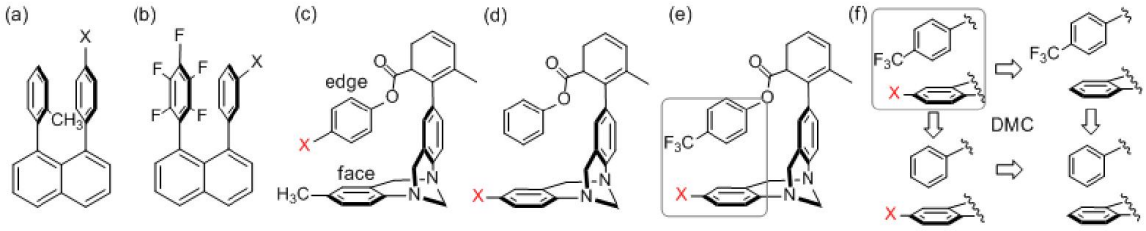

Figure 1.1 Unimolecular models for the studies of substituent (X) effects in aromatic stacking interactions (a-b) and in edge-to-face interactions (c-e) and a double mutant cycle (f) for the model (e)

The significance of the electrostatic contributions to substituent effects was also tested in aryl edge-to-face interactions using unimolecular models. In the mid-1990's, Wilcox developed a molecular torsion balance based on an atropisomeric Troger's base framework (Figure 1.1 c).[7] Various substituents were introduced on the perpendicular edge ring, and the folding energies of the Troger's base models were varied over a 0.4 kcal/mol range. Both electron-donating and electron-withdrawing substituents raised the *folded/unfolded* conformational ratios. The lack of correlation with electrostatic substituent parameters led to the conclusion that dispersion effects of the substituent effects were dominant. Later, substituents were introduced on the face ring and the folding energies only varied over a small 0.1 kcal/mol range (Figure 1.1 d).[8] Again, no correlation between the folding energies and the electrostatic Hammett parameters was observed, and thus electrostatic interactions did not seem to play a dominant role in the substituent effects in this model system.

Diederich recently reexamined the Troger's base edge-to-face models and observed strong electrostatic substituent effects in the edge-to-face interactions when strongly polarizing substituents were placed on the opposing ring. (Figure 1.1 e).[9] A couple of differences in this study were in the model system design and data analysis. First, a *para*-CF_3 group was introduced on the edge ring. This strongly polarizing substituent increased the acidity of the hydrogens of the edge ring leading to a more pronounced electrostatic component of the edge-to-face interaction. Second, a double mutant cycle (DMC) analysis was employed to more accurately isolate the substituent effects by subtracting out other influences on the conformational equilibria (Figure 1.1 f). The folding energies of the substituted balances spanned a larger 1 kcal/mol range and were linearly correlated with the electrostatic Hammett σ_m parameter. Electron-withdrawing groups were destabilizing, and electron-donating groups were stabilizing. Therefore, the magnitude of the substituent effects seemed to be significantly influenced by electrostatic interaction changes. However, an alternative explanation for the observation of electrostatic effects in Diederich's model systems could be direct electrostatic interactions between the *para*-CF_3 and various substituents.

In the 2000's, Hunter developed bimolecular models called hydrogen-bonded supramolecular zipper complexes. One of the terminal phenyl rings was substituted with various electron-donating and electron-withdrawing groups (Figure 1.2 a).[10] Association constants of the zipper complexes were measured via NMR titration, and DMC analyses were used to isolate the substituent effects from the measured association constants. More electron-withdrawing substituents stabilized the face-to-face interactions. When pentafluorophenyl ring was introduced instead of a phenyl ring, the same series of

substituents displayed the reversed trend. Thus, the results showed that the substituent effects in the aromatic stacking interactions were dominated by electrostatic effects. A complementary set of zipper complexes was also designed to form intermolecular edge-to-face interactions (Figure 1.2 b).[11] When the substituents on the edge-ring were changed, again electron-withdrawing groups stabilized and electron-donating groups destabilized the interaction. The substituent effects on the edge-ring showed larger changes when there were electron-donating groups on the face ring. When the face ring substituent effects were examined, the opposite electrostatic trend was observed. Electron-withdrawing groups destabilized and electron-donating groups stabilized the interaction. This is consistent with the model where the face ring is an electron donor via its π-electrons. In summary, the series of studies on hydrogen-bonding zipper complexes provided experimental evidence for the significant role of electrostatic contributions in arene-arene interactions and in their substituent effects.

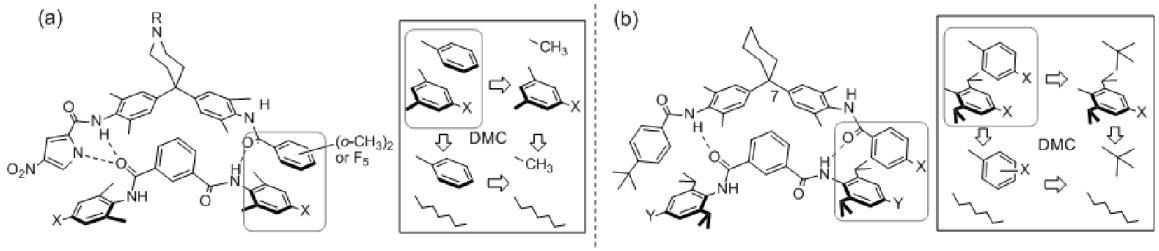

Figure 1.2 Bimolecular models of hydrogen-bonding zipper complexes for the study of substituent (X) effects in an aromatic stacking interaction (a) and an edge-to-face interaction (b)

Arene ring size effects have been used to test the importance of solvophobic or dispersion interactions in aromatic stacking interactions. Early studies by Gellman found significant solvophobic effects using unimolecular amide rotamer models.[12] Rotamer ratios for two series of model systems (Figure 1.3 a), one with Na cations for study in

water and the other with CH_3 groups for study in chloroform, were compared to find how different or similar the stacking interaction trends were for different sized aromatic rings in different solvent environments. In water, the rotamer ratios significantly increased as the aryl size increased. For example, the aryl change from phenyl to diphenyl caused stabilization of 0.6 kcal/mol. In contrast, the change in the rotamer ratio in chloroform from phenyl to diphenyl was less than the experimental error (0.1 kcal/mol) in chloroform. Thus, the stacking interaction changes in water appeared to be dominated by solvophobic interactions and were much weaker or negligible in the organic solvent.

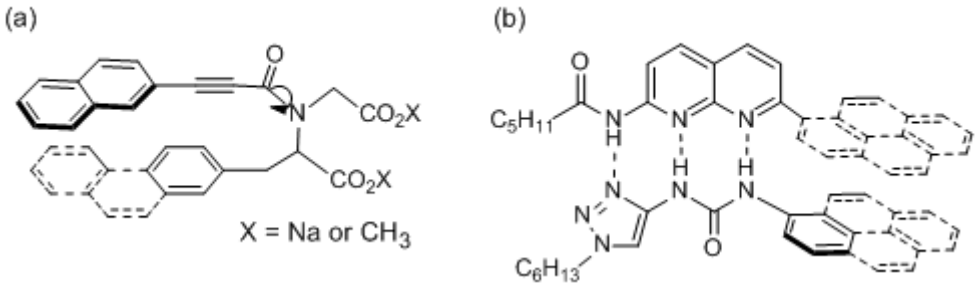

Figure 1.3 Unimolecular (a) and bimolecular (b) models to test the significance of solvophobic or dispersion contributions in aromatic stacking interactions

More recently, Cockroft measured the association constants for a series of naphthyridine and urea hydrogen-bonding complexes in 5% acetonitrile in chloroform via NMR titrations (Figure 1.3 b).[13] The measured aromatic stacking interactions varied over a large 1.8 kcal/mol range, and could be linearly correlated with the dispersion energy terms of symmetry-adapted perturbation theory (SAPT) calculations of the complexes. Their conclusion was that dispersion interactions were much weaker in organic solution then in the gas-phase. However, they were strong enough to be measurable and were stronger than the solvophobic interactions in organic solvents.[13]

1.2 Functional groups-arene interactions

Interactions between various functional groups and arene surfaces have been investigated. Motherwell used unimolecular dibenzopanoanthracene model systems to study substituent-arene interactions by measuring the *D/U* conformational equilibria (Figure 1.4 a).[14] In the *D* conformation, the more electronegative atom points towards the phenyl surface, and in the *U* conformation, the more electronegative atom points away from the phenyl surface. The low interconversion energy barrier between the two conformers (< 7 kcal/mol) required determination of the conformer ratios based on the coupling constants of the diasteromeric H_a and H_b protons with the adjacent bridge head proton H_x. The model systems verified the impact of steric effects on the strength of interactions with an arene surface and how hydrogen-bonding interactions change in different solvents. To study steric effects, the conformational ratio of the system with H/OH groups was measured, in which the major conformation with the H-arene interaction was the more stable due to larger steric hindrance of the OH-arene interaction. In another system with OH/CH_3 groups, the major conformation was the one with the OH-arene interaction due to larger steric repulsion of the CH_3-arene interaction. This model system was also used to study solvent effects on the OH-arene interactions. The OH-arene interactions appeared to be consistently stronger in non-polar solvents where the OH-arene versus CH_3-arene conformational ratios were above 9:1. In contrast, the interactions were largely attenuated in polar or protic solvents such as DMSO and methanol where conformational ratios were near 1:1, presumably due to hydrogen bonding interactions between the more polar solvents and the OH groups in the CH_3-arene conformers.

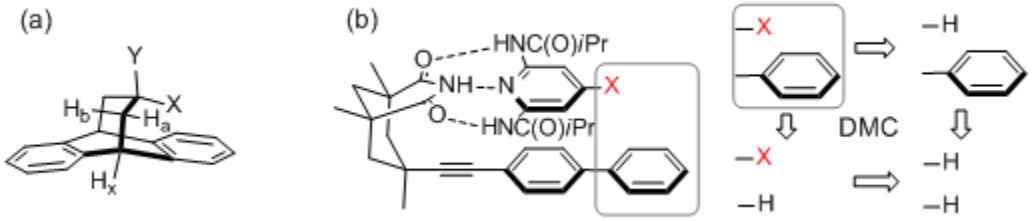

Figure 1.4 Unimolecular (a) and bimolecular (b) models for the studies of direct substituent (X)-π interactions

Diederich employed bimolecular models based on Rebek's hydrogen-bonding imide receptor with a 2,6-di(isobutylamido)pyridine guests (Figure 1.4 b).[15] Association constants of these model systems were measured via NMR titration in 1,1,2,2-tetrachloroethane, and substituent-π interaction strengths were isolated using DMC analyses. A substituent on the 2,6-di(isobutylamido)pyridine guest formed intermolecular interactions with the terminal phenyl ring of the Rebek imide receptor. In the study, a surprisingly strong stabilizing interaction (-0.34 kcal/mol) was observed with the *N*-methylcarboxamide group, which was much stronger than the interactions from other groups such as phenyl (-0.03 kcal/mol), methylthio (-0.01 kcal/mol), and ethyl groups (0.06 kcal/mol). The large stabilization of the *N*-methylcarboxamide-arene interactions was attributed to the ability of the *N*-methylcarboxamide group to form π-π stacking and attractive electrostatic interactions with an arene surface.

References

(1) Riley, K. E.; Hobza, P. *Acc. Chem. Res.* **2013**, *46*, 927.
(2) Hoeben, F. J. M.; Jonkheijm, P.; Meijer, E. W.; Schenning, A. P. H. J. *Chem. Rev.* **2005**, *105*, 1491.
(3) Cozzi, F.; Cinquini, M.; Annunziata, R.; Dwyer, T.; Siegel, J. S. *J. Am. Chem. Soc.* **1992**, *114*, 5729.
(4) Cozzi, F.; Ponzini, F.; Annunziata, R.; Cinquini, M.; Siegel, J. S. *Angew. Chem. Int. Ed.* **1995**, *34*, 1019.
(5) Cozzi, F.; Annunziata, R.; Benaglia, M.; Baldridge, K. K.; Aguirre, G.; Estrada, J.; Sritana-Anant, Y.; Siegel, J. S. *Phys. Chem. Chem. Phys.* **2008**, *10*, 2686.
(6) Cozzi, F.; Annunziata, R.; Benaglia, M.; Cinquini, M.; Raimondi, L.; Baldridge, K. K.; Siegel, J. S. *Org. Biomol. Chem.* **2003**, *1*, 157.
(7) Paliwal, S.; Geib, S.; Wilcox, C. S. *J. Am. Chem. Soc.* **1994**, *116*, 4497.
(8) Kim, E.; Paliwal, S.; Wilcox, C. S. *J. Am. Chem. Soc.* **1998**, *120*, 11192.
(9) Hof, F.; Scofield, D. M.; Schweizer, W. B.; Diederich, F. *Angew. Chem. Int. Ed.* **2004**, *43*, 5056.
(10) Cockroft, S. L.; Hunter, C. A.; Lawson, K. R.; Perkins, J.; Urch, C. J. *J. Am. Chem. Soc.* **2005**, *127*, 8594.
(11) Carver, F. J.; Hunter, C. A.; Livingstone, D. J.; McCabe, J. F.; Seward, E. M. *Chem. Eur. J.* **2002**, *8*, 2848.
(12) Gardner, R. R.; Christianson, L. A.; Gellman, S. H. *J. Am. Chem. Soc.* **1997**, *119*, 5041.
(13) Yang, L.; Brazier, J. B.; Hubbard, T. A.; Rogers, D. M.; Cockroft, S. L. *Angew. Chem. Int. Ed.* **2016**, *55*, 912.
(14) Motherwell, W. B.; Moise, J.; Aliev, A. E.; Nic, M.; Coles, S. J.; Horton, P. N.; Hursthouse, M. B.; Chessari, G.; Hunter, C. A.; Vinter, J. G. *Angew. Chem. Int. Ed.* **2007**, *46*, 7823.
(15) Harder, M.; Corrales, M. A. C.; Trapp, N.; Kuhn, B.; Diederich, F. *Chem. Eur. J.* **2015**, *21*, 8455.

CHAPTER 2

ADDITIVITY OF SUBSTITUENT EFFECTS IN AROMATIC STACKING INTERACTIONS[1]

[1] Reproduced with permission from: Hwang, J.; Li, P.; Carroll, W. R.; Smith, M. D.; Pellechia, P. J.; Shimizu, K. D. *J. Am. Chem. Soc.* **2014**, *136*, 14060. Copyright © 2014 American Chemical Society.

Aromatic stacking interactions play an important role in determining the structure, property, and function of many synthetic[1-4] and biological systems.[4–7] For example, attractive interactions of aromatic surfaces have been cited as a major stabilizing interaction in nucleic acid and protein structures,[8] host−guest complexes,[9,10] solid-state structures,[11] and transition states of asymmetric catalysts.[12,13] A common strategy for modulating the strengths of aromatic stacking interactions is via the introduction of substituents on the aromatic rings. Theoretical[14–18] and experimental[19–22] studies have found that electron-withdrawing groups stabilize and electron-donating groups generally destabilize aromatic stacking interactions. In addition, theoretical studies have predicted that the electronic substituent effects (SEs) in multisubstituted aromatic rings will be additive.[23] For example, Sherrill et al. demonstrated an excellent linear correlation between the interaction energy and the number of substituents. However, these theoretical studies were carried out in vacuo and examined the aligned face-to-face stacking geometry, where one aromatic ring is directly over the opposing ring. In this study, we experimentally test whether the electrostatic SEs are additive for the more commonly observed offset aromatic stacking geometry (Figure 2.1). SE additivity would provide a simple means of rationally designing systems that utilize aromatic stacking and aid in rational design of host−guest, drug−receptor, and substrate−catalysts systems that incorporate aromatic stacking interactions. In addition, the verification of additive SEs could help differentiate the different theoretical models of the aromatic stacking SEs.[24-28]

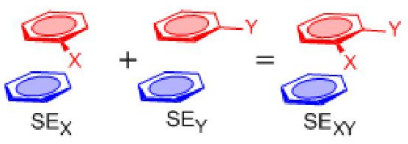

Figure 2.1 General depiction of additive SEs for aromatic stacking interaction in the offset face-to-face geometry

Our strategy was to prepare and study a series of small molecule model systems (Figure 2.2), which could form and measure the strength of an intramolecular offset face-to-face (or parallel) aromatic stacking interaction. Five different substituents (OCH_3, CH_3, Cl, CN, NO_2) were introduced on the aromatic ring yielding a total of 21 different combinations (Figure 2.3). This range of substituents and substitution patterns allowed us to systematically test whether the SEs of the monosubstituted systems could be added together to accurately predict the SEs for the multisubstituted systems (Figure 2.1).

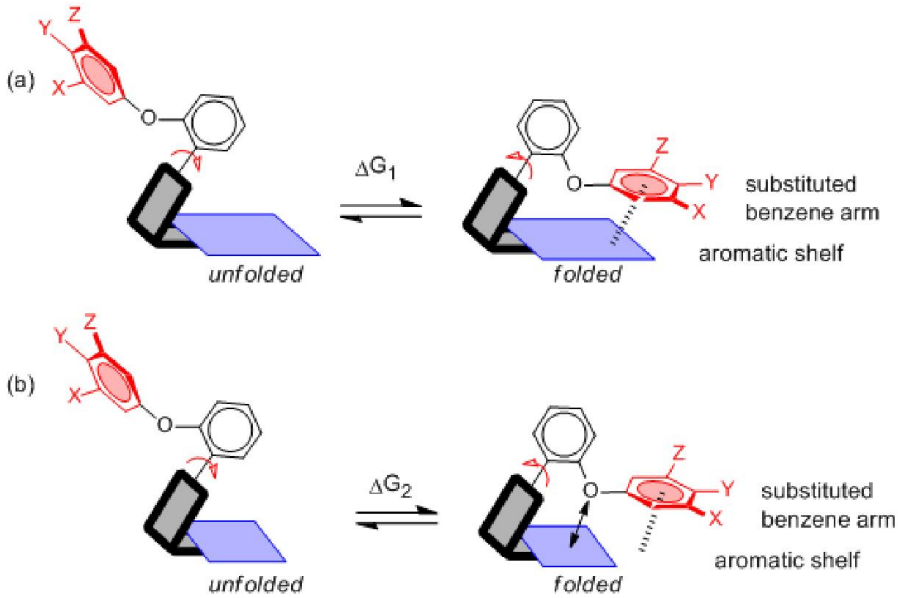

Figure 2.2 Representation of (a) the molecular torsional balance designed to measure the SEs of an intramolecular aromatic stacking interaction via changes in the *folded/unfolded* equilibrium ratio and (b) the control balance designed to measure the solvent and repulsive lone pair to π interactions of the oxygen linker

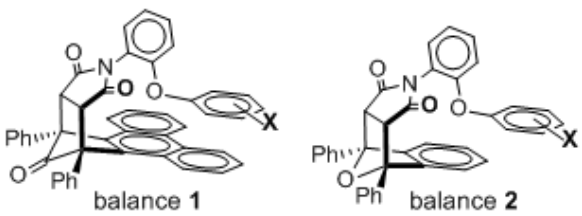

X =		
a *p*-CH_3	**h** *m,m*-$(Cl)_2$	**o** *m*-CN
b *m*-CH_3	**i** *m,p*-$(Cl)_2$	**p** *m,p*-$(CN)_2$
c *m,m*-$(CH_3)_2$	**j** *p*-Cl, *m*-CH_3	**q** *m*-CN, *p*-NO_2
d *m,p*-$(CH_3)_2$	**k** *m*-Cl, *p*-CH_3	**r** *p*-OCH_3
e *m,m,p*-$(CH_3)_3$	**l** *p*-NO_2	**s** *m*-OCH_3
f *p*-Cl	**m** *m*-CH_3, *p*-NO_2	**t** *m,p*-$(OCH_3)_2$
g *m*-Cl	**n** *p*-CN	**u** H

Figure 2.3 *Folded* conformers of aromatic stacking balance **1** and nonstacking control balance **2**, which contain 21 different substituted benzenes arms (**a**–**u**).

There have been a number of experimental studies that have examined the additivity of SEs in face-to-face aromatic stacking interactions. However, these previous studies examined a limited number of substituents, measured the interaction energies via an indirect method, and yielded to opposing conclusions. Two separate studies examined the additivity of SEs in aromatic stacking interactions indirectly via measuring changes in a rotational barrier. Cozzi and Siegel showed that benzene rings with varying numbers of fluorines appeared to show SE additivity for the stacking interaction within a rigid 1,8-diarylnaphthalene model system.[29] Conversely, Waters and Rashkin found that the SEs for CH_3, CF_3, and F groups fell short of additivity by an average of 19% in their benzylpyridinium model system.[22] A possible explanation for the opposing conclusions is the indirect method of measuring aromatic stacking energies used in both studies. The face-to-face aromatic stacking interaction energies in the ground states were measured via the rotational barrier of one of the aromatic surfaces. However, both systems could form additional edge-to-face or edge-to-substituent interactions in their transition states. Therefore, the observed SE trends could be a combination of the trends for the face-to-face and these other interactions. Another experimental study of note is Schneider's comprehensive study of the SEs in the host−guest interactions of porphyrins in water.[30] The observed additive SEs were attributed to dispersion and solvophobic effects as opposed to aromatic stacking interactions.

Our recently reported molecular torsional balance model system has a number of attractive attributes for the study of SE additivity.[31,32] First, we previously established that this rigid bicyclic model system forms a well defined intramolecular aromatic stacking interaction in the folded conformer. The X-ray crystal structure (Figure 2.4) showed that

the aromatic surfaces of the phenyl ether arm and the phenanthrene shelf were held in a parallel geometry and at a proper distance (3.76 Å, centroid-to-plane). Second, the aromatic stacking energy can be easily and accurately measured via a conformational equilibrium (Figure 2.2). Due to restricted rotation around the C_{aryl}–N_{imide} single bond, **1** and **2** adopt distinct *folded* and *unfolded* conformers that form and break the intramolecular stacking interaction. Thus, the *folded/unfolded* conformer ratio provides a sensitive (±0.008 to±0.03 kcal/mol) measure of the interaction.[33,34] This ratio was easily measured from the peak areas of the two conformers in the ^{1}H NMR spectra, which were in slow exchange at room temperature. Third, the balance exclusively forms the face-to-face geometry and cannot form alternative stacking geometries due to the rigidity of the bicyclic framework. Molecular modeling simulations confirmed that there was insufficient distance between the aromatic surfaces in the *folded* conformer to form the edge-to-face geometry. Fourth, we could introduce up to three substituents on the arm of the balance that would only electrostatically attenuate the stacking interaction. The X-ray structure (Figure 2.4) showed that substituents at these positions could not form steric or dispersion interactions with the aromatic shelf. Due to the offset geometry, the benzene arm juts out beyond the edge of the phenanthrene shelf, and substituents at the *para*-and *meta*-positions are not over the aromatic shelf. The elimination of these secondary interactions was important, as experimental[24,22] and theoretical studies[35] have shown that they can disrupt the electrostatic SE trends of interest. While the crystal structure shows the two *meta*-positions are in different geometries, they are equivalent on the NMR time scale. This is because, as shown by calculations by Datta et al.,[36] the arm is moving back and forth rapidly between the two outer benzenes of the phenanthrene shelf.

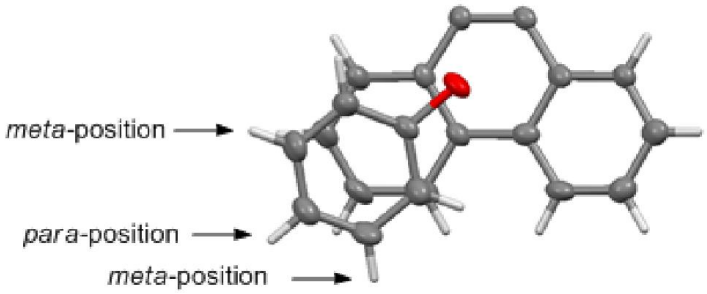

Figure 2.4 Top view of the *folded* conformer of the X-ray crystal structure of a two-armed version of unsubstituted balance **1u** highlighting the intramolecular aromatic stacking interaction between the phenyl ether of the arm (top) and the phenanthrene shelf (bottom).[31] For clarity, the bicyclic framework is hidden.

Finally, control balances **2a**−**u** could be used to measure and remove other possible influences on the *folded/unfolded* ratios in balance **1**. These included repulsive the lone pair to π interactions of the oxygen linker[31,36,37] or solvent effects of the substituted aryl ether arms.[38,39] The control balances **2a**−**u** contained the same substituted aromatic arms but had a smaller benzene shelf that could not form the aromatic stacking interactions. This can be visualized using the crystal structure in Figure 2.4. The control balance **2** contains only the central benzene ring of the phenanthrene shelf in **1**, which can form lone pair to π interactions with the linker ether oxygen. Thus, the aromatic interaction energies were measured using the difference in the folding energies of the aromatic stacking balances **1** and the control balances **2** ($\Delta G_1 - \Delta G_2$).

First, the 21 substituted balances **1a**−**u** and the matching 21 substituted control balances **2a**−**u** (Figure 2.3) were prepared. These were all rapidly and efficiently assembled using a common modular synthesis route (Figure 2.5). The substituted aromatic rings of the arms and the aromatic shelves were synthesized independently and then condensed together in the last step. Five representative substituents were chosen spanning the range from electron-donating (CH_3, OCH_3) to electron-withdrawing (Cl,

CN, and NO_2).[40] A variety of substitution patterns were examined including 1 unsubstituted (**1u**), 9 monosubstituted (**1a**, **b**, **f**, **g**, **n**, **o**, **r**, **s**), 10 disubstituted (**1c**, **d**, **h**−**m**, **p**, **q**, **t**), and 1 trisubstituted (**1e**) arm.

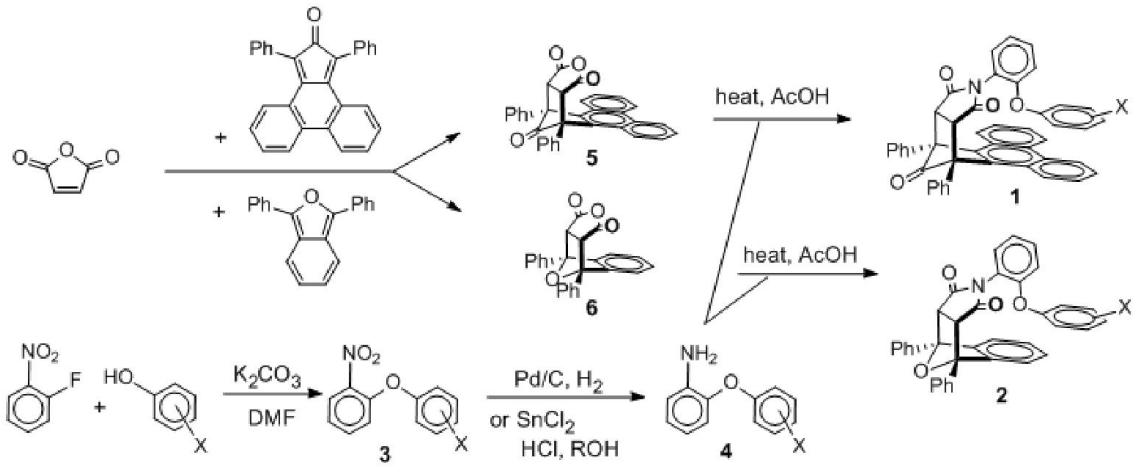

Figure 2.5 Modular synthetic route used to prepare balances **1** and **2** with substituted arms **a**−**k**, **n**, **o**, **r**−**t**

All of the aromatic arms **4** were assembled via an S_NAr reaction. The majority of the arms (**4a**−**k**, **n**, **o**, **r**−**t**) were made by the reaction of the appropriately substituted phenolate with 2-fluoronitrobenzene to form diphenyl ethers **3**. Then 2-nitro groups were reduced to the primary amines. For arms with strong electron-withdrawing substituents (**l**, **m**, **p**, **q**), their phenolates were not sufficiently nucleophilic. Therefore, **4l**, **m**, **p**, **q** were prepared in one step via the S_NAr reaction of 2-aminophenol with the appropriately substituted fluoro- or nitrobenzene (not shown).

The aromatic shelves were synthesized via the Diels−Alder reaction of maleic anhydride with either phencyclone or diphenylisobenzofuran to yield the *endo*-bicyclic anhydrides **5** or **6**containing phenanthrene or benzene surfaces.[41] Finally, thermal condensation reaction of a substituted aniline arm (**4a**−**u**) and a bicyclic anhydride shelf (**5** or **6**) yielded the *endo*-bicyclic **1** and **2**.

The ability of balances **1** and **2** to form the desired intramolecular aromatic stacking interactions was established by ^{1}H NMR. The expected upfield shifts were observed for the protons on the substituted benzene arms of **1a−u**, which were indicative of the benzene arm being positioned over the phenanthrene shelf. In particular, the *ortho*-protons (adjacent to the ether oxygen) of the benzene arms shifted from 1.0 to 1.2 ppm upfield. By comparison, upfield shifts were not observed for the benzene arm protons of control balances **2a−u**, which have a shorter benzene shelf that cannot form intramolecular aromatic stacking.

The ability to measure the intramolecular stacking interactions was confirmed by examination of the ^{1}H NMR spectra. The presence of distinct *folded* and *unfolded* conformers was observed via the separate set of peaks in the ^{1}H NMR spectra ($CDCl_3$, 25°C) for most of the protons in **1a−u** and **2a−u**. Thus, the two conformers were in slow exchange, and *folded/unfolded* ratio could be easily measured from the corresponding peak areas. The succinimide methine protons were used for this analysis because they were singlets in a relatively clear region of the spectra (4.2−4.7 ppm). To ensure the accuracy and consistency of the measurement, the line-fitting method was applied to high-concentration NMR samples (30 mM).[42,43] In this manner, the *folded/unfolded* ratios for **1** and **2** were measured (Table 2.1), and the corresponding folding energies (ΔG_1 and ΔG_2) were calculated.

Table 2.1 Measured folding energies (kcal/mol) of balances **1** (ΔG_1) and control balances **2** (ΔG_2) systems and SEs ($SE_x = (\Delta G_{1x} - \Delta G_{2x}) - (\Delta G_{1u} - \Delta G_{2u})$)

arm	substituents	ΔG_1[a]	ΔG_2[a]	SE_{measd}[b]
a	*m*-CH_3	0.40	1.50	-0.19
b	*p*-CH_3	0.44	1.31	0.05
c	*m,m*-$(CH_3)_2$	0.29	1.56	-0.35
d	*m,p*-$(CH_3)_2$	0.35	1.35	-0.08
e	*m,m,p*-$(CH_3)_3$	0.34	1.52	-0.27
f	*p*-Cl	0.15	1.22	-0.15
g	*m*-Cl	-0.02	1.45	-0.54
h	*m,m*-$(Cl)_2$	-0.46	1.38	-0.92
i	*m,p*-$(Cl)_2$	-0.37	1.28	-0.73
j	*p*-Cl, *m*-CH_3	0.03	1.25	-0.30
k	*m*-Cl, *p*-CH_3	-0.01	1.30	-0.39
l	*p*-NO_2	0.22	1.51	-0.36
m	*p*-NO_2, *m*-CH_3	0.03	1.56	-0.61
n	*p*-CN	0.24	1.47	-0.31
o	*m*-CN	-0.24	1.31	-0.63
p	*m,p*-$(CN)_2$	-0.31	1.61	-1.00
q	*p*-NO_2, *m*-CN	-0.28	1.58	-0.94
r	*p*-OCH_3	0.34	1.26	0.01
s	*m*-OCH_3	0.33	1.41	-0.16
t	*m,p*-$(OCH_3)_2$	0.21	1.29	-0.15
u	none	0.48	1.40	0.00

[a]ΔG_1 and ΔG_2 were measured at 25°C with an error of $<\pm 0.008$ and ± 0.03 kcal/mol, respectively. [b]SE with an error of $<\pm 0.03$ kcal/mol.

The folding energies of **1** and **2** (ΔG_1 and ΔG_2) were analyzed to verify that *folded/unfolded* equilibrium provided a measure of the intramolecular aromatic stacking energies in **1**. The ΔG_1 values (−0.46 to 0.48 kcal/mol) were consistently lower in energy than the ΔG_2 values (1.22 to 1.61 kcal/mol). This was consistent with the expected stabilization of the *folded* conformer in **1** by aromatic stacking interactions. The average difference of −1.3 kcal/mol was consistent with previous measures of benzene−benzene stacking interactions in organic solution.[20,24]

Hammett plot analyses were conducted to establish that the electrostatic SEs in our aromatic stacking model system were similar to those in previous theoretical and experimental studies.[19−22] To isolate the intramolecular stacking energies, the difference in folding energies of **1** and **2** ($\Delta G_1 - \Delta G_2$) of the monosubstituted balances were plotted against their σ_{meta} parameters (Figure 2.6). The σ_{meta} parameters was used because it more closely correlates to the purely electrostatic SEs than σ_{para}, which also includes resonance effects.[15,24] Interestingly, the *meta*- and *para*-systems displayed distinct linear trends with slopes of (−0.95 and−0.55 kcal/mol). The origins of this positional dependence will be discussed in more detail below. However, the overall sign and magnitudes of these slopes were consistent with those measured by Hunter (−0.62 kcal/mol)[21] and Gung (−1.06 kcal/mol)[20] for face-to-face aromatic stacking interactions in organic solvents.

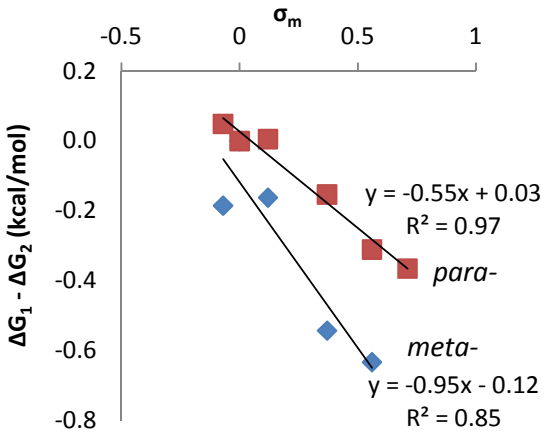

Figure 2.6 Hammett σ_{meta} plots of $\Delta G_1 - \Delta G_2$ for the monosubstituted balances with substituents in the *meta*- (blue diamond) or *para*-substitutes (red square) (the substituents from left to right - CH_3, H, OCH_3, Cl, CN, NO_2)

The importance of the control balances **2** in improving the accuracy of the analysis was tested by comparing the Hammett plots with ($\Delta G_1 - \Delta G_2$) and without (ΔG_1) the balance **2** corrections. Although the Hammett plots without balance **2** had similar magnitude negative slopes, there was considerably more scatter in the linear correlation. For example, the R^2 value for the *para*-substituted values for ΔG_1 was 0.69 as compared to 0.97 for $\Delta G_1 - \Delta G_2$. The improved correlation with ΔG_2 suggests that secondary factors other than the electron-withdrawing and -donating effects of the substituents influence the folding ratios in **1**. These secondary factors include solvation effects, changes in the dipoles of the *folded* and *unfolded* conformers, and resonance effects on the oxygen linker that could modulate the repulsive lone pair to π interactions.

Once the viability of our model system was established, the additivity of the SEs was assessed. The SEs in **1** were calculated using an equation: $SE_{(x)} = (\Delta G_{1x} - \Delta G_{2x}) - (\Delta G_{1u} - \Delta G_{2u})$. The SE for an arm with substituents x was defined as the difference in the folding energies of **1** and **2** containing the substituents x. In addition, the $SE_{(x)}$ was

normalized by subtracting out the stacking interactions in the unsubstituted balances **1u** and **2u**. Thus, the SE for the unsubstituted arm (SE_u) was 0.0 kcal/mol.

$$SE_{(x)} = (\Delta G_{1x} - \Delta G_{2x}) - (\Delta G_{1u} - \Delta G_{2u}) \quad (1)$$

An initial analysis of the SE_{measd} values for the 11 multisubstituted arms in Table 2.2 was consistent with SE additivity. There was a good correlation between the SE_{measd} and SE_{calcd} values calculated from the sum of the SE_{measd} for the individual substituents. For example, the SE_{measd} (−0.35 kcal/mol) for the *m,m*-$(CH_3)_2$ arm **c** is very similar to the SE_{calcd} value (−0.37 kcal/mol) calculated from the sum of two SE_{measd} from the *m*-CH_3 arms. The agreement between the measured and calculated SEs spanned a diverse set of substituent types. These included arms with electron-donating CH_3 and OCH_3 groups (arms **c**, **d**, **e**, **s**), electron-withdrawing Cl, NO_2, and CN groups (arms **h**, **i**, **p**, **q**), and mixtures of electron-donating and -withdrawing groups (arms **j**, **k**, **m**).

However, there was not perfect agreement between the measured and calculated SE values in Table 2.2. Therefore, additional analyses were conducted to determine whether these deviations were systematic or random error. First, a correlation plot of the calculated and measured SE values (Figure 2.7) showed an excellent linear correlation with an R^2 value of 0.96 and a slope near unity (0.99). The residuals ($SE_{calcd} - SE_{measd}$) had a standard error ±0.02 kcal/mol, which was less than the error of the analysis of ±0.03 kcal/mol. Most importantly, the SE_{measd} values were not consistently lower than the SE_{calcd} values. In addition, a plot of the residuals did not show any systematic variations. Specifically, the residuals for arms with electron-donating or -withdrawing groups did not show systematic variance.

Table 2.2 Comparison of the calculated (SE_{calcd}) and measured (SE_{measd}) multisubstituent effects. SE_{calcd} were calculated from the sum of the SE_{measd} for the constituent mono-SE.

multisubst arm	sum of monosubst SE_{measd}[a]	SE_{calcd}[b]	SE_{measd}[a]
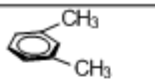	2 x  (-0.19)	-0.37	**-0.35**
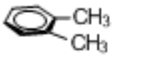	 (-0.19) +  (0.05)	-0.14	**-0.08**
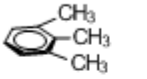	2 x  (-0.19) + 2 x  (0.05)	-0.32	**-0.27**
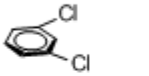	2 x  (-0.54)	-1.09	**-0.92**
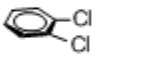	 (-0.54) +  (-0.15)	-0.70	**-0.73**
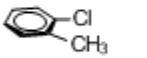	 (-0.19) +  (-0.15)	-0.34	**-0.30**
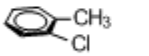	 (-0.54) +  (0.05)	-0.49	**-0.39**
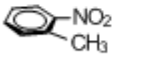	 (-0.19) +  (-0.36)	-0.55	**-0.61**
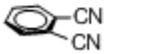	 (-0.63) +  (-0.31)	-0.94	**-1.00**
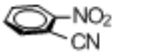	 (-0.63) +  (-0.36)	-1.00	**-0.94**
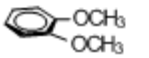	 (-0.16) +  (0.01)	-0.16	**-0.15**

[a]SE_{measd} (kcal/mol) in $CDCl_3$ at 25 °C with an error of <±0.03 kcal/mol. [b]SE_{calcd} of disubstituents with an error of <±0.04 kcal/mol. [c]SE_{calcd} of trisubstituents with an error of <±0.05 kcal/mol.

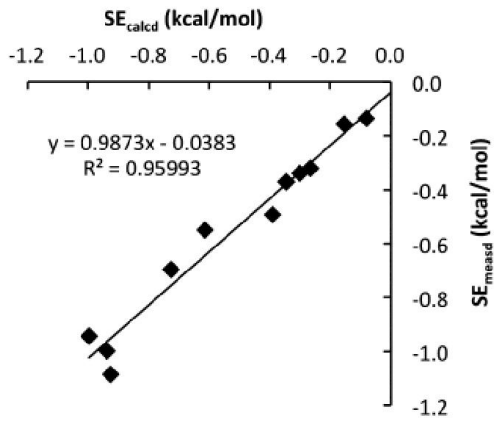

Figure 2.7 Correlation plot of the calculated and measured SEs for the aromatic stacking interactions in the 11 multisubstituted arms in **1** and **2**. The SE_{calcd} values are based on the sum of the individual SE_{measd} values for each multisubstituted arm.

Building on the success of the above additivity model, a more complex additivity model was developed to provide a more accurate estimate of the SEs. A multivariate approach was employed similar to that used by Schneider et al. for the analysis of SE additivity in porphyrin host−guest complexes.[30] This multivariate model incorporated data from the multisubstituted and monosubstituted arms. Thus, each of the 9 individual SEs (*m*-CH_3, *p*-CH_3, *m*-Cl, *p*-Cl, *m*-CN, *p*-CN, *m*-OCH_3, *p*-OCH_3, *p*-NO_2) were estimated based on multiple SE measurements instead of just the monosubstituted SE measurements used in the previous analysis.

To estimate the 9 individual SEs, a matrix of 21 algebraic equations was created using an equation (eq 2) to calculate the SE for each substituted arm in Table 2.1. This equation calculates the SE for a substituted benzene via the sum of the number of the individual substituents of type z (n_z) multiplied by the SE of substituent z (SE_z). Using the solver function in Excel, a set of SE_z values was found for the 9 different types of substituents that best fit the SE_{calcd2} and SE_{measd} values for all 21 arms.

$$SE_{calcd2} = \sum n_z \cdot SE_z \quad (2)$$

The improved accuracy was evident from the better correlation of the SE_{calcd2} and SE_{measd} values. The standard error of the difference was only ±0.01 kcal/mol. A plot of SE_{measd} versus SE_{calcd2} (Figure 2.8) also showed the improved correlation with an R^2 = 0.99 and a slope was closer to unity (1.00). An additional advantage of this analysis is that it could be used to predict SE_{calcd2} values for monosubstituted arms.

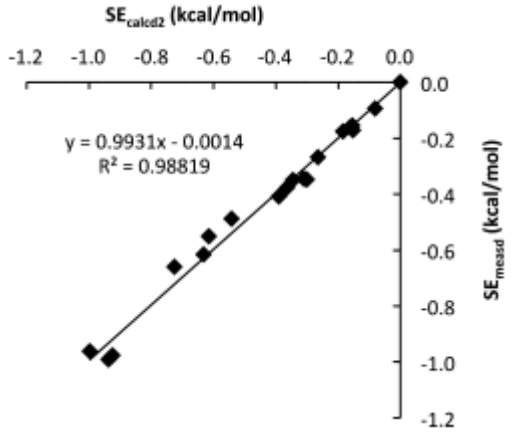

Figure 2.8 Correlation plot of the calculated (SE_{calcd2}) and measured SEs (SE_{measd}) for all 21 arms using a simple additive model based on the sum of the constituent monosubstituted arms

The existence or absence of SE additivity can also be used to test fundamental models of the aromatic stacking interaction. Two general models have been proposed for the origins of the SEs (Figure 2.9). In the direct interaction model, the substituents interact directly with the edges of the opposing aromatic ring.[27,35,44] Alternatively in the indirect interaction model, the substituents modulate the electrostatic potential of the attached π-system. The polarized aromatic ring, in turn, will have a stronger or weaker electrostatic attraction for the opposing aromatic ring.[14,45]

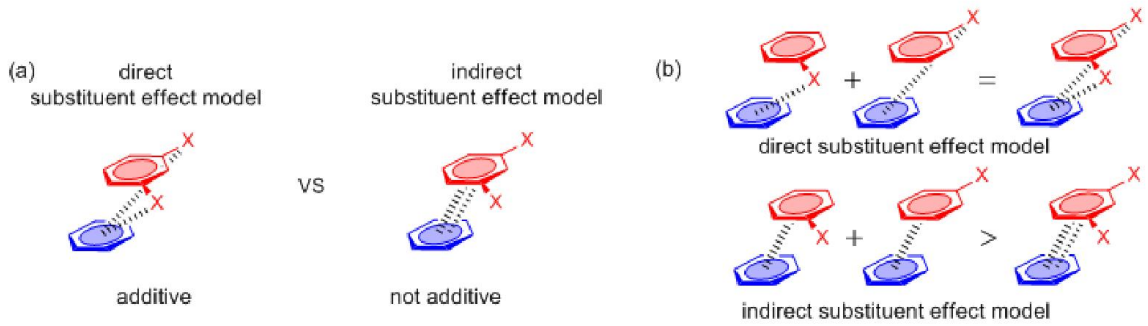

Figure 2.9 Representation of (a) the direct and indirect SE models for the aromatic stacking interaction and (b) the presence and absence of additive SEs for the direct and indirect SE models

The two SE models predict different degrees of SE additivity. The direct model predicts additive SEs.[44] Each substituent forms a separate interaction with the edge of the opposing aromatic ring. In contrast, the indirect model predicts SEs that are smaller than estimated by an additivity model. In the indirect model, the first substituent will impart the largest electrostatic polarization of the attached π-system. However, each additional substituent has a successively smaller SE as the buildup of charge on the aromatic ring makes the π-surface more difficult to polarize.

Therefore, the additivity of the SEs in our experimental model systems appeared to support the direct SE model. The near unity slopes of the correlation plots (Figures 2.7 and 2.8) and trend lines intersecting the origin provide support for the 1:1 correlation of the SE_{measd} to the additivity-based SE_{calcd} values. However, a concern was that the deviation for the indirect model from the additivity model could be too small to be accurately measured. To address this concern, we estimated the deviations from the additivity model for the indirect model by calculating the electrostatic potential (ESP) for a series of benzene rings with varying numbers of substituents (0−6). ESP provides a measure of the electrostatic polarization of the π-system by substituents and was shown

by Hunter et al. to correlate to the measured SEs in the aromatic stacking interactions.[21,24] The ESP calculations were made using the same method and level of theory (B3LPY, 6-31G*) as used by Hunter et al. Three representative substituents were examined that matched the substituents used in our model system: two electron-withdrawing groups (CN and Cl) and one electron-donating (CH_3) group. ESP for symmetrical substitution patterns were calculated from benzenes bearing one to six substituents. Similar trends were observed when the ESPs for asymmetric substitution patterns.

The ESP calculations showed the expected deviations from additivity (Figure 2.10). The first substituent had the largest effect, and each successive substituent had a smaller effect. This yielded asymptotic ESP curves that increasingly deviated from the linear additivity model with an increasing number of substituents. However, the deviations from the additivity model were small for benzenes with 2 and 3 substituents, which was the number of substituents in our model systems. The average difference from the additivity model was only −8% with 2 substituents and −11% with 3 substituents. Furthermore, the majority of these differences were due to the electron-donating CH_3 groups that had small SEs, and thus small variations became large percentage differences. Excluding the CH_3 group data, the deviations from the additivity model were only slightly larger than the error in our model system. Therefore, we cannot definitively rule out the indirect SE model.

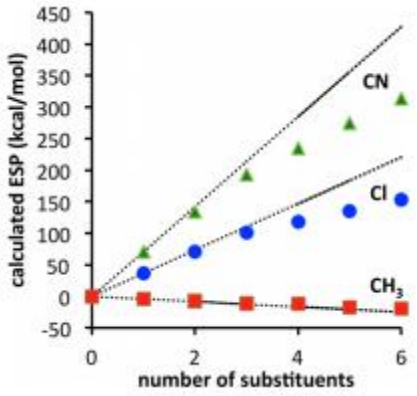

Figure 2.10 Calculated ESPs (kcal/mol) at the center of benzene rings bearing 0-6 symmetrically positioned substituents (CN, Cl, and CH_3). The broken lines show the expected ESPs for a perfectly additive system.

We examined other ways of differentiating the direct and indirect SE models. Larger deviations (>20%) from the additivity models were predicted for benzenes with 4 or more substituents. However, our current model system is limited to 3 substituents because one position is occupied by the oxygen linker, and the two adjacent *ortho*-positions can form additional steric and dispersion interactions. Alternatively, the distinct SE trends for the *meta*- and *para*-substituents in our model system provide support for the direct SE model. The direct SE model was originally developed for the aligned stacking geometry. However, the direct SE model has also been shown to be applicable to the offset stacking geometry.[44] A key difference in the offset geometry is that the substituents are no longer symmetrically arranged. Thus, the direct SE model predicts that substituents will have different magnitude SEs depending upon the distance of the substituents from the edge of the opposing aromatic surface. This positional dependence was observed in our system, as the close *meta*-substituents have a much stronger influence than the *para*-substituents. Quantitatively, the ratios of the SE for the *meta*- and *para*-positions averaged 1.7:1 as judged by the ratio of the slopes for their Hammett plots (Figure 2.6).

The indirect model predicts a weaker positional SE dependence than the direct model. To the first approximation, the indirect model should not have a positional dependence, as the *meta*- and *para*-substituents polarize the π-system of the attached aromatic ring to a similar extent. However, the orientation of the polarization of the π-surface will differ depending upon the position of the substituent relative to the dipole or quadrupole of the opposing aromatic surface. Therefore, we cannot entirely rule out the possibility that the indirect model, as the magnitude of its positional dependence is not easily calculated.

In this study, we have utilized a small molecule model system to experimentally test the additivity of the SEs for the offset stacking aromatic interaction in organic solution. A series of molecular torsional balances **1a−u** and control balances **2a−u** with 21 different substituted benzene arms were prepared containing 5 different substituents (CH_3, OCH_3, Cl, CN, NO_2) that ranged for strongly electron-withdrawing to electron-donating groups. The formation of intramolecular aromatic stacking interactions and the ability to electrostatically influence the interaction energies by the introduction of substituents in our model system were confirmed by NMR, X-ray crystallography, and the observation of linear Hammett plots for the monosubstituted systems. These SEs ranged from slightly destabilizing (+0.05 kcal/mol for *p*-CH_3) substituted to strongly stabilizing (−1.00 kcal/mol for *m,p*-$(CN)_2$).

An analysis of the SEs for the 11 multisubstituted balances demonstrated that simple additivity models could provide a good estimate (±0.01 to ±0.02 kcal/mol) of the measured SEs. Specifically, the SEs for multisubstituted systems could be accurately estimated from the sum of the individual SEs. These individual SEs could be estimated

from SE_{measd} of the monosubstituted balances or via multivariate analysis using the SE_{measd} of the mono- and multisubstituted balances. The observation of SE additivity for the aromatic stacking interaction in this solution-phase study was consistent with previous theoretical studies conducted in vacuo. [23]

The additivity of SEs for the aromatic stacking interactions has both theoretical and practical applications. First, the SE additivity and the positional dependence of the SEs in our model system provide support for the direct SE model, in which the SEs are due to the direct interaction of the substituents with the edge of the opposing aromatic ring. However, due to the limitation in the number of substituents in our system and the measurement error, we cannot definitively exclude the indirect SE model. Second, the additivity of the SEs for the aromatic stacking interaction has practical applications. This should aid in the rational design and optimization of systems that utilize aromatic stacking, as the magnitude of the stabilization or destabilization by substituents can be accurately predicted using an additive SE model. As demonstrated in this study, the aromatic stacking energies of multisubstituted benzenes can be accurately predicted from the measured stacking energies of the analogous monosubstituted systems. Alternatively, the stacking energies of monosubstituted systems can be predicted from stacking energies of multisubstituted systems. For example from Table 2.2, the stacking energy of *m*-CH_3 can be estimated from half of the measured stacking energy of *m,m*-$(CH_3)_2$.

References

(1) Resconi, L.; Cavallo, L.; Fait, A.; Piemontesi, F. *Chem. Rev*. **2000**, *100*, 1253−1345.
(2) Roesky, H. W.; Andruh, M. *Coord. Chem. Rev*. **2003**, *236*, 91−119.
(3) Zhao, D. H.; Moore, J. S. *Chem. Commun*. **2003**, 807−818.
(4) Meyer, E. A.; Castellano, R. K.; Diederich, F. *Angew. Chem. Int. Ed.* **2003**, *42*, 1210−1250.
(5) Salonen, L. M.; Ellermann, M.; Diederich, F. *Angew. Chem. Int. Ed*. **2011**, *50*, 4808−4842.
(6) Draper, D. E. *J. Mol. Biol*. **1999**, *293*, 255−270.
(7) Whitten, D. G.; Chen, L. H.; Geiger, H. C.; Perlstein, J.; Song, X. D. J. *Phys. Chem. B* **1998**, *102*, 10098−10111.
(8) Riley, K. E.; Hobza, P. *Acc. Chem. Res*. **2013**, *46*, 927−936.
(9) Klosterman, J. K.; Yamauchi, Y.; Fujita, M. *Chem. Soc. Rev*. **2009**, *38*, 1714−1725.
(10) Schneider, H. J. *Angew. Chem. Int. Ed*. **2009**, *48*, 3924−3977.
(11) Moulton, B.; Zaworotko, M. *J. Chem. Rev*. **2001**, *101*, 1629−1658.
(12) Wei, Y.; Held, I.; Zipse, H. *Org. Biomol. Chem*. **2006**, *4*, 4223−4230.
(13) Ruano, J. L. G.; Aleman, J.; Alonso, I.; Parra, A.; Marcos, V.; Aguirre, *J. Chem. Eur. J*. **2007**, *13*, 6179−6195.
(14) Hunter, C. A.; Sanders, J. K. M. *J. Am. Chem. Soc*. **1990**, *112*, 5525−5534.
(15) Watt, M.; Hardebeck, L. K. E.; Kirkpatrick, C. C.; Lewis, M. *J. Am. Chem. Soc*. **2011**, *133*, 3854−3862.
(16) Wheeler, S. E.; McNeil, A. J.; Muller, P.; Swager, T. M.; Houk, K. N. *J. Am. Chem. Soc.* **2010**, *132*, 3304−3311.
(17) Lee, E. C.; Kim, D.; Jurecka, P.; Tarakeshwar, P.; Hobza, P.; Kim, K. S. *J. Phys. Chem. A* **2007**, *111*, 3446−3457.
(18) Sinnokrot, M. O.; Sherrill, C. D. *J. Am. Chem. Soc*. **2004**, *126*, 7690−7697.
(19) Cozzi, F.; Cinquini, M.; Annunziata, R.; Dwyer, T.; Siegel, J. S. *J. Am. Chem. Soc*. **1992**, *114*, 5729−5733.
(20) Gung, B. W.; Xue, X. W.; Reich, H. J. *J. Org. Chem*. **2005**, *70*, 3641−3644.
(21) Cockroft, S. L.; Hunter, C. A.; Lawson, K. R.; Perkins, J.; Urch, C. J. *J. Am. Chem. Soc*. **2005**, *127*, 8594−8595.
(22) Rashkin, M. J.; Waters, M. L. *J. Am. Chem. Soc*. **2002**, *124*, 1860−1861.
(23) Ringer, A. L.; Sinnokrot, M. O.; Lively, R. P.; Sherrill, C. D. *Chem. Eur. J*. **2006**, *12*, 3821−3828.
(24) Cockroft, S. L.; Perkins, J.; Zonta, C.; Adams, H.; Spey, S. E.; Low, C. M. R.; Vinter, J. G.; Lawson, K. R.; Urch, C. J.; Hunter, C. A. *Org. Biomol. Chem*. **2007**, *5*, 1062−1080.
(25) Ringer, A. L.; Sherrill, C. D. *J. Am. Chem. Soc*. **2009**, *131*, 4574−4575.
(26) Cozzi, F.; Annunziata, R.; Benaglia, M.; Baldridge, K. K.; Aguirre, G.; Estrada, J.; Sritana-Anant, Y.; Siegel, J. S. *Phys. Chem. Chem. Phys*. **2008**, *10*, 2686−2694.
(27) Wheeler, S. E.; Houk, K. N. *J. Am. Chem. Soc*. **2008**, *130*, 10854−10855.
(28) Seo, J.-I.; Kim, I.; Lee, Y. S. *Chem. Phys. Lett*. **2009**, *474*, 101−106.
(29) Cozzi, F.; Ponzini, F.; Annunziata, R.; Cinquini, M.; Siegel, J. S. *Angew. Chem. Int. Ed.* **1995**, *34*, 1019−1020.
(30) Liu, T. J.; Schneider, H. J. *Angew. Chem. Int. Ed*. **2002**, *41*, 1368−1370.
(31) Carroll, W. R.; Pellechia, P.; Shimizu, K. D. *Org. Lett*. **2008**, *10*, 3547−3550.
(32) Li, P.; Zhao, C.; Smith, M. D.; Shimizu, K. D. *J. Org. Chem*. **2013**, *78*, 5303−5313.

(33) Paliwal, S.; Geib, S.; Wilcox, C. S. *J. Am. Chem. Soc*. **1994**, *116*, 4497−4498.
(34) Mati, I. K.; Cockroft, S. L. *Chem. Soc. Rev*. **2010**, *39*, 4195−4205.
(35) Arnstein, S. A.; Sherrill, C. D. *Phys. Chem. Chem. Phys*. **2008**, *10*, 2646−2655
(36) Nijamudheen, A.; Jose, D.; Shine, A.; Datta, A. *J. Phys. Chem. Lett*. **2012**, *3*, 1493−1496.
(37) Mooibroek, T. J.; Gamez, P.; Reedijk, *J. CrystEngComm* **2008**, *10*, 1501−1515.
(38) Hunter, C. A. *Angew. Chem. Int. Ed*. **2004**, *43*, 5310−5324.
(39) Muchowska, K. B.; Adam, C.; Mati, I. K.; Cockroft, S. L. *J. Am. Chem. Soc*. **2013**, *135*, 9976−9979.
(40) Hansch, C.; Leo, A.; Taft, R. W. *Chem. Rev*. **1991**, *91*, 165−195.
(41) Yoshitake, Y.; Misaka, J.; Setoguchi, K.; Abe, M.; Kawaji, T.; Eto, M.; Harano, K. *J. Chem. Soc., Perkin Trans*. *2* **2002**, 1611−1619.
(42) Soininen, P.; Haarala, J.; Vepsalainen, J.; Niemitz, M.; Laatikainen, R. *Anal. Chim. Acta* **2005**, *542*, 178−185.
(43) Pauli, G. F.; Goedecke, T.; Jaki, B. U.; Lankin, D. C. *J. Nat. Prod*. **2012**, *75*, 834−851.
(44) Wheeler, S. E. *J. Am. Chem. Soc*. **2011**, *133*, 10262−10274.
(45) Hunter, C. A.; Lawson, K. R.; Perkins, J.; Urch, C. J. *J. Chem. Soc., Perkin Trans*. *2* **2001**, 651−669.
(46) Rizzo, V.; Pinciroli, V.J. *Pharm. Biomed. Anal*. **2005**, *38*, 851−857.
(47) Bauer, M.; Bertario, A.; Boccardi, G.; Fontaine, X.; Rao, R.; Verrier, D. *J. Pharm. Biomed. Anal.* **1998**, *17*, 419−425.
(48) Barding, G. A. J.; Salditos, R.; Larive, C. K. *Anal. Bioanal. Chem*. **2012**, *404*, 1165−1179.
(49) Soininen, P.; Haarala, J.; Vepsalainen, J.; Niemitz, M.; Laatikainen, R. *Anal. Chim. Acta* **2005**, *542*, 178−185.

CHAPTER 3

IMPORTANCE OF DISPERSION INTERACTIONS TO THE STRENGTH OF AROMATIC STACKING INTERACTIONS IN SOLUTION[2]

[2] Reproduced with permission from: Hwang, J.; Dial, B. E.; Li, P.; Kozik, M. E.; Smith, M. D.; Shimizu, K. D. *Chem. Sci.* **2015**, *6*, 4358. Copyright © 2015 Royal Society of Chemistry.

Aromatic stacking interactions play a key role in determining the stability, activity, and utility of many supramolecular processes such as the structure of biopolymers,[1-3] host-guest complex stability,[4-7] and the selectivity of asymmetric catalysts.[8-10] The importance and utility of aromatic stacking interactions have provided the motivation to study the fundamental nature of the interaction and to develop models that can accurately predict their stability trends.[11,12] Thus, the influence of variables to the strength of stacking interactions such as charge,[13,14] substituent effects,[15,16] and solvent effects[17,18] has been an active area of research.

The goal of this study was to experimentally assess the role that dispersion interactions play in the aromatic stacking interaction in solution.[19-21] London dispersion interactions are the most fundamental attractive non-covalent interaction as all types of molecules including: charged, polarized, and non-polar molecular surfaces.[12,22] In the gas-phase, dispersion interactions have been identified as the dominant contributing term for aromatic stacking interactions.[23-25] For example, Sherrill's component analysis estimated that the dispersion term comprises 61% of the overall stacking energy for the benzene dimer.[26] However, the role of dispersion forces in solution has been much more controversial. Specifically, the dispersion contributions in solution have been proposed to be much smaller or even negligible.[27] The rationale is that there are roughly an equal number of dispersion interactions on either side of the stacking equilibrium (Figure 3.1). The aromatic surfaces still form attractive dispersion interactions in the stacking complex. However, solvent molecules form additional dispersion interactions on either side of the binding equilibrium with the uncomplexed aromatic surfaces and with each

other.[27] Thus, the question is whether the net dispersion interactions on the right-hand side of the equilibrium are stronger than those on the left-hand side of the equilibrium.

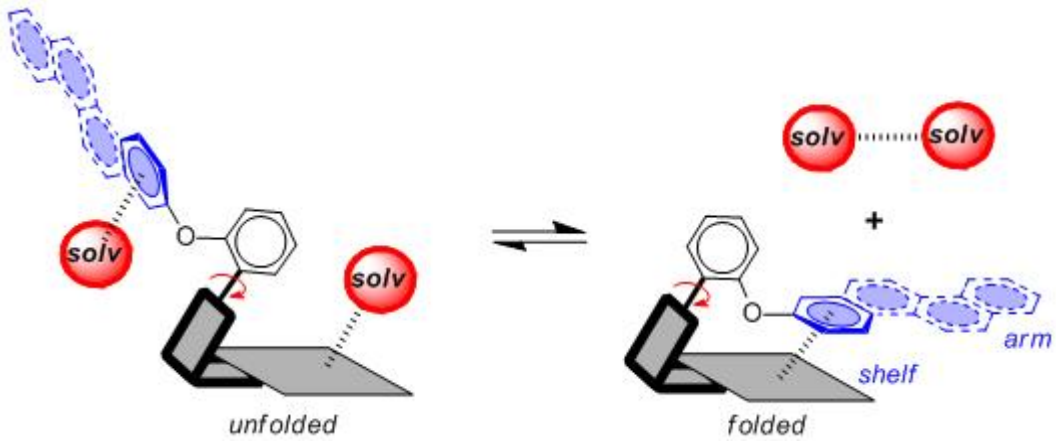

Figure 3.1 Representation of the intramolecular aromatic stacking interaction in the *folded* conformer of a molecular torsion balance model system and the influence of solvent molecules (red spheres) on the stability of the *folded-unfolded* conformational equilibrium

The measurement of dispersion interaction in solution has posed a number of experimental challenges.[28,29] First, the dispersion contributions are expected to be small, and thus a very sensitive method with sub kcal/mol accuracy is required. Second, in contrast to electrostatic or solvent trends, it is difficult to systematically vary the dispersion term of a non-covalent interaction. Third, dispersion interactions are very difficult to differentiate from solvophobic interactions because both scale with increasing size of the aromatic surfaces.[30,31] Thus, studies that have observed a correlation between the size of the aromatic surface and the strength of the stacking interaction could be attributed to solvophobic or dispersion effects.[32-34]

In this study, a small molecule model system was designed to specifically address the above challenges.[35,36] First, the model system is an example of a "molecular torsion balance", which has been demonstrated to provide a very accurate and sensitive measure of non-covalent interactions.[36] Variations in the strength of the intramolecular interaction

as small as ±0.03 kcal/mol can be measured by monitoring their influence on the *folded-unfolded* equilibrium (Figure 3.1).[37-40] Second, the dispersion term was systematically varied by increasing the conjugation length and polarizability of one of the interacting surfaces. Dispersion interactions are known to increase with increasing molecular polarizability because dispersion interactions are the result of the electrostatic attraction between polarizable molecular surfaces.[41-43] Third, the dispersion effects were differentiated from the solvophobic effects by keeping the contact area between the two stacking aromatic surfaces constant. The rigid bicyclic framework of the molecular balances fixes the geometry and contact area of the aromatic surfaces in **1a-f** (Figure 3. 2). Only the first benzene ring of the aromatic arm, regardless of its size, was in contact with the phenanthrene shelf. Thus, the extended aromatic surfaces in **1b-f** did not form any additional stacking or solvophobic interactions.

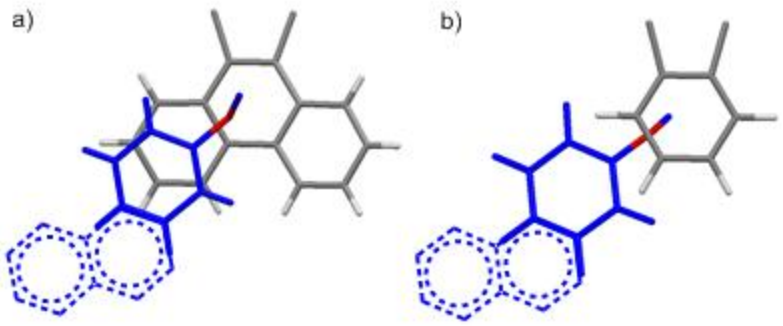

Figure 3.2 Top views of the aromatic arm (colored blue) and shelf (colored gray) surfaces in the *folded* conformers of the (a) balance **1a** and (b) control balance **2a**. The models are based on the crystal structures of an analogue of **1a**[41] and DFT molecular modelling (M06-2X, 6-31G*)[46] for **2a**. For viewing clarity, only the aromatic surfaces of the arm and shelf are shown. The extrapolated extended surfaces in arms of **b** and **d** are depicted as dotted lines.

An additional advantage of these molecular systems was that the results could be directly compared with computational studies.[39,41,44] These computational studies provided theoretical in vacuo benchmarks to compare the magnitudes of our

experimentally measured trends in solution. The most similar computational studies were by Zeinalipour-Yazdi and Pullman, which measured the stacking energy of a benzene with aromatic surfaces of varying size.[41] The molecular balances performed an analogous comparison as the outer most benzene ring of the phenanthrene shelf forms stacking interactions with the aromatic arms of varying size. In the computational studies, the stacking energies of the benzene unit were found to systematically increase with the increasing size and polarizability of the opposing aromatic surface. A steep linear correlation was predicted between the size of the opposing aromatic surfaces and the stacking energies. This trend is consistent with the dispersion term representing a significant portion of the stacking energy in vacuo. For example, the stacking interaction energy of the benzene-naphthalene complex was 2.3 times larger than the benzene-benzene complex. Similarly, the stacking interaction energy of the benzene-anthracene complex was 3.9 times larger than the benzene-benzene complex.

The rigid bicyclic N-arylimide framework of the molecular balances utilized in this study had been previously employed to study a range of non-covalent interactions such as aromatic stacking, CH-π, and cation-π interactions.[37-40] This molecular balance framework has a number of attractive features. First, restricted rotation of the N-arylimide rotor leads to the formation of distinct *folded* and *unfolded* conformers that are in equilibrium at room temperature. Second, the bicyclic framework holds the aromatic surfaces of the arm and shelf at different distances in the two conformers. In the *folded* conformer, the arm and shelf surfaces are in close proximity allowing formation of an intramolecular off-set stacking interaction. In the *unfolded* conformer, the arm and shelf surfaces are held apart and cannot form a stacking interaction. Thus, the *folded*/*unfolded*

equilibrium ratio provides a very sensitive measure of variations in the strength of the intramolecular interactions. A strengthening of the intramolecular stacking interactions is evident by a shift in the *folded*/*unfolded* ratio towards the *folded* conformer.

We have previously demonstrated that the parent balance **1a** with a phenyl arm forms a well-defined off-set stacking interaction in the *folded* conformer (Figure 3.2).[39,40] X-ray and NMR analyses of **1a** found that the phenyl arm and phenanthrene shelf adopt a parallel stacking geometry in the *folded* conformer. The phenyl ring of the arm is in contact with outer most ring of the phenanthrene shelf with a center-to-center distance of 3.75 Å. Furthermore, the proximity of the arm and shelve surfaces and the rigidity of the bicyclic framework do not provide sufficient freedom and space to form the alternative arene-arene geometries such as the perpendicular edge-to-face and T-shaped geometries. The rigidity of the balance framework also ensures that the extended aromatic surfaces of the arms in balances **1b-f** (represented as dotted lines in Figure 3.2) should not form additional stacking interactions with the phenanthrene shelf. In addition, the contact area between the arm and shelf surfaces should remain constant despite the variations in the size of the aromatic arms.

We have also confirmed that the parent control balance **2a** with the phenyl arm is unable to form an intramolecular stacking interaction in the *folded* conformer due to its shorter benzene shelf (Figure 3.2).[40] The absence of stacking interactions in **2a** was confirmed by NMR and modeling studies. Thus, control balances **2a-f** should provide a measure of the other factors that influence the *folded-unfolded* equilibria such as solvent, dipole, linker, and secondary interaction effects. The subtraction of the folding energy of **2** from the folding energy of **1** should isolate the intramolecular stacking energy.

For this study, six balances (**1a-f**) and six control balances (**2a-f**) were prepared via previously described synthetic routes.[39,40] The six aromatic arms (**a-f**) include aromatic surfaces of varying size, conjugation length, and polarizability. These aromatic surfaces fell into three groups (Figure 3.3). The first was the unsubstituted phenyl arm (**a**) that had the smallest common aromatic surface. The next were the fused aromatic surfaces with naphthyl and phenanthryl arms (**b** and **c**). The last group was the non-fused aromatic surfaces (**d**, **e**, and **f**). These include the biphenyl (**d**), stilbene (**e**), and diphenylethynyl (**f**) arms, which extend the conjugation of the parent phenyl ring from a single substitution point at the *para*-position.

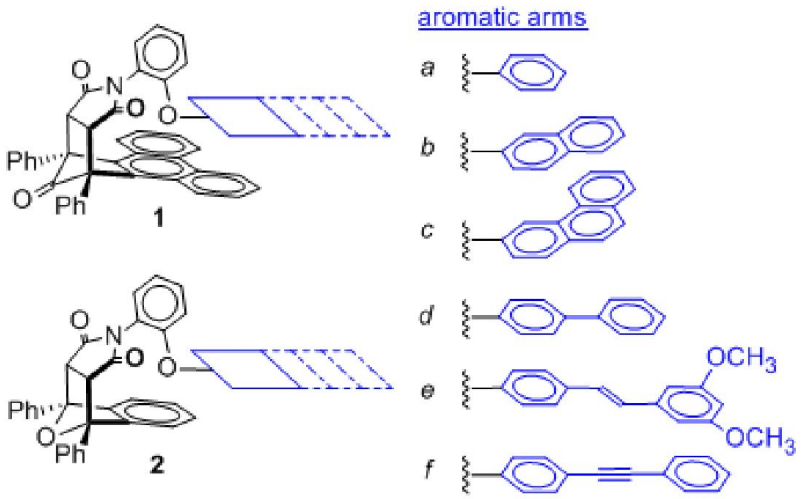

Figure 3.3 The structures of aromatic stacking balances **1a–f** and control balances **2a–f** (shown in the *folded* conformation), which have six different aromatic arms (**a–f**) with varying conjugation lengths and polarizabilities.

The formation of the expected intramolecular stacking interactions within the new balances **1b-f** was established by comparison of their ^{1}H NMR spectra ($CDCl_3$, 298 K) with those of the parent balance **1a** and control balances **2a-f**. The NMR analyses were facilitated by a separate set of peaks for the *folded* and *unfolded* conformers due to slow exchange on the NMR time scale. The first indication of stacking interactions in **1b-f** was

the observation of the expected upfield shifts of the aromatic arm and shelf protons. Due to the proximity of the arm and shelf aromatic surfaces in the stacked structure, upfield shifts of up to 1.0 ppm were observed in the *folded* versus the *unfolded* conformers. The direction and magnitude of these peak shifts were identical to those observed in the parent stacking phenyl balance **1a**.[40] By comparison, these same aromatic protons did not display upfield shifts in the *folded* versus *unfolded* conformers of control balances **2a-f**, which cannot form intramolecular stacking interactions.

The formation of stacking interaction was also evident from a comparison of their folding energies. The *folded*/*unfolded* ratios of **1a-f** and **2a-f** and their corresponding folding energies were measured from their peak areas in the ^{1}H NMR spectra (Table 3.1). The folding energies of the stacking balances **1a-f** were consistently stronger (more negative) than the folding energies of the corresponding control balances **2a-f**. This was consistent with the stabilization of the *folded* conformers of **1a-f** by the formation of attractive stacking interactions. The intramolecular stacking interactions were estimated from the difference in the folding energies of **1a-f** and **2a-f** ($\Delta\Delta G_{1\text{-}2}$). The stacking energies ranged from -0.92 to -1.33 kcal/mol, which were comparable with previous measurements of stacking interactions of benzene surfaces in organic solution.[15]

Table 3.1 ^{1}H NMR measured folding energies of balances **1** and **2** (ΔG_1 and ΔG_2), the aromatic stacking energies ($\Delta\Delta G_{1\text{-}2}$)

	arm	ΔG_1[a]	ΔG_2[a]	$\Delta\Delta G$[b]
a	phenyl	0.48	1.40	-0.92
b	naphthyl	0.17	1.33	-1.16
c	3-phenanthrene	-0.08	1.26	-1.33
d	diphenyl	0.31	1.41	-1.10
e	1,3-dimethoxy-5-styrylbenzene	0.38	1.33	-0.95
f	diphenylethynyl	0.29	1.33	-1.05

[a]Folding energies (kcal/mol) measured in $CDCl_3$ at 298 K, with an error less than ±0.03 kcal/mol. [b]π-Stacking interactions (kcal/mol) with an error less than ±0.04 kcal/mol.

Next, the influence of the different sized aromatic arms on the stacking energies was examined. This analysis suggested that the dispersion contributions to the stacking interaction in solution were either small or negligible. These conclusions were based on two observations. First, the stacking energies in **1a-f** were very similar despite the large variations in size of the arm surfaces. The $\Delta\Delta G_{1\text{-}2}$ values spanned a relatively narrow range from -0.92 to -1.33 kcal/mol. These variations were an order of magnitude smaller than those predicted by the computational studies.[41] For example, the stacking interaction energy of the naphthyl arm in **1b** was only 26% greater than the phenyl arm in **1a** (-1.16 versus -0.92 kcal/mol). By comparison, the computational studies predicted a 230% increase in the stacking energies of naphthalene versus benzene surfaces.[41]

Second, no clear correlation was observed between the stacking energies and the polarizabilities of the respective arms. The polarizabilities of the aromatic surfaces in the arms were estimated using computational methods (B3LYP, 6-31G*).[47] The most polarizable arms such as the diphenyl acetylene and stilbene did not show the strongest stacking energies. More convincingly, a plot of the calculated polarizabilities versus the measured stacking energies ($\Delta\Delta G_{1\text{-}2}$) did not show a clear correlation (Figure 3.4). The stacking energies of the different sized arms appeared to strengthen (more negative) with increasing polarizability of the fused arms (**b** and **c**). However, an inverse correlation was observed between polarizability and stacking energy for the non-fused arm (**d-f**).

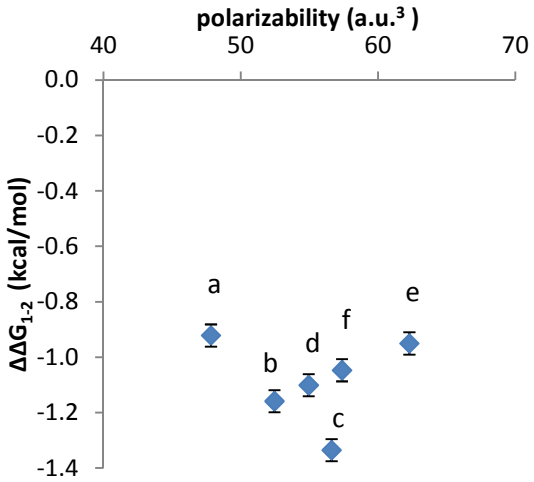

Figure 3.4 Plot of the correlation between the measured stacking energies ($\Delta\Delta G_{1\text{-}2}$) in balance **1a**–**f** and the polarizability of the aromatic arms **a**–**f**.

The inability to observe the dispersion of the stacking interaction energies in solution was consistent with the hypothesis that the dispersion contributions would be smaller in solution because of the counter-balancing dispersion interactions of the solvent molecules. However, alternative explanations were also explored. First, the possibility was that the variations in the stacking energies were within the error for the measurement. The standard deviation of the stacking energies was 0.15 kcal/mol. While this value is small, it is greater than the error for the analysis which was estimated to be ±0.04 kcal/mol. The second possible explanation was that the variations in the stacking energies were due to electrostatic substituent effects (ESEs). Substituents on aromatic rings have been shown to stabilize and destabilize the aromatic stacking interaction in computational and experimental studies.[15,16,48-50] Along these lines, we have previously characterized the electrostatic substituent effects (ESE) of this specific stacking model system.[46] This allowed us to estimate the influence of the substituent effects and to test

whether the substituent effects can explain the observed minor variations in stacking interaction energies.

To assess the ESEs in this system, the extended conjugation of arms **b**-**f** was classified as *meta*- and/or *para*-substituents on the core phenyl arm **a** (Table 3.2). Arms **d**-**f** were treated as monosubstituted phenyl rings. For example, the biphenyl arm in balance **1d** was categorized as a phenyl ring with a *para*-phenyl substituent. The fused naphthyl and phenanthryl arms **b** and **c** were treated as disubstituted phenyl rings with one *meta*- and one *para*-substituent. The expected stabilizing or destabilizing ESEs were calculated based on the Hammett σ_{meta} parameters for respective substituents in Table 3.2 and the slopes of the previously measured Hammett plots for this balance system.[51] For the disubstituted arms (**b** and **c**), the ESEs were calculated as the sum of the individual substituent effects. This analysis is based on the recent finding that the substituent effects for stacking interactions are additive.[46]

Table 3.2 Classification of aromatic surfaces in arms **a**–**f** as *meta*- and *para*-substituted phenyl rings for use in estimating their electrostatic substituent effects

arms	*meta*-substituent	*para*-substituent
(a)	—H	—H
(b)		
(c)		
(d)	—H	
(e)	—H	
(f)	—H	

The estimated ESEs were able to explain half of the variation in the $\Delta\Delta G_{1\text{-}2}$ values. The ESEs for arms **b-f** were all weakly stabilizing, which was consistent with the observed stronger stacking energies for the extended arms **b-f**. The vinyl, phenyl, styrene, and phenylacetylene substituents in the arms are all weak electron-withdrawing groups with small positive Hammett σ_{meta} values (0.03 to 0.14). Electron-withdrawing substituents have been shown to stabilize stacking interactions due to the formation of attractive electrostatic interactions.[52] To assess the importance of the substituent effects, the predicted ESE values were subtracted from the measured $\Delta\Delta G_{1\text{-}2}$ values to give a substituent corrected stacking energy ($\Delta\Delta G_{1\text{-}2}$ – ESE). The corrected stacking energies (-0.92 to -1.11 kcal/mol) had approximately half the variation than the uncorrected stacking energies (-0.92 to -1.33 kcal/mol).

The third alternative explanation was that the substituent effects had been obscuring the smaller dispersion effects. To test this possibility, the correlation between the substituent corrected stacking energies and polarizability was examined (Figure 3.5). The plot of $\Delta\Delta G_{1\text{-}2}$ – ESE versus polarizability was relatively flat, as the majority of variance had been removed. However, the remaining variance did not show a correlation with the polarizabilities of the aromatic surfaces.

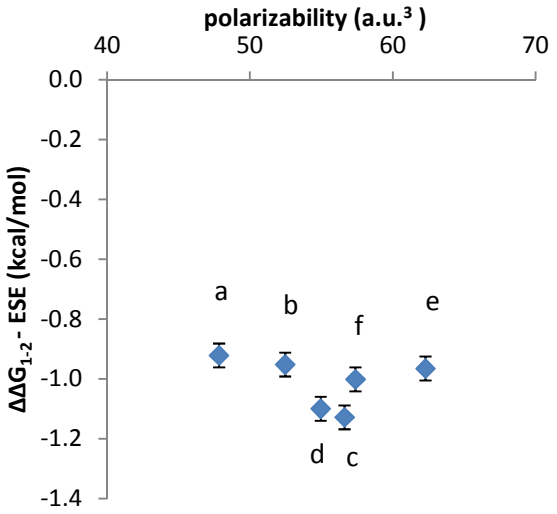

Figure 3.5 Plot of the correlation between the substituent effects corrected stacking energies ($\Delta\Delta G_{1\text{-}2}$ - ESE) and the polarizability of the aromatic arms **a**–**f**

The final explanation for the inability to observe the dispersion effects was that the experimental design has not properly isolated the stacking energy from the *folded-unfolded* equilibrium energies. Of particular concern were solvophobic effects, which have been cited as the dominant term for the weak non-covalent interactions of non-polar surfaces in solution.[53,54] However, there were two observations that suggested that solvent and solvophobic effects had been effectively isolated in this study. First, relatively small differences in the stacking energies in **1a-f** were observed despite the large variation in the size of the aromatic arms. Thus, the geometric constraints in the balance framework appear to have been effective in keeping the surface area contact and solvophobic effects constant for the series. Second, the folding energies of balances **1a-f** and **2a-f** were measured in two additional solvent systems. The folding energies of balances **1a-f** and control balances **2a-f** were measured in a more polar, acetone- d_6, and a less polar, bromobenzene-d_5, solvent. The overall trends and conclusions were analogous to those observed in $CDCl_3$, suggesting that the solvent effects were not the reason for the

inability to observe dispersion effects. The uncorrected ($\Delta\Delta G_{1\text{-}2}$) and corrected ($\Delta\Delta G_{1\text{-}2}$ – ESE) stacking energies in these two additional solvents had relatively small variations and did not show any clear correlation with the polarizabilities of the aromatic surfaces.

In this study, we designed a series of molecular torsion balances **1a-f** to assess the importance of dispersion interactions to the aromatic stacking interactions in solution. These model systems measured the strength of an intramolecular stacking interaction via changes in a *folded-unfolded* conformational equilibrium. The contribution of the dispersion term was assessed by systematically varying the size and polarizability of one of the aromatic surfaces and measuring the effect on the stacking energies. Through the use of control systems **2a-f**, geometrical constraints, and studies in multiple solvents, the stacking interaction energies were separated from other factors that influence the conformational equilibrium such as solvophobic, dipole, linker, and steric effects.

No clear correlation was observed between the polarizabilities of the aromatic surfaces and the stacking energies. There was relatively little variance in the strengths of the stacking energies despite the wide range in the sizes and conjugation lengths of the aromatic surfaces. These results suggest that the dispersion contributions to the aromatic stacking interaction in solution are small or negligible. This conclusion is in contrast to computational studies, which have found a dramatic correlation between the stacking energy versus the size and polarizability of an aromatic surface.[41]

The minimal influence of dispersion interactions to stacking interactions in solution is not due to the absence of dispersion interactions. Aromatic surfaces still form attractive dispersion interaction in solution just as they do in vacuo. However, the

aromatic surfaces in solution also form dispersion interactions with solvent molecules, which attenuates the overall magnitude of the dispersion term.

The approach and results of this study nicely complement a recent study of the origin of alkyl-alkyl interactions in solution.[53] Cockroft and co-workers used a perpendicular approach of assessing the contributions of dispersion interactions in solution. Instead of varying the size and polarizability of the interacting surfaces, they systematically varied the solvent environment, which allowed them to measure and subtract out the solvent effects from the overall interaction energy. Although the approach was different, the conclusions were the same as this study as the dispersion term of the interaction could not be observed in solution. The majority of the interaction energy was attributed to the solvent and solvophobic effects and the small residual interaction energy was within the error of the analysis.

Refereneces

(1) Riley, K. E.; Hobza, P. *Acc. Chem. Res.* **2013**, *46*, 927.
(2) Kool, E. T.; Morales, J. C.; Guckian, K. M. *Angew. Chem. Int. Ed.* **2000**, *39*, 990.
(3) Heddi, B.; Phan, A. T. *J. Am. Chem. Soc.* **2011**, *133*, 9824.
(4) Klarner, F. G.; Kahlert, B. *Acc. Chem. Res.* **2003**, *36*, 919.
(5) T Webb, T. H.; Wilcox, C. S. *Chem. Soc. Rev.* **1993**, *22*, 383.
(6) Yoshizawa, M.; Klosterman, J. K.; Fujita, M. *Angew. Chem. Int. Ed.* **2009**, *48*, 3418.
(7) Harmata, M. *Acc. Chem. Res.* **2004**, *37*, 862.
(8) Erkkila, A.; Majander, I.; Pihko, P. M. *Chem. Rev.* **2007**, *107*, 5416.
(9) Kolb, H. C.; Vannieuwenhze, M. S.; Sharpless, K. B. *Chem. Rev.* **1994**, *94*, 2483.
(10) Krenske, E. H.; Houk, K. N. *Acc. Chem. Res.* **2013**, *46*, 979.
(11) Lee, E. C.; Kim, D.; Jurecka, P.; Tarakeshwar, P.; Hobza, P.; Kim, K. S. *J. Phys. Chem. A* **2007**, *111*, 3446.
(12) Ehrlich, S.; Moellmann, J.; Grimme, S. *Acc. Chem. Res.* **2013**, *46*, 916.
(13) Yamada, S.; Fossey, J. S. *Org. Biomol. Chem.* **2011**, *9*, 7275.
(14) Kano K.; Minamizono, H.; Kitae, T.; Negi, S. *J. Phys. Chem. A* **1997**, *101*, 6118.
(15) Gung, B. W.; Xue, X. W.; Reich, H. J. *J. Org. Chem.* **2005**, *70*, 3641.
(16) Cockroft, S. L.; Perkins, J.; Zonta, C.; Adams, H.; Spey, S. E.; Low, C. M. R.; Vinter, J. G.; Lawson, K. R.; Urch, C. J.; Hunter, C. A. *Org. Biomol. Chem.* **2007**, *5*, 1062.
(17) Cubberley, M. S.; Iverson, B. L. *J. Am. Chem. Soc.* **2001**, *123*, 7560.
(18) Rehm, T.; Schmuck, C. *Chem. Commun.* **2008**, 801.
(19) Waters, M. L. *Curr. Opin. Chem. Biol.* **2002**, *6*, 736.
(20) Sponer, J.; Riley, K. E.; Hobza, P. *Phys. Chem. Chem. Phys.* **2008**, *10*, 2595.
(21) da Costa, L. M.; Stoyanov, S. R.; Gusarov, S.; Seidl, P. R.; Carneiro, J. W. D.; Kovalenko, A. *J. Phys. Chem. A* **2014**, *118*, 896.
(22) Zeinalipour-Yazdi, C. D.; Pullman, D. P. *J. Phys. Chem. B* **2006**, *110*, 24260.
(23) Hobza, P.; Sponer, J. *Chem. Rev.* **1999**, *99*, 3247.
(24) Tsuzuki, S.; Honda, K.; Uchimaru, T.; Mikami, M.; Tanabe, K. *J. Am. Chem. Soc.* **2002**, *124*, 104.
(25) Sinnokrot, M. O.; Sherrill, C. D. *J. Phys. Chem. A* **2004**, *108*, 10200.
(26) Jaffe, R. L.; Smith, G. D. *J. Chem. Phys.* **1996**, *105*, 2780.
(27) Sherrill, C. D. *Acc. Chem. Res.* **2013**, *46*, 1020.
(28) Hunter, C. A. *Angew. Chem. Int. Ed.* **2004**, *43*, 5310.
(29) Schneider, H. J. *Angew. Chem. Int. Ed.* **2009**, *48*, 3924.
(30) Hunter, C. A.; Lawson, K. R.; Perkins, J.; Urch, C. J. *J. Chem. Soc., Perkin Trans. 2*, **2001**, 651.
(31) Gardner, R. R.; Christianson, L. A.; Gellman, S. H. *J. Am. Chem. Soc.* **1997**, *119*, 5041.

(32) Chen, Z. J.; Lohr, A.; Saha-Moller, C. R.; Wurthner, F. *Chem. Soc. Rev.* **2009**, *38*, 564.
(33) Sebaoun, L.; Maurizot, V.; Granier, T.; Kauffmann, B.; Huc, I. *J. Am. Chem. Soc.* **2014**, *136*, 2168.
(34) Jonkheijm, P.; Hoeben, F. J. M.; Kleppinger, R.; van Herrikhuyzen, J.; Schenning, A. P. H. J.; Meijer, E. W. *J. Am. Chem. Soc.* **2003**, *125*, 15941.
(35) Duan, P. F.;Liu, M. H. *Langmuir **2009**, 25, 8706*.
(36) Paliwal, S.; Geib, S.; Wilcox, C. S. *J. Am. Chem. Soc.* **1994**, *116*, 4497.
(37) Mati, I. K.; Cockroft, S. L. *Chem. Soc. Rev.* **2010**, *39*, 4195.
(38) Zhao, C.; Parrish, R. M.; Smith, M. D.; Pellechia, P. J.; Sherrill, C. D.; Shimizu, K. D. *J. Am. Chem. Soc.* **2012**, *134*, 14306.
(39) Carroll, W. R.; Zhao, C.; Smith, M. D.; Pellechia, P. J.; Shimizu, K. D. *Org. Lett.* **2011**, *13*, 4320.
(40) Li, P.; Zhao, C.; Smith, M. D.; Shimizu, K. D. *J. Org. Chem.* **2013**, *78*, 5303.
(41) Carroll, W. R.; Pellechia, P.; Shimizu, K. D. *Org. Lett.* **2008**, *10*, 3547.
(42) Hobza, P.; Selzle, H. L.; Schlag, E. W. *J. Am. Chem. Soc.* **1994**, *116*, 3500.
(43) Sinnokrot, M. O.; Valeev, E. F.; Sherrill, C. D. *J. Am. Chem. Soc.* **2002**, *124*, 10887.
(44) Grimme, S. *Angew. Chem. Int. Ed.* **2008**, *47*, 3430.
(45) Hwang, J.; Li, P.; Carroll, W. R.; Smith, M. D.; Pellechia, P. J.; Shimizu, K. D. *J. Am. Chem. Soc.* **2014**, *136*, 14060.
(46) Gu, J. D.; Wang, J.; Leszczynski, J.; Xie, Y. M.; Schaefer, H. F. *Chem. Phys. Lett.* **2008**, *459*, 164.
(47) Calculated polarizabilities were used for the analysis because values for the molar refractivities (MR) of all of the aromatic arm surfaces were not available. The calculated polarizabilities were shown to linearly correlate with the MR for aromatic surfaces, which had literature MR values.
(48) Wheeler, S. E.; Houk, K. N. *J. Am. Chem. Soc.* **2008**, *130*, 10854.
(49) Sinnokrot, M. O.; Sherrill, C. D. *J. Phys. Chem. A* **2003**, *107*, 8377.
(50) Gung, B. W.; Patel, M.; Xue, X. W. *J. Org. Chem.* **2005**, *70*, 10532..
(51) The Hammett σ_{meta} parameter was used to characterize the ESE *meta*- and *para*-substituents. The reason is that the σ_{meta} parameter gives a 'purer' measure of the inductive electrostatic substituent effects. The σ_{para} parameter also includes resonance substituent effects. The *para*- and *meta*-substituent effects were differentiated based on the use of separate measured Hammett plots to characterize the magnitude of the ESEs.
(52) Cockroft, S. L.; Hunter, C. A.; Lawson, K. R.; Perkins, J.; Urch, C. J. *J. Am. Chem. Soc.* **2005**, *127*, 8594.
(53) Yang, L. ; Adam, C.; Nichol, G. S.; Cockroft, S. L. *Nat. Chem.* **2013**, *5*, 1006.
(54) Smithrud, D. B.; Diederich, F. *J. Am. Chem. Soc.* 1990, **112**, 339-343.
(55) Adam, C.; Yang, L. ; Cockroft, S. L. *Angew. Chem. Int. Ed.* **2015**, *54*, 1164
(56) Lima, C. F. R. A. C.; Rocha, M. A. A.; Gomes, L. R.; Low, J. N.; Silva, A. M. S.; Santos, L. M. N. B. F. *Chem. Eur. J.* **2012**, *18*, 8934.
(57) Bauer, M.; Bertario, A.; Boccardi, G.; Fontaine, X.; Rao, R.; Verrier, D. *J. Pharm. Biomed.* **1998**, *17*, 419.

CHAPTER 4

DISTANCE-DEPENDENT ATTRACTIVE AND REPULSIVE INTERACTIONS OF BULKY ALKYL GROUPS[3]

[3] Reproduced with permission from: Hwang, J.; Li, P.; Smith, M. D.; Shimizu, K. D. *Angew. Chem. Int. Et.* **2016**, DOI: 10.1002/anie.201602752. Copyright © 2016 John Wiley & Sons, Inc.

Large alkyl groups, such as, *tert*-butyl and adamantyl groups, are commonly incorporated into molecular systems to fix the conformational preference of flexible molecules[1,2] or to enhance the selectivity of chemical reactions[3-6] and catalysts.[7-9] In these applications, the influence of bulky alkyl groups is primarily ascribed to repulsive steric interactions.[10,11] However, recent theoretical and experimental studies have shown that bulky alkyl groups can also form stabilizing non-covalent interactions.[12-17] For example, the introduction of 12 *t*Bu groups on the periphery of hexaphenylethane appears to stabilize this kinetically unstable framework by the formation of attractive intramolecular dispersion interactions.[18-21] Another recent example showed that larger alkyl substituents, such as adamantyl and cyclohexyl groups, preferentially stabilize the *cis*-azobenzene conformer.[12]

In the course of studying the substituent effects of aromatic stacking interactions with our molecular balance model system, we observed that bulky alkyl groups displayed opposite stability trends when placed at different distances from the opposing aromatic rings (Figure 4.1). Alkyl groups of increasing size (Me, Et, *i*Pr, and *t*Bu) were introduced at the *meta*- and *para*-positions, and their influence on the stability of the intramolecular aromatic stacking interaction was measured. At the closer *meta*-position, the trend followed the conventional steric paradigm, as increasingly larger alkyl groups systematically destabilized the aromatic stacking interaction (Figure 4.1).[22-23] However, in the *para*-position, the opposite trend was observed, with larger alkyl groups stabilizing the aromatic stacking interaction. Thus, the goal of this study was to quantitatively measure these trends in solution and to study their origins using X-ray crystallography.

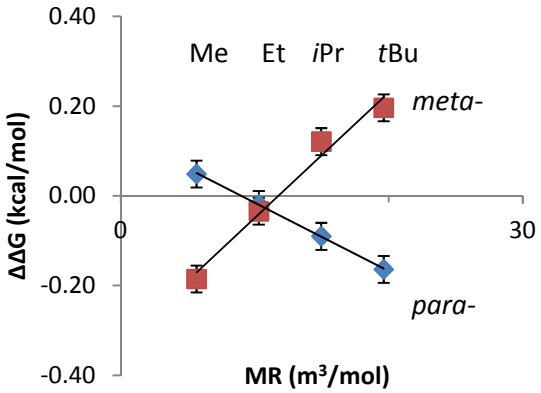

Figure 4.1 Correlation of the alkyl group (Me, Et, *i*Pr, *t*Bu from left to right) interaction energies (ΔΔG) measured in $CDCl_3$ (25 °C) for balances **1b-i** via the double mutant cycle analysis versus their molar refractivity substituent parameters

The influence of the alkyl groups were assessed from the *folded/unfolded* equilibrium ratios of molecular balances **1a-i** and control balances **2a-i** in solution (Figure 4.2). The phenyl ether arms of the balances were functionalized with alkyl substituents of varying size (H, Me, Et, *i*Pr, or *t*Bu) at the *meta*- or *para*-position. This bicyclic model system has been successfully employed to measure the stability trends,[24,25] the additivity of substituent effects,[26] and the dispersion contributions for off-set aromatic stacking interactions.[27] Because of restricted rotation of the N-arylimide rotor, the balances and control balances adopt two distinct conformational states. In the *folded* conformation, the aromatic surfaces of the substituted phenyl ether arms and phenanthrene shelves are held in a parallel geometry, thus forming an intramolecular stacking interaction. The off-set stacking geometry with the phenyl arm extending beyond the phenanthrene shelf was confirmed by X-ray, NMR, and modeling studies.[24,25] This stacking geometry positions the *meta*- and *para*-substituents on the phenyl ether arm at different distances from the phenanthrene shelf. In the *unfolded* conformation, the aromatic surfaces of the arm and shelf are far apart and cannot form an intramolecular interaction. Thus, the *unfolded-folded* conformational equilibrium provides a very

sensitive measure (±0.03 kcal/mol)[26] of the intramolecular stacking and substituent effects.

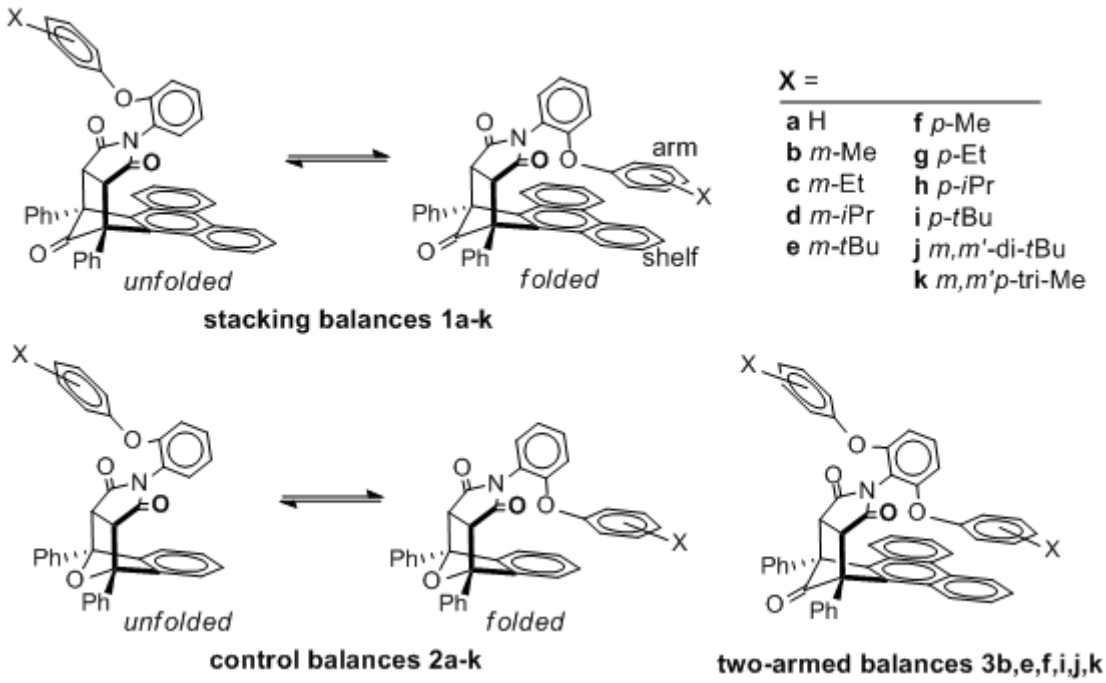

Figure 4.2 The *unfolded-folded* conformational equilibrium (top) of aromatic stacking molecular balances **1a-k** containing alkyl substituents of varying size and position (**a-k**), control balances **2a-k** (bottom left), which cannot form intramolecular stacking interactions, and two-armed balances **3** (bottom right), which were used in the X-ray crystallographic studies

Balances **1a-i** and control balances **2a-i** were prepared with different sized alkyl substituents at the *meta*- or *para*-positions of the phenyl ether arm. The *folded*/*unfolded* ratios in $CDCl_3$ (25 °C) were measured via integration of the ^1H NMR spectra. Folding energies (ΔG) were calculated from the folding ratios. The interaction energies ($\Delta\Delta G_x$) for each alkyl substituent **x** (where **x** is an alkyl substituent **b-i**) were isolated using a double mutant cycle (DMC) analysis (Figure 4.3).[28,29] The DMC required the ΔGs for four balances to measure each alkyl group interaction energy: $\Delta\Delta G_x = (\Delta G_{1x} - \Delta G_{2x}) - (\Delta G_{1a} - \Delta G_{2a})$. The DMC analysis subtracts out the effects of aromatic stacking, repulsive lone pair-π, dipole, and solvation effects on the folding ratios in **1x**. An initial analysis of

$\Delta\Delta G_x$'s showed a clear correlation with the size of the alkyl groups (Figure 4.1). The molecular descriptor molar refractivity (MR), was used to parameterize the size of the alkyl substituents **x**, as MR is closely correlated with molecular van der Waals (VDW) volumes, polarizabilities, and dispersion energies.[30-32] An excellent linear correlation was observed between MR and the alkyl group interaction energies ($\Delta\Delta G$) for the *meta*- or *para*-positions. Interestingly, the slopes of the linear regressions were opposite for the *meta*- and *para*-alkyl series. The *meta*-alkyl group trend followed the conventional paradigm where alkyl groups form repulsive steric interactions. The bulkiest *meta*-*t*Bu group was the most destabilizing (+0.20 kcal/mol) and each successively smaller alkyl group was less destabilizing. In contrast, in the *para*-position, the bulkiest *para*-*t*Bu group was the most stabilizing (-0.16 kcal/mol) and each successively smaller *para*-alkyl group was less stabilizing. Similar opposing trends of the *meta*- and *para*-alkyl substituents were observed in two additional solvents, bromobenzene-d_5 and acetone-d_6, thus suggesting that the trends in Figure 4.1 were not due to an artifact of solvent effects in chloroform.

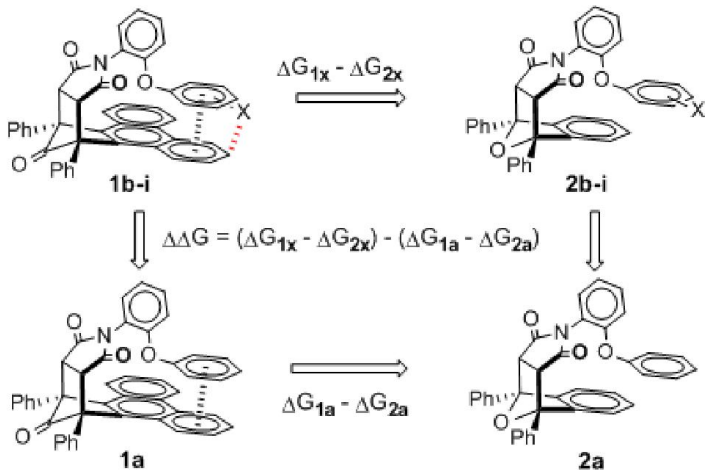

Figure 4.3 Double mutant cycle analysis isolating the alkyl group interaction energies in balances **1x** (**x** = alkyl substituents **b-i**) in the *folded* conformers. For each alkyl substituent, the analyses required ΔG values for four balances: **1x**, **2x**, **1a**, and **2a**.

X-ray structure analysis was used to study the origins of the substituent trends. Specifically, the relationship between the solution interaction energies and the solid-state geometries was investigated. Balances **1a-i** do not consistently crystallize in the *folded* conformation because of the destabilizing lone pair-π interactions of the ether oxygen.[24,33] Therefore, a series of two-armed balances (**3b, 3e, 3f,** and **3i**) were prepared. These balances had identical substituted phenyl arms at both *ortho*-positions of the N-arylimide rotors, ensuring that one phenyl ring would always be in the *folded* conformation. Two-armed balances with the smallest Me (**3b** and **3f**) and largest *t*Bu (**3e** and **3i**) substituents were crystallized and analyzed by X-ray crystallography. In each structure, the off-set aromatic stacking interaction was observed between one of the substituted phenyl arms and the phenanthrene shelf (Figure 4.4).[24,25] This confirmed that the alkyl substituents do not significantly change or disrupt the stacking interaction. Even in cases with a large *t*Bu group (**3e** and **3i**), the phenyl arm was roughly parallel and in close contact to an outer six-membered ring of the phenanthrene shelf.

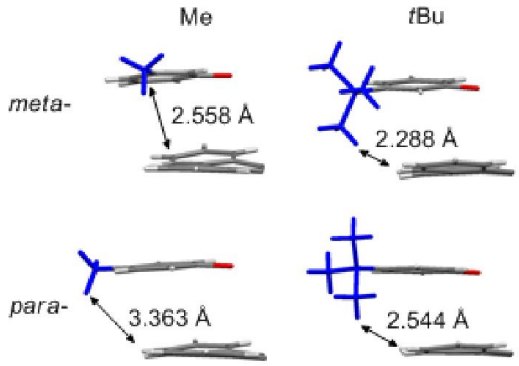

Figure 4.4 Side-views of the X-ray[35] crystal structures of the substituted phenyl arm and phenanthrene shelf surfaces which form an intramolecular aromatic off-set stacking interaction in two-armed molecular balances with *meta*-Me (**3b**), *meta*-*t*Bu (**3e**), *para*-Me (**3f**), and *para*-*t*Bu (**3i**) substituents. The other atoms were omitted for viewing clarity. The shortest H···H contacts between the alkyl substituent of the arm and the phenanthrene shelf are highlighted with double-headed arrows. For structures containing multiple crystallographically independent molecules and/or structural disorder (**3b**, **3f**, and **3i**), the structure with the shortest H···H contact distance is shown.

Surprisingly, the stabilizing *meta*-Me and *para*-*t*Bu groups did not form intramolecular CH-π interactions and instead were in close contact with the edge of the phenanthrene shelves. Similar stabilizing close H···H contacts (2.6 to 3.0 Å) have been observed in the stacked 2,5,8-tri-*tert*-butyl-phenalenyl dimer in the solid-state.[34] Therefore, the shortest H···H distances between each alkyl substituent and the phenanthrene shelf in the crystal structures were measured and compared with the corresponding solution alkyl group interaction energies (Figure 4.5 a). The H···H distances for the stabilizing substituents (*para*-*t*Bu and *meta*-Me) fell into a narrow intermediate range (2.5 to 3.0 Å). The destabilizing substituents fell outside this optimal distance. They were either too close (*meta*-*t*Bu < 2.5 Å), thus forming repulsive VDW interactions or were too far (*p*-Me > 3.0 Å) to form effective stabilizing interactions.

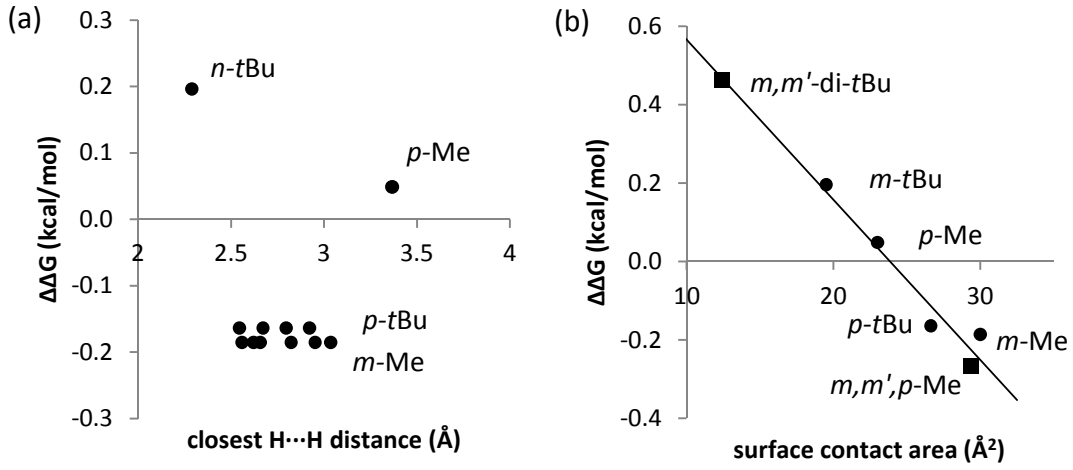

Figure 4.5 (a) Correlation of the alkyl group interaction energies (ΔΔG) in solution versus the observed shortest H···H distances (Å) between the alkyl substituent and aromatic shelf in X-ray crystal structures. In the cases where more than one crystallographically independent molecule and/or a structural disorder were observed, the shortest H···H contact for each structure was measured. (b) Correlation of the measured alkyl group interaction energies (ΔΔG) in solution with the surface contact area (SCA) of the arm-shelf stacking complexes calculated from the VDW surface areas of the X-ray structures. The units with the shortest H···H contact were chosen for SCA assessments.

The shape of the plot in Figure 4.5 a is similar to a Lennard-Jones potential. The position of the minimum (2.5 to 3.0 Å) is consistent with the other crystallographic database studies of optimal H···H distances for two hydrocarbon units.[36,37] However, the slopes of the energy well are much steeper than a conventional Lennard-Jones potential. This is likely due to the horizontal mobility of the substituted phenyl arm above the plane of the phenanthrene shelf that allows it to maximize its intramolecular interaction energy.[33] Thus, alkyl substituents forming repulsive interactions will shift to longer H···H distances to minimize these destabilizing interactions, and alkyl substituents that are too far apart to interact with the phenanthrene shelf can shift to shorter H···H distances to form stabilizing interactions.

An analysis of the contact areas of the interacting surfaces in the *folded* conformers of the X-ray structures provided evidence that the same forces were responsible for the opposing *meta*- and *para*-alkyl group interaction energy trends (Figure 4.5 b). The surface contact areas (SCAs) were calculated from the VDW surface areas of the interacting surfaces in the X-ray crystal structures. The SCA parameter was defined as the difference in VDW surface areas of the uncomplexed substituted phenyl arms and phenanthrene shelves and the corresponding stacking complex. An excellent linear correlation was found between the SCAs of the four substituted intramolecular stacking complexes (*meta*-Me, *meta*-*t*Bu, *para*-Me, *para*-*t*Bu) in the crystal structures and the alkyl group interaction energies measured in solution (Figure 4.5 b, circles). Thus, the similar stabilizing effects of the *para*-*t*Bu and *meta*-Me groups appear to be due to their optimal fit with the corresponding stacking complexes, thus yielding large SCAs. Conversely, the destabilizing interactions of the *meta*-*t*Bu and *para*-Me groups were due

to their poor fit as evident from their smaller SCAs in their stacking complexes. The SCAs provided an excellent predictive parameter for the attractive and repulsive substituent effects of the alkyl groups. For example, the linear correlation for the four mono-substituted balances (Figure 4.5 b, circles) accurately modeled two additional balances with multiple alkyl substituents (Figure 4.5 b, squares). The solid-state SCAs of the *meta,meta'*-di-*t*Bu (**3k**) and *meta,meta',para*-tri-Me (**3j**) balances were well correlated to the solution alkyl group interaction energies in the corresponding **1k** and **1j** balances.

In this study, alkyl groups were found to form stabilizing interactions through non-electrostatic mechanisms.[38-42] More interestingly, large and small alkyl groups were either stabilizing or destabilizing depending upon their position rather than size. For example in the *para*-position, the largest and bulkiest alkyl groups formed the strongest stabilizing interaction. This observation is consistent with the recent concept of dispersion energy donors in which bulky alkyl groups form stabilizing dispersion interactions.[17,20] However, we also observed the reverse trend at the *meta*-position, as smaller alkyl groups formed the most stabilizing interactions. An analysis of the common factors in these opposing trends found that the relative distances and VDW surface contact areas were excellent predictors for the alkyl group interaction energies. These position dependent stabilizing interactions of large and small alkyl groups extend the types of interactions that they can form beyond the conventional steric effects. Finally, we are currently studying the relative contributions of dispersion[45] and solvophobic effects[15] to these stabilizing alkyl group interactions in solution.

References

(1) Ikeda, A; Shinkai, S *Chem. Rev.* **1997**, *97*, 1713-1734.
(2) Bentrude, W. G.; Tan, H. W.; Yee, K. C. *J. Am. Chem. Soc.* **1975**, *97*, 573-582.
(3) Clayden, J; Worrall, C. P.; Moran, W. J.; Helliwell, M. *Angew. Chem.* **2008**, *120*, 3278-3281; *Angew. Chem. Int. Ed.* **2008**, *47*, 3234-3237.
(4) Nakamura, M.; Hirai, A.; Sogi, M.; Nakamura, E. *J. Am. Chem. Soc.* **1998**, *120*, 5846-5847.
(5) You, L.; Berman, J. S.; Lucksanawichien, A.; Anslyn, E. V. *J. Am. Chem. Soc.* **2012**, *134*, 7126-7134.
(6) Gunawan, M. A.; Hierso, J. C.; Poinsot, D.; Fokin, A. A.; Fokina, N. A.; Tkachenko, B. A.; Schreiner, P. R. *New J. Chem.* **2014**, *38*, 28-41.
(7) Nillson Lill, S. O.; Ryberg, P.; Rein, T.; Bennstrom, E.; Norrby, P. O. *Chem. Eur. J.* **2012**, *18*, 1640-1649.
(8) Foley, S. R.; Zhou, Y. L.; Yap, G. P. A.; Richeson, D. S. *Inorg. Chem.* **2000**, *39*, 924-929.
(9) Cogan, D. A.; Liu, G. C.; Kim, K. J.; Backes, B. J.; Ellman, J. A. *J. Am. Chem. Soc.* **1998**, *120*, 8011-8019.
(10) Charton, M. *Top. Curr. Chem.* **1983**, *114*, 57-91.
(11) Gallo, R. *Prog. Phys. Org. Chem.* **1983**, *14*, 115-163.
(12) Schweighauser, L.; Strauss, M. A.; Bellotto, S.; Wegner, H. A. *Angew. Chem.* **2015**, *127*, 13636-13639; *Angew. Chem. Int. Ed.* **2015**, *54*, 13436-13439.
(13) Wagner, J. P.; Schreiner, P. R. *Angew. Chem.* **2015**, *127*, 12446-12471; *Angew. Chem. Int. Ed.* **2015**, *54*, 12274-12296.
(14) Lyngvi, E.; Sanhueza, I. A.; Schoenebeck, F. *Organometallics* **2015**, *34*, 805-812.
(15) Yang, L.; Adam, C.; Nichol, G. S.; Cockroft, S. L. *Nat. Chem.* **2013**, *5*, 1006-1010.
(16) Sedov, I. A.; Solomonov, B. N. *J. Struct. Chem.* **2013**, *54*, 262-270.
(17) Grimme, S.; Huenerbein, R.; Ehrlich, S. *ChemPhysChem* **2011**, *12*, 1258-1261.
(18) Kahr, B; Vanengen, D.; Mislow, K. *J. Am. Chem. Soc.* **1986**, *108*, 8305-8307.
(19) Schreiner, P. R.; Chernish, L. V.; Gunchenko, P. A.; Tikhonchuk, E. Y.; Hausmann, H.; Serafin, M.; Schlecht, S.; Dahl, J. E. P.; Carlson, R. M. K.; Fokin, A. A. *Nature* **2011**, *477*, 308-311.
(20) Grimme, S.; Schreiner, P. R. *Angew. Chem.* **2011**, *123*, 12849-12853; *Angew. Chem. Int. Ed.* **2011**, *50*, 12639-12642.
(21) Fokin, A. A.; Chernish, L. V.; Gunchenko, P. A.; Tikhonchuk, E. Y.; Hausmann, H.; Serafin, M.; Dahl, J. E. P.; Carlson, R. M. K.; Schreiner, P. R. *J. Am. Chem. Soc.* **2012**, *134*, 13641-13650.
(22) Lund, H; Lund, V. *Acta Chem. Scand.* **1973**, *27*, 383-390.
(23) Lund, H. *Acta Chem. Scand.* **1973**, *27*, 391-395.
(24) Carroll, W. R.; Pellechia, P.; Shimizu, K. D. *Org. Lett.* **2008**, *10*, 3547-3550.
(25) Li, P.; Zhao, C.; Smith, M. D.; Shimizu, K. D. *J. Org. Chem.* **2013**, *78*, 5303-5313.

(26) Hwang, J; Li, P.; Carroll, W. R.; Smith, M. D.; Pellechia, P. J.; Shimizu, K. D. *J. Am. Chem. Soc.* **2014**, *136*, 14060-14067.
(27) Hwang, J.; Dial, B. E.; Li, P.; Kozik, M. E.; Smith, M. D.; Shimizu, K. D. *Chem. Sci.* **2015**, *6*, 4358-4364.
(28) Carter, P. J.; Winter, G.; Wilkinson, A. J.; Fersht, A. R. *Cell* **1984**, *38*, 835-840.
(29) Cockroft, S. L.; Hunter, C. A. *Chem. Soc. Rev.* **2007**, *36*, 172-188.
(30) Greaves, T. L.; Drummond, C. J. *Chem. Rev.* **2008**, *108*, 206-237.
(31) Charton, M.; Charton, B. I. *J. Org. Chem.* **1979**, *44*, 2284-2288.
(32) Pauling, L.; Pressman, D. *J. Am. Chem. Soc.* **1945**, *67*, 1003-1012.
(33) Nijamudheen, A.; Jose, D.; Shine, A.; Datta, A. *J. Phys. Chem. Lett.* **2012**, *3*, 1493-1496.
(34) Goto, K.; Kubo, T.; Yamamoto, K.; Nakasuji, K.; Sato, K.; Shiomi, D.; Takui, T.; Kubota, M.; Kobayashi, T.; Yakusi, K.; Ouyang, J. *J. Am. Chem. Soc.* **1999**, *121*, 1619-1620.
(35) CCDC 1469080 (3b), 1469085 (3e), 1469084 (3f), 1469082 (3i), 1469079 (3j), and 1469083 (3k) contain the supplementary crystallographic data for this paper. These data can be obtained free of charge from The Cambridge Crystallographic Data Centre.
(36) Echeverria, J.; Aullon, G.; Danovich, D.; Shaik, S.; Alvarez, S. *Nat. Chem.* **2011**, *3*, 323-330.
(37) Danovich, D.; Shaik, S.; Neese, F.; Echeverria, J.; Aullon, G.; Alvarez, S. *J. Chem. Theory Comput.* **2013**, *9*, 1977-1991.
(38) Hunter, C. A.; Sanders, J. K. M. *J. Am. Chem. Soc.* **1990**, *112*, 5525-5534.
(39) Cozzi, F.; Cinquini, M.; Annunziata, R.; Dwyer, T.; Siegel, J. S. *J. Am. Chem. Soc.* **1992**, *114*, 5729-5733.
(40) Hunter, C. A.; Lawson, K. R.; Perkins, J.; Urch, C. J. *J. Chem. Soc. Perkin Trans. 2* **2001**, 651-669.
(41) Gung, B. W.; Xue, X.; Reich, H. J. *J. Org. Chem.* **2005**, *70*, 3641-3644.
(42) Cozzi, F.; Annunziata, R.; Benaglia, M.; Cinquini, M.; Raimondi, L.; Baldridge, K. K.; Siegel, J. S. *Org. Biomol. Chem.* **2003**, *1*, 157-162.
(43) Cozzi, F.; Annunziata, R.; Benaglia, M.; Baldridge, K. K.; Aguirre, G.; Estrada, J.; Sritana-Anant, Y.; Siegel, J. S. *Phys. Chem. Chem. Phys.* **2008**, *10*, 2686-2694.
(44) Yang Y.; Brazier J. B; Hubbard T. A.; Rogers D. M.; Cockroft S. L., *Angew. Chem.* **2016**, *128*, 924-928; *Angew. Chem. Int. Ed.* **2016**, *55*, 912-916.

CHAPTER 5

EXPERIMENTAL COMPARISONS OF THE S-Π AND O-Π INTERACTIONS

The primary evidence for attractive sulfur-π interactions has come from statistical analyses of crystal structure databases that have shown close contacts between sulfur atoms and π-systems are observed with greater frequency than would be expected from simply statistical distributions.[1-4] For example, the sulfur atoms of cysteine or methionine residues were often observed in close contact with the aromatic ring of phenylalanine, tryptophan, or tyrosine residues in protein crystal structures.[1,2] The possible origins of favorable S-π contacts were proposed to be due to charge-transfer, enhanced dispersion, or favorable disulfide bond to aromatic ring interactions.[5] Charge-transfer interactions could arise from the unoccupied 3d orbitals on sulfur, which can function as an acceptor for the electrons in an adjacent π-system. Alternatively, the greater polarizability of sulfur atoms could result in enhanced dispersion interactions with aromatic carbons that are also more polarizable due to their extended π-systems. Finally, disulfide bonds have partial double bond character that could form attractive interactions. Computational studies have suggested that S-π interactions are mainly due to dispersion interactions.[6] For example, computational studies of H_2S with varying aromatic systems such as benzene,[7] indole,[8] naphthalene,[9] or azulene[10] found that dispersion interactions were the dominant stabilizing term followed by a smaller attractive electrostatic term. The exchange-repulsion component was the largest destabilizing term. In these studies,

the dominance of the dispersion interactions of S-π interactions was tested by comparisons of S-π and O-π interactions, which found larger differences in the dispersion component and relatively smaller differences in the electrostatic component. For example, in computational studies comparing of the interactions of H_2O-benzene and H_2S-benzene complexes found differences in dispersion and electrostatic energies of 1.03 kcal/mol and 0.59 kcal/mol.[7] In these computational studies, the dispersion term was always larger for the S-π interactions. However, even high level ab initio methods did not agree on whether the S-π or O-π interaction was the more stable.[9] Therefore, accurate calculations of S-π interactions are still challenging. Generally, computational studies of S-π interactions were carried out using small heterodimers to reduce computational cost, in which the sulfur atoms were connected to one or two hydrogen atoms.[7-10] This complicated the analyses as the optimized geometries often formed competing SH-π interactions where the acidic thiol hydrogen forms a hydrogen bond with the opposing π-system.[6,11,12]

Only a few experimental measurements of S-π interactions have been reported, and these studies have mainly focused on whether the S-π interactions form a stabilizing or destabilizing interaction in comparison to O-π interactions. In some experimental model systems, the S-π interactions were measured to be more stable than the O-π interactions, which was attributed to the stronger dispersion interactions of the more polarizable sulfur atoms.[13,14] However, other experimental studies found the opposite trend where S-π interactions were weaker than O-π interactions. These trends were attributed to the greater steric repulsion of the larger sulfur atoms.[15,16] Four experimental

model systems will be briefly discussed. The first two observed more stabilizing S-π interactions, and the last two observed the more stabilizing O-π interactions (Figure 5.1).

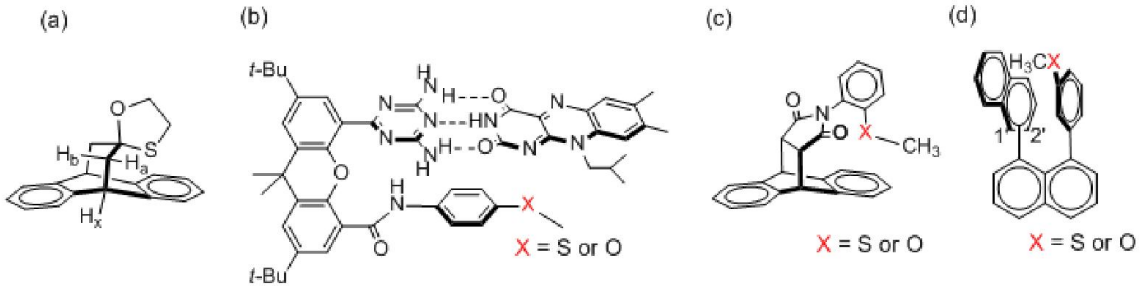

Figure 5.1 Model systems employed in previous experimental studies to compare S/O-π interactions

First, the study of a dibenzobicylo[3,2,2]nonane derivative (Figure 5.1 a) by Motherwell[14] measured the conformational ratio based on the coupling constants between H_x and H_a/H_b. The conformer that formed intramolecular S-π interactions was more stable by 2.9 kcal/mol than the O-π conformer. The preference for the S-π conformer was attributed to the greater polarizability of sulfur which formed stronger dispersion interactions. However, a couple of concerns in this study were: 1) only one example of this model system was studied and 2) the observed conformational preference could have alternatively been due to intermolecular solvent interactions with the sulfur and oxygen atoms. Rotello's experimental study involved H-bonding complexes of a flavin with a synthetic receptor (Figure 5.1 b). The differences in association constants of a series of receptors with different aryl substituents were measured via NMR titration.[13] Both methylthio and methoxy substituted receptors had larger association energies than the unsubstituted aromatic receptor by 5.0 kcal/mol and 4.5 kcal/mol, respectively. The slightly larger association energy of the methylthio substituted receptor was attributed to the greater polarizability of the sulfur atom. One concern was that the structure of the

intermolecular complex could change with the different substituents making the comparisons involve slightly different interaction geometries.

Cozzi's experimental studies of the N-aryl-3,4-(9',10'-dihydroanthracene-9',10'-diyl)succinimides with methylthio or methoxy groups (Figure 5.1 c) concluded that the differences in interaction energy were due to steric repulsion.[16] The conformational ratios measured via NMR indicated that the intramolecular S/O-π interactions were both unfavorable as the *exo*-conformers that could not form an intramolecular S-π or O-π interaction were found to be more stable. *Endo/exo*-ratios of 17:83 for the methylthio group and 21:79 for the methoxy group were measured. The smaller conformational ratio for the methylthio substituted model was attributed to the larger size and greater steric repulsion of the sulfur atom. Similar results were reported in Zoltewicz studies of the conformational preference of 1,8-diaryl naphthalenes (Figure 5.1 d).[15] The interacting naphthyl moiety was connected via the 1' or 2' position and formed close contacts with an adjacent OCH_3 or SCH_3 group substituted aryl groups. The methylthio group showed slightly less favorable S-π interactions (conformational ratios: 1.0 and 1.1) than the methoxy group's O-π interactions (conformational ratios: 1.2 and 1.3). Again, the conformational ratio differences were attributed to the greater steric repulsion of sulfur.

All of these previous experimental studies involve a small number of examples. This small data set was extremely limited with respect to the relative S-π interaction distances, geometry, electrostatics, and substituent groups, which might explain the discrepancies in their overall conclusions. Therefore, we embarked on a more comprehensive study which involved a much larger set of individual models (28 in total) which might provide a more complete picture of the S-π interaction.

As shown in Figure 5.2, we prepared 28 molecular balances that measure intramolecular S-π or O-π interaction strengths via their conformational ratios. Preparation of the 14 pairs of balances can help us understand how different variables influence the S/O-π interactions. Different substituents, aryl ring sizes, and interaction distances were employed. Varying R-groups were attached to the sulfur or oxygen atoms, eliminating the possibility of competing SH-π hydrogen bonding interactions. As in the previous experimental studies that compared S-π and O-π interactions, differences in the conformational ratios for each pair of S-π and O-π balances would indicate the existence of additional or enhanced forces contributing to the S-π interactions.

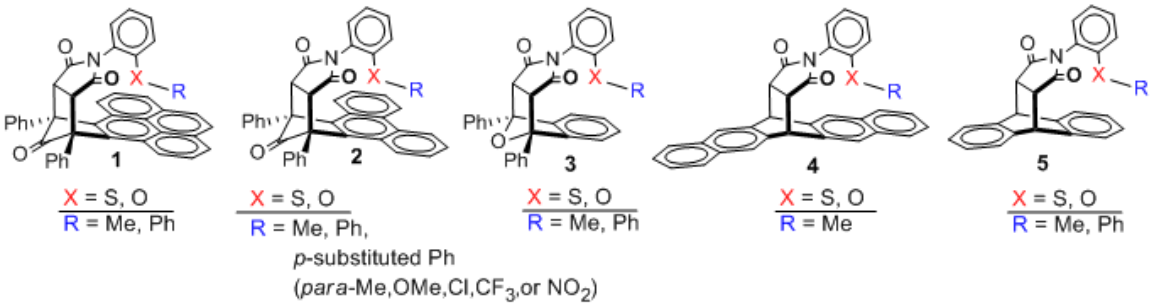

Figure 5.2 The 28 molecular balances used in our experimental comparison of S/O-π interactions

As shown in Table 5.1, all of the folding energies for the balances **1-5** were positive, which indicated that the *unfolded* conformers that could not form the intramolecular S/O-π interactions were the more stable. First, the impact of variations in the substituent (R) between phenyl and methyl was compared. As the $\Delta\Delta G_{Me\text{-}Ph}$ values in Table 5.2 showed, the differences in folding energies of the two R-groups were similar. Thus, the Me and Ph groups had an equal or similar impact on the S-π and O-π interactions. This suggests that the geometries of the S-π and O-π balances are similar despite the differences in size and bond lengths of the sulfur and oxygen.

Table 5.1 All of the folding energies ΔG (kcal/mol)[a] for the balances **1**-**5** .

	1		**2** (*p-substituent*)							**3**		**4**	**5**	
-X-\R	Me	Ph	Me	Ph	*Me*	*OMe*	*Cl*	*CF_3*	*NO_2*	Me	Ph	Me	Me	Ph
S	0.1	0.3	0.5	0.5	0.6	0.5	0.1	0.1	0.1	2.0	2.0	0.0	1.1	1.2
O	0.2	0.3	0.5	0.5	0.4	0.3	0.1	0.1	0.2	1.4	1.4	0.1	0.8	0.9

[a]in $CDCl_3$, at 298 K with an error < ±0.03 kcal/mol.

Table 5.2 Differences in the folding energies ($\Delta\Delta G_{Me-Ph}$)[a] of the same balance system with Me or Ph

-X-/balance	**1**	**2**	**3**	**4**
-S-	-0.12	0.01	0.04	-0.14
-O-	-0.10	-0.02	-0.02	-0.17

[a]$\Delta\Delta G$ (kcal/mol) = $\Delta G_{Me} - \Delta G_{Ph}$, in $CDCl_3$, at 298 K with < ±0.04 kcal/mol.

Second, the electrostatic effects were tested using balances **2** with different *para*-substituted SPh or OPh groups. As shown in Table 5.1, strong electron-withdrawing groups such as CF_3 and NO_2 had larger stabilizing effects on the S-π than the O-π interaction. Similarly, weak electron-donating groups also had a larger destabilizing effect on the S-π interactions. Thus, the S-π interaction was more sensitive to changes in electrostatics than the O-π interaction.

Third, the impact of the size of the aromatic surfaces was examined. As shown in Figure 5.3, the folding energies for both the S- and O-balances decreased as larger π-surfaces were introduced. With the exception of benzene that showed the significantly different folding energies for the S/O-π interactions, the other arenes showed similar folding energies for the both interactions. The greater stability of the O-benzene versus S-benzene interaction could be due to additional steric interactions in the S-benzene system due to the larger sulfur atoms. Why this steric difference between sulfur and oxygen was not also observed in the larger arene balances **1** and **2** is unclear. Possibly, the larger

arene surfaces could form more stabilizing dispersion interactions with the sulfur versus oxygen atoms that offset the steric differences. Alternatively, the R-groups on sulfur might be able to form stronger R-group to arene interactions.

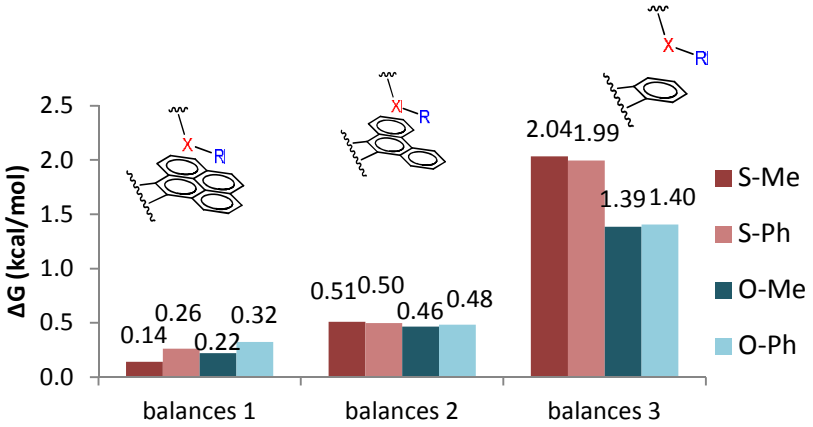

Figure 5.3 Comparisons of π-surface size impacts on the folding energies of balances **1**-**3**.

Lastly, the influences of the S-π and O-π distances were examined. The [2.2.2] bicyclic balances **5** showed lower folding energies than the [2.2.1] bicyclic balances **3** (Figure 5.4). The folding energy changes between the different bicyclic frameworks were larger for the S-balances. For example, the balances **3** and **5** with methyl group showed the folding energy differences 0.9 kcal/mol and 0.6 kcal/mol for the S-balances and the O-balances, respectively. Previous analyses of these two bicyclic frameworks showed different angles between the five membered imide ring and the π-surface in X-ray crystallographic structures.[17] The larger angle in the [2.2.2] bicyclic balances **5** (58˚) versus the [2.2.1] bicyclic balances **3** (52˚) positions the sulfur and oxygen atoms further from the π surface, decreasing steric repulsion, which seemed to have larger impacts on the S-π interactions.

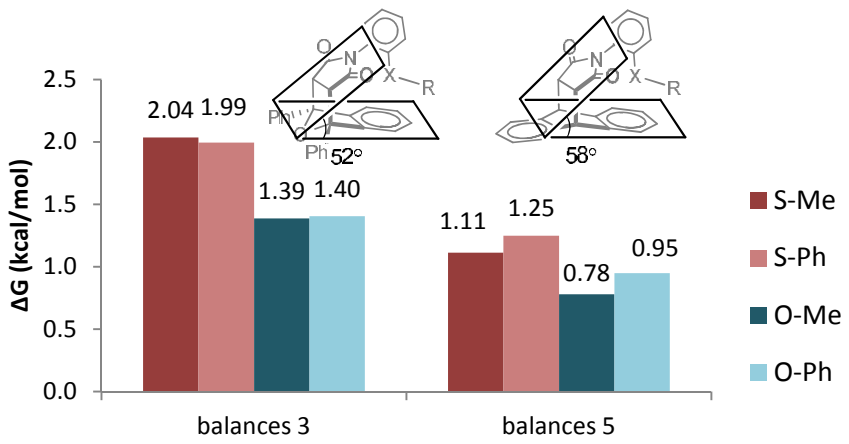

Figure 5.4 Comparisons of distance effects on the folding energies balances **3** and **5**

A general comparison between the 14 S-π and 14 O-π balances was made to test whether any of the above factors were uniquely responsible for the differences. This would be seen by outliers from the correlation plot corresponding to a particular type of balance. However, an excellent linear correlation was observed without any systematic deviations (Figure 5.5, red squares). To verify the quantitative correlations of the S-π and O-π interactions, we carried out the analysis in another solvent DMSO-d_6, which has different properties from chloroform (Figure 5.5, blue diamonds). Unlike chloroform that is a moderate hydrogen-bond donor, dimethylsulfoxide is a strong hydrogen-bond acceptor and is also considerably more polar.[18] The results in DMSO were in accordance with the chloroform solvent study as shown in Figure 5.5. A difference found in two solvents was that the folding energies were consistently smaller in the polar solvent. The trend lines with the same slope in the two solvents showed that the differences in the S/O-π interactions were not due to variations in the electrostatic interaction but presumably due to dispersion or/and solvophobic[19] interactions.

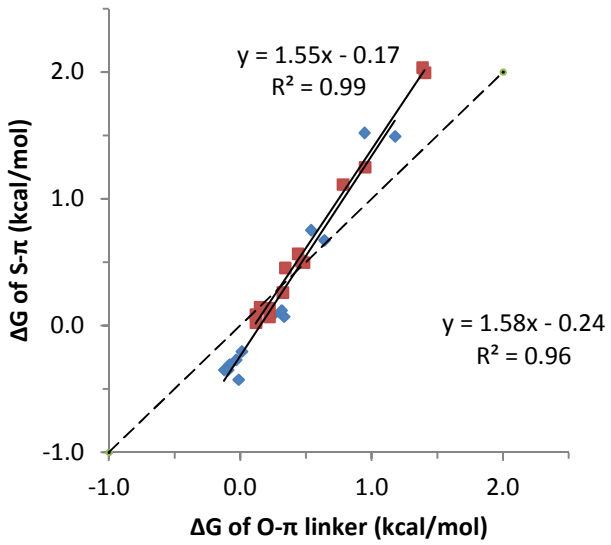

Figure 5.5 Correlations of the folding energies of the balances **1**-**5** in $CDCl_3$ (red squares) and DMSO-d_6 (blue diamond). The black dotted line Y = X indicates more stabilizing S-π interactions under the line and more destabilizing S-π interactions above the line.

While an excellent correlation was observed for all variables and correlations between the S- and O-balances, the slope of the correlation fit was greater than unity. Therefore, the balances on the upper of the plot had lower O-balance folding energies than S-balance folding energies. The number of the O-balance with relatively lower folding energies decreased as the solvent became polar. This could be attributed to larger solvophobic effects for the S-π interactions.

Intramolecular contact distances for the S/O-π interactions were compared via X-ray crystallographic structures to find whether differences in the close contacts in the *folded* conformers could be correlated with the folding energy trend observed in solution. The crystal were prepared from two-armed balances to ensure that one of two arms always forms a *folded* conformational geometry, except balance crystal **1** with Me group due to difficulty in synthesis. However, we previously showed that the intermolecular interaction geometries in two-armed and one-armed balance crystal structures were

similar.[20] We found surprisingly short S···C distances, which were smaller their van der Waals radii (3.5 Å).[21] As shown in Figure 5.6, all of three crystal structures forming the S-arene interactions showed shorter intramolecular distances than the structures forming the O-arene interactions by 0.16-0.30 Å. The short S···C distances could be indicative of stronger dispersion interactions in the interactions of the sulfur atoms.

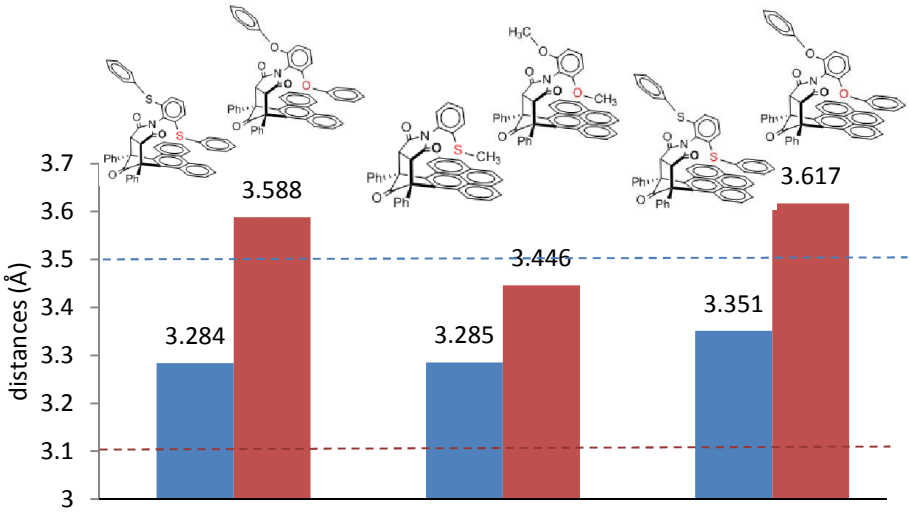

Figure 5.6 Three pairs of the S-balance (blue bars) and O-balance (red bars) crystal structures of **1** and **2** with their shortest intramolecular distance. The red and blue dotted lines show the van der Waals radii of O···C and S···C, respectively.

In summary, we prepared 14 pairs of S/O-molecular balances that compared how substituent effects, π-surfaces, and interaction frameworks impact the S/O-π interactions. The methyl and phenyl group impacts were almost the same in the both S-π and O-π interactions. However, the electrostatic substituent effects with electron-donating to –withdrawing characters showed variations in the S/O-π interaction strengths suggesting that there is an electrostatic component to the S-π interaction. With increasing π-surface size, the S/O-π interactions were generally stabilized. Distance effects were observed via comparison of the [2.2.1] bicyclic and [2.2.2] bicyclic systems for the balances **3** and **5**,

which showed more significant effects for the S-π interactions. This might be due to longer intramolecular interaction distances that greatly reduced steric repulsion of sulfur atoms. The strong correlation between the S-π and O-π interactions clearly showed that the strengths of the S-π interactions were more sensitive to changes in sterics and electrostatics. Since the same correlations of the S-π and O-π interactions were observed in different solvents, the interaction differences in the S-π interactions were presumably due to differences in dispersion and steric interactions and not due to different solvent or solvophobic effects. The solid-state studies found closer contacts in the S-π interactions than in the O-π, which might be due to larger dispersion interactions of sulfur atoms.

References

(1) Morgan, R. S.; Mcadon, J. M. *Int. J. Pept. Prot. Res.* **1980**, *15*, 177.
(2) Warme, P. K.; Morgan, R. S. *J. Mol. Biol.* **1978**, *118*, 289.
(3) Zauhar, R. J.; Colbert, C. L.; Morgan, R. S.; Welsh, W. J. *Biopolymers* **2000**, *53*, 233.
(4) Reid, K. S. C.; Lindley, P. F.; Thornton, J. M. *Febs. Lett.* **1985**, *190*, 209.
(5) Morgan, R. S.; Tatsch, C. E.; Gushard, R. H.; Mcadon, J. M.; Warme, P. K. *Int. J. Pept. Prot. Res.* **1978**, *11*, 209.
(6) Duan, G. L.; Smith, V. H.; Weaver, D. F. *Mol. Phys.* **2001**, *99*, 1689.
(7) Crittenden, D. L. *J. Phys. Chem. A* **2009**, *113*, 1663.
(8) Biswal, H. S.; Wategaonkar, S. *J. Phys. Chem. A* **2009**, *113*, 12774.
(9) Cabaleiro-Lago, E. A.; Rodriguez-Otero, J.; Pena-Gallego, A. *J. Phys. Chem. A* **2008**, *112*, 6344.
(10) Cabaleiro-Lago, E. M.; Rodriguez-Otero, J.; Pena-Gallego, A. *J. Chem. Phys.* **2008**, *129*.
(11) Hussain, H. B.; Wilson, K. A.; Wetmore, S. D. *Aust. J. Chem.* **2015**, *68*, 385.
(12) Tauer, T. P.; Derrick, M. E.; Sherrill, C. D. *J. Phys. Chem. A* **2005**, *109*, 191.
(13) Breinlinger, E. C.; Keenan, C. J.; Rotello, V. M. *J. Am. Chem. Soc.* **1998**, *120*, 8606.
(14) Motherwell, W. B.; Moise, J.; Aliev, A. E.; Nic, M.; Coles, S. J.; Horton, P. N.; Hursthouse, M. B.; Chessari, G.; Hunter, C. A.; Vinter, J. G. *Angew. Chem. Int. Ed.* **2007**, *46*, 7823.
(15) Lavieri, S.; Zoltewicz, J. A. *J. Org. Chem.* **2001**, *66*, 7227.
(16) Raimondi, L.; Benaglia, M.; Cozzi, F. *Eur. J. Org. Chem.* **2014**, 4993.
(17) Zhao, C.; Parrish, R. M.; Smith, M. D.; Pellechia, P. J.; Sherrill, C. D.; Shimizu, K. D. *J. Am. Chem. Soc.* **2012**, *134*, 14306.
(18) Hunter, C. A. *Angew. Chem. Int. Ed.* **2004**, *43*, 5310.
(19) Tatko, C. D.; Waters, M. L. *Protein Sci.* **2004**, *13*, 2515.
(20) Li, P.; Zhao, C.; Smith, M. D.; Shimizu, K. D. *J. Org. Chem.* **2013**, *78*, 5303.
(21) Morgado, C. A.; McNamara, J. P.; Hillier, I. H.; Burton, N. A. *J. Chem. Theory. Comput.* **2007**, *3*, 1656.

CHAPTER 6

TESTING THE DIRECT SUBSTITUENT EFFECT MODEL OF AROMATIC STACKING INTERACTIONS

The goal of this study was to experimentally test the recently proposed direct substituent effect model of aromatic stacking interactions. This model was developed by Wheeler and Houk to describe the substituent effects (SEs).[1] The model postulated that the interaction energy changes upon introducing substituents are governed by the direct interactions of the substituent with the opposing aromatic surface and not by indirect electrostatic polarization by the substituent of the attached π-surface as previously proposed by Hunter and Sanders[2] and Cozzi and Siegel.[3] Wheeler and Houk compared the SE's from 24 substituted stacked benzene dimers (Figure 6.1 a) and found the same energy trend with and without the benzene ring attached to the substituent. This seems to rule out the possibility that the SEs were due to the substituents polarizing the attached aromatic ring. Later, Sherrill computationally confirmed that the substituent effects are mostly due to these direct substituent-arene interactions using the F-SAPT computational method.[4,5]

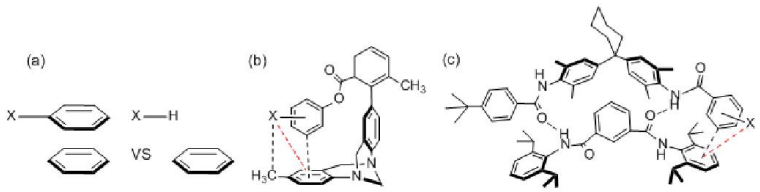

Figure 6.1 (a) Wheeler and Houk's computational models to prove the significance of direct substituent-arene interactions. (b) Wilcox's experimental model system. (c) Hunter's experimental model system. In two experimental model systems, red dotted lines indicate direct substituent-arene interactions, and black dotted lines indicate other interactions.

Previously, we provided indirect experimental evidence for the direct SE model by demonstrating the additivity of the substituent effects in our aromatic stacking balances.[6] While it is relatively simple to measure SEs with and without π-system in computational studies, it is far more challenging to conduct the same study experimentally. Specifically, the substituents without the attached aromatic stacking ring must somehow be covalently connected to the balance framework. Furthermore, the analysis must also take into account other factors that the substituents might influence such as secondary interactions or supporting interactions.

Possible examples of model systems that could be used to form and measure direct substituent-arene interactions include the edge-to-face arene-arene model system by Wilcox (Figure 6.1 b)[9] and Hunter (Figure 6.1 c)[11]. However, both model systems form additional interactions such as aryl CH-π interactions, methyl-substituent interactions, or framework effects which could have their own SEs. Since both of these studies were designed to study edge-to-face interactions of the perpendicular top ring, there were no control model systems to examine the contributions of these additional interactions.

Herein, we designed a series of molecular balances that form direct substituent-arene interactions without the accompanying aromatic stacking interactions. The three goals of this study were: 1) to measure the direct substituent-arene interactions in a system that cannot form aromatic stacking interactions; 2) to verify whether electrostatic interactions play a major role in the substituent-arene interactions by testing their correlation with the electrostatic Hammett σ_m parameter; 3) to find whether the dispersion contributions to the substituent effects are observable.

Three series of balances (**1**-**3**) were prepared as shown in Figure 6.2. Balances **1** have a substituent X that can form a direct substituent-arene interaction with the benzene shelf in the *folded* conformation. The strength of the substituent-arene interactions were monitored via their influence on the *folded/unfolded* conformational ratios. To help remove the other influences on the folding energy differences for balances **1,** control balances **2** and **3** were prepared, and their folding energies were measured. Control balances **2** and **3** measured the methyl CH-arene interactions, aryl CH-arene interactions, and framework effects in the folding energies of balances **1**. Control balances **2** had the same substituents but at different positions as balances **1** and could not form direct substituent-arene interactions. Therefore, the folding energy differences in balances **2** show the magnitude of the substituent effects for the methyl CH-arene and aryl edge-to-face interaction in balances **1**. The second control balances **3** had the same substituents at the same position as balances **1** but lacked an opposing phenyl surface. Therefore, the folding energies of control balances **3** show the significance of solvent interactions and dipole effects in the absence of the intermolecular interactions.

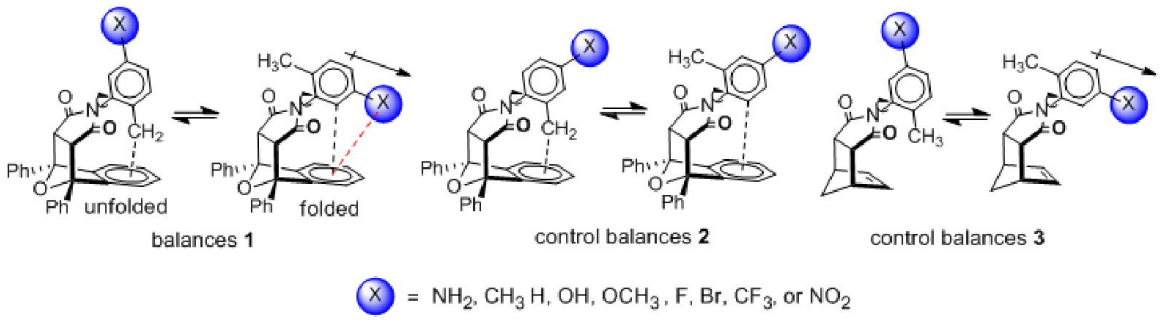

Figure 6.2 Balances **1**, **2**, and **3** with nine substituents. A red dotted line indicates direct substituent-π interactions, and black dotted lines indicate other interactions that may affect the folding energies of the balances.

All of the balances had an *ortho*-methyl group on the rotor ring to slow C_{aryl}-N_{imide} bond rotation at room temperature. Any potential contributions from the CH-arene

interactions of the methyl group in the unfolded conformation of balances **1** were measured using control balances **2**. For all three balances, nine substituents were used which ranged from strongly electron-donating to strongly electron-withdrawing groups to test the significance of electrostatic interactions in the direct substituent-arene interactions.

The measured negative folding energies (-ΔG) are shown in Table 6.1. The -ΔG values for balances **1** and **2** were of similar magnitudes (~ 0.8 kcal/mol) in contrast to the near zero folding energies of balances **3**. This demonstrated that the CH_3–phenyl interactions in the *unfolded* conformations of balances **1** and **2** were sterically repulsive and destabilized the *unfolded* conformer. Thus, for all nine substituents, the -ΔG values for balances **1** were all positive and spanned a 0.24 kcal/mol range. In contrast, the folding energies of control balances **2** and **3** were fairly constant and spanned a small range of 0.09 kcal/mol and 0.08 kcal/mol, respectively. The minimal variations in the folding energies of the control balances indicated the significance of the direct substituent-arene interactions in balances **1**. One concern was that the larger variations in -ΔG for balances **1** could also be due to substituent effects on the CH_3-π interactions. However, this possibility could be discounted based on two observations. First, if the resonance effects on CH_3 were significant, the opposite SE trend would have been observed in balances **1** as electron-withdrawing groups should stabilize the CH-π interactions in the *unfolded* conformation leading to smaller -ΔG values. Instead, the opposite trend was observed. Second, if the SEs on the CH-π interactions were significant, they would have been also observed for control balances **2**. However, control

balances **2** showed very little variation with different substituents and no general trend with respect to the electron-donating or –withdrawing character of the substituents.

Table 6.1 Negative folding energies (kcal/mol) of balances **1**, **2**, and **3**.

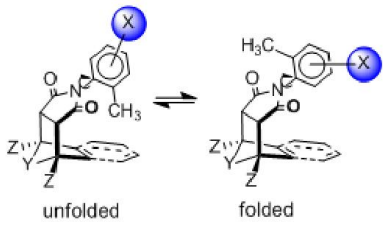

substituent **X**	$-\Delta G_{\text{balance 1}}$ [a]	$-\Delta G_{\text{control balance 2}}$ [a]	$-\Delta G_{\text{control balance 3}}$ [a]
NH_2	0.85	0.80	0.04
CH_3	0.89	0.89	0.05
H	0.84	0.84	0.02
OH	0.90	0.82	0.05
OCH_3	1.05	0.83	0.00
F	0.97	0.84	0.05
Br	0.95	0.83	0.06
CF_3	1.06	0.84	-0.02
NO_2	1.08	0.81	0.03

[a]298 K, $CDCl_3$, with an error less than ±0.03 kcal/mol.

Next, the significance of the electrostatic contributions to the direct substituent-arene interactions was examined by correlating the folding energies with the electrostatic Hammett σ_m parameters. As shown in Figure 6.3 a, a significant slope was only observed for the folding energies of balance **1**. This is consistent with the computational studies which found that the direct substituent-arene interactions can be qualitatively predicted based on their Hammett parameters.[1] Other influences such as substituent effects on the

CH_3-π interactions, dipole, or framework effects showed no variation with the electrostatic parameters as seen by the near zero slopes of control balances **2** and **3**.

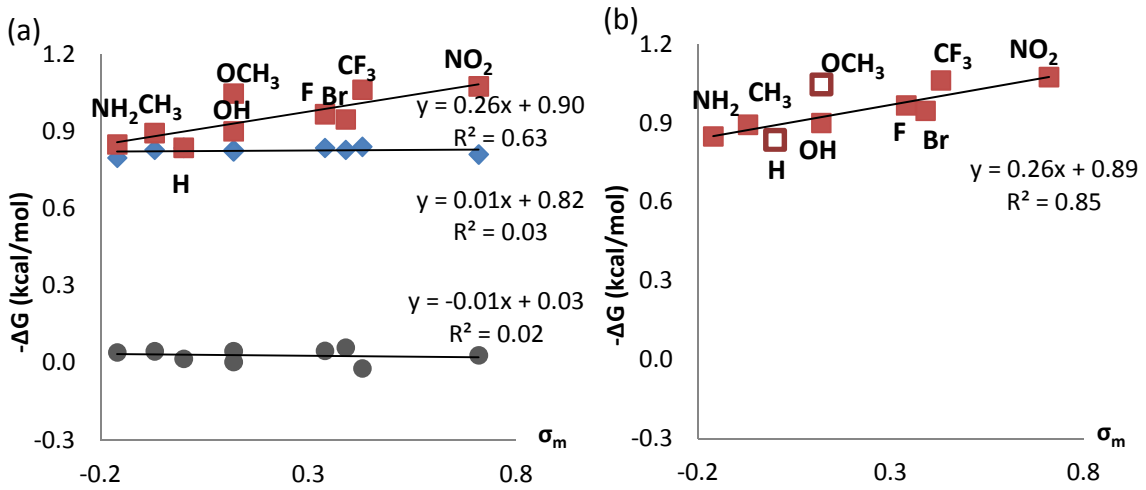

Figure 6.3 (a) Correlations of the folding energies of balances **1** (red square), **2** (blue diamond), and **3** (gray circle) with Hammett σ_m parameters. (b) A correlation of the folding energies of balance **1** and Hammett σ_m parameters without H and OCH_3 group.

The relatively poor linear fit of the nine balance **1**'s can be explained by the varying contributions of dispersion interactions of the substituents. For example, Wheeler and Houk excluded the unsubstituted arene (X = H) from their Hammett analysis because the smaller hydrogen atom formed significantly weaker dispersion interactions compared to the other non-H substituents in their computational study.[1] Another substituent that can form unusually strong or weak dispersion interactions was OCH_3 group. This can be seen by the different folding energies of the OH and OCH_3 groups that have the same Hammett σ_m values. The higher -ΔG value for the OCH_3 group was attributed to greater stabilizing dispersion effects of the larger OCH_3 group. Thus, the data points for the H and OCH_3 groups were removed from the Hammett correlation, which improved the fit to $R^2 = 0.85$ (Figure 6.3 b).

Perhaps the closest comparison to the current study was Diederich's studies using the Troger's base torsion balances. This study had longer substituent-arene distances and eliminated competing SEs of the secondary CH-π interactions using multiple control balances and a DMC analysis. The folding energies of the CF_3 and F groups measured in the Diederich's studies were different by 0.15 kcal/mol, with the CF_3 forming the stronger interactions.[7] Our results also showed stronger CF_3–arene interactions than F-arene interactions by a similar 0.10 kcal/mol.

Next, we examined the structures of balances **1** and **2** via X-ray crystallography (Figure 6.4 a).[8] The aryl carbon attached to the substituents in balances **1** was positioned over the edge of the benzene shelf. This positioned the substituents slightly past the hydrogens on the edge of the benzene shelf, which was very similar to the position of the substituents in Wheeler and Houk's studies. The more distant substituent position in balances **2** was also confirmed to not be able to form a direct substituent-arene interaction in either conformation.

Analysis of the distances in our model system versus previous aromatic stacking models found farther distances. For example, the centroid-centroid distances between the substituted phenyl rotor ring and the phenyl shelf ring ranged 4.98 Å - 5.31 Å, which were slightly longer than the distances found Wilcox's edge-to-face balances (4.95 Å and 5.09 Å).[9] They were also significantly longer than the centroid to centroid distances for off-set face-to-face stacking balances 3.8 Å (Figure 6.4 b).[10] These larger distances help explain the smaller slope of the Hammett plot in our balance system (0.26 kcal/mol) than in our off-set face-to-face balances which had Hammett slopes of 0.55 to 0.95 kcal/mol.[6]

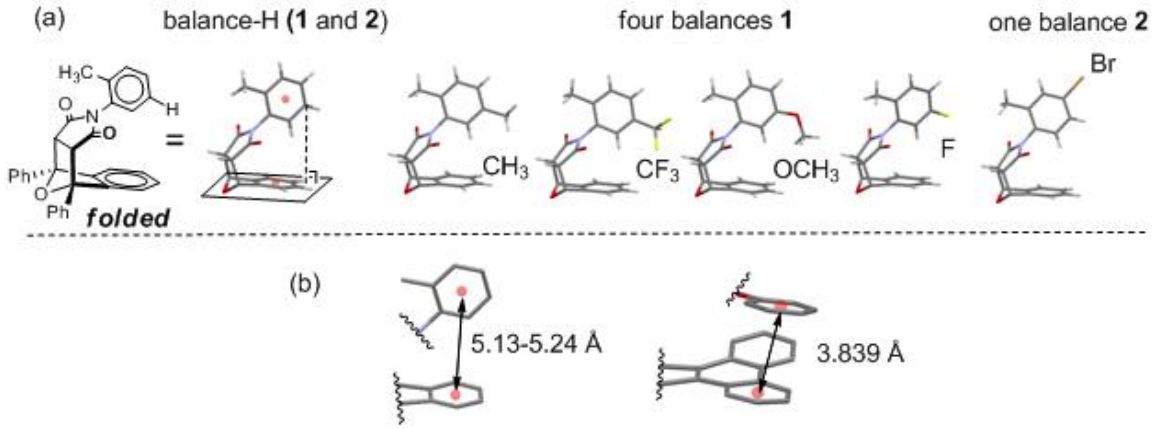

Figure 6.4 (a) Crystal structures of balances **1** and control **2**. The very left ChemDraw structure is equivalent to the crystal structure of *folded* unsubstituted (H) balance **1** (**2**) where two phenyl wings are omitted for viewing clarity, and four substituted balances **1** and one substituted balance **2** are shown. (b) Comparison of intramolecular centroid-centroid distances in the crystal structures of the unsubstituted balance **1** (left) and the aromatic stacking balance in our previous study (right).

In summary, we experimentally measured the direct substituent-arene interactions in systems that cannot form substituent polarized arene-arene interactions. Three series of balances **1**, **2**, and **3** were prepared to quantify direct substituent-arene interactions as well as other influences in the molecular balances. Balances **1** that could form direct substituent-arene interactions showed significant folding energy changes while control balances **2**, and **3** showed little change in their folding energies. Thus, the folding energy changes of balances **1** provided a direct measure of the direct substituent-arene interactions. The linear Hammett σ_m correlation of the folding energies of balances **1** showed significant electrostatic contributions in the substituent-arene interactions. Although the magnitudes were small, ranging 0.24 kcal/mol, this study showed the significant direct substituent-arene interactions that were primarily due to electrostatic interactions. In addition, dispersion seemed to play a minor but measurable role because balances **1** with H showed the lowest folding energy and OCH_3 group formed a

significantly stronger interaction than OH despite their similar electrostatic Hammett parameter.

Refereces

(1) Wheeler, S. E.; Houk, K. N. *J. Am. Chem. Soc.* **2008**, *130*, 10854.
(2) Hunter, C. A.; Sanders, J. K. M. *J. Am. Chem. Soc.* **1990**, *112*, 5525.
(3) Cozzi, F.; Cinquini, M.; Annunziata, R.; Dwyer, T.; Siegel, J. S. *J. Am. Chem. Soc.* **1992**, *114*, 5729.
(4) Parrish, R. M.; Sherrill, C. D. *J. Am. Chem. Soc.* **2014**, *136*, 17386.
(5) Parrish, R. M.; Parker, T. M.; Sherrill, C. D. *J. Chem. Theory. Comput.* **2014**, *10*, 4417.
(6) Hwang, J.; Li, P.; Carroll, W. R.; Smith, M. D.; Pellechia, P. J.; Shimizu, K. D. *J. Am. Chem. Soc.* **2014**, *136*, 14060.
(7) Gardarsson, H.; Schweizer, W. B.; Trapp, N.; Diederich, F. *Chem. Eur. J.* **2014**, *20*, 4608.
(8) Li, P.; Hwang, J.; Maier, J. M.; Zhao, C.; Kaborda, D. V.; Smith, M. D.; Pellechia, P. J.; Shimizu, K. D. *Cryst. Growth. Des.* **2015**, *15*, 3561.
(9) Paliwal, S.; Geib, S.; Wilcox, C. S. *J. Am. Chem. Soc.* **1994**, *116*, 4497.
(10) Carroll, W. R.; Pellechia, P.; Shimizu, K. D. *Org. Lett.* **2008**, *10*, 3547.
(11) Carver, F. J.; Hunter, C. A.; Livingstone, D. J.; McCabe, J. F.; Seward, E. M. *Chem. Eur. J.* **2002**, *8*, 2847.

APPENDIX A - SUPPORTING INFORMATION

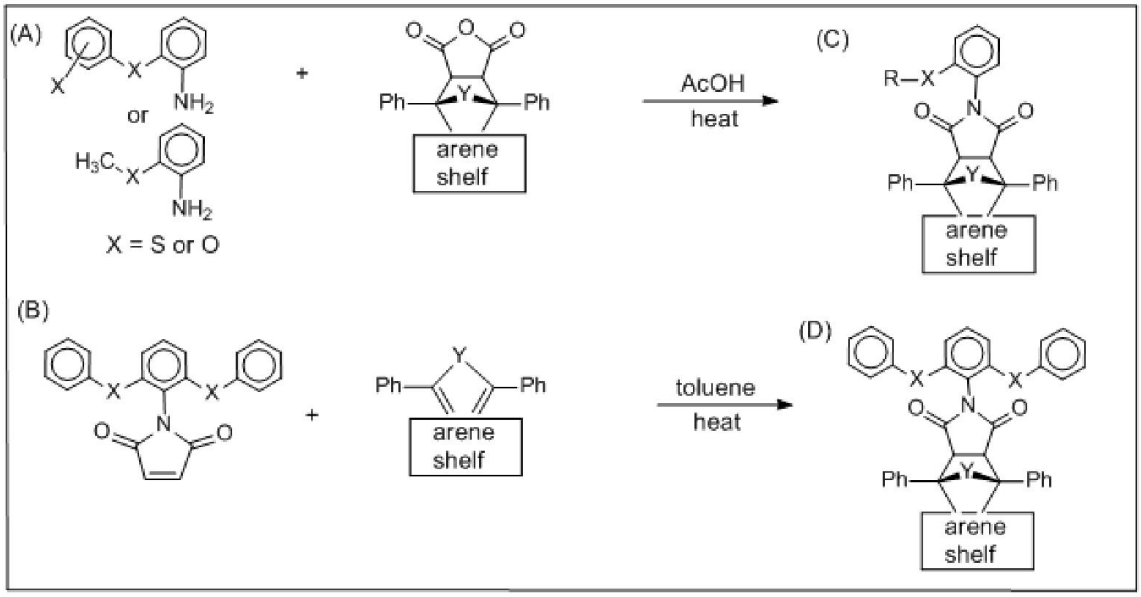

Scheme 1. Overview of synthetic procedure of S- and O-balances.

Preparation of (A) from its corresponding nitrophenyl ether and NMR data for (A)

2-(4-Chlorophenoxy)aniline: the nitrophenyl ether (0.77 g, 3.1 mmol) and $SnCl_2$ $2H_2O$ (5.4 g, 24 mmol) in 10 mL of hydrochloric acid and 10 mL of CH_3OH were refluxed for 15 min. 1M NaOH (aq) was added until the reaction mixture became basic (pH > 9). The product was extracted with EtOAc (20 mL x 2) and then washed with water (50 mL x 3). The crude product was purified by flash chromatography using silica gel (EtOAc:hex 1:4). The product was obtained as a brown liquid (0.48 g, 71%). ^{1}H NMR (400 MHz $CDCl_3$) δ 7.26 (dd, J_1 = 9.2, J_2 = 0.8 Hz, 2H), 7.04-6.99 (m, 1H), 6.91 (dd, J_1 = 9.2 Hz, J_2 = 0.8 Hz, 2H), 6.87 (ddd, J_1 = 8.0 Hz, J_2 = 1.2 Hz, J_3 = 1.2 Hz, 1H), 6.83 (dd, J_1 = 8.0 Hz, J_2 = 1.2 Hz, 1H), 6.72-6.76 (m, 1H), 3.79 (br, 2H).

2-(3-Chlorophenoxy)aniline: the nitrophenyl ether (0.99 g, 4.0 mmol) and $SnCl_2$ $2H_2O$ (5.4 g, 24 mmol) were used. The product was obtained as a brown liquid (0.41 g, 45%). ^{1}H NMR (400 MHz $CDCl_3$) δ 7.65 (dd, J_1 = 8.0 Hz, J_2 = 1.2 Hz, 1H), 7.27 (dd, J_1 = 8.0 Hz, J_2 = 8.0 Hz, 1H), 7.17-7.06 (m, 4H), 6.88 (dd, J_1 = 8.0 Hz, J_2 = 8.0 Hz, 1H), 6.71 (d, J = 8.0 Hz, 1H), 3.30 (br, 2H).

2-(3,5-Dichlorophenoxy)aniline: the nitrophenyl ether (0.77 g, 2.7 mmol) and $SnCl_2$ $2H_2O$ (3.1, 14 mmol) were used. The product was a yellow liquid (0.25 g, 36%). 1H NMR (400 MHz, CDCl3) δ 7.07-8.05 (m, 2H), 6.93 (d, J = 8.0 Hz, 1H), 6.88-6.87 (m, 2H), 6.84 (dd, J1 = 8.0 Hz, J2 = 1.3 Hz, 1H), 6.80-6.75 (m, 1H), 3.74 (br, 2H).

2-(3,4-Dichlorophenoxy)aniline: the nitrophenyl ether (0.97 g, 3.4 mmol) and $SnCl_2{\cdot}2H_2O$ (3.9 g, 17 mmol) were used. The product was a brown liquid (0.34 g, 40%). ^{1}H NMR (400 MHz, $CDCl_3$) δ 7.34 (d, J = 8.8 Hz, 1H), 7.07-7.02 (m, 2H), 6.89 (d, J = 7.6 Hz, 1H), 6.85-6.81 (m, 2H), 6.78-6.72 (m, 1H), 3.73 (br, 2H).

Preparation and NMR data of (B)

1-(2,6-Bis(phenylthio)phenyl)-1*H*-pyrrole-2,5-dione: 2,6-Bis(phenylthio)aniline (2.2 g, 7.1 mmol) and maleic anhydride (0.70 g, 7.1 mmol) in 5mL of AcOH were heated at reflux for 1d. After AcOH was removed under reduced pressure, 50 mL of ethyl acetate was added. The organic solution was washed with water (50 mL x 3). The crude product was purified by flash chromatography using silica gel (EtOAc:hex 1:4). The product was obtained as a yellow solid (1.2 g, 43%). ^{1}H NMR (400 MHz, $CDCl_3$) δ 7.41-7.28 (m, 10H), 7.15 (dd, J_1 = 8.4 Hz, J_2 = 7.2 Hz, 1H), 7.04 (d, J = 7.8 Hz, 2H), 6.84 (s, 2H). ^{13}C NMR (100 MHz, $CDCl_3$) δ 168.6, 139.3, 134.2, 133.0, 132.9, 130.4, 129.5, 129.3, 129.2, 128.1. HRMS (EI) Calcd for $C_{22}H_{15}NO_2S_2$: 389.0544; found: 389.0545.

Preparation and NMR data of (C)

One of a hydride among benzene, pheananthrene, and pyrene anhydrides, was dissolved in 5 mL acetic acid, and the reaction mixture was heated at 110℃ for 1 d. After the solvent was removed under reduced pressure, the residue was dissolved in 30 mL of EtOAc and washed with water (40 mL x 3) using saturated sodium bicarbonate and brine. The organic layer was obtained and the solvent of the organic layer was removed under reduced pressure. The crude product was washed with CH_3OH. The product was obtained as an off-white solid (0.064 g, 73%).

A pyrene anhydride (0.070 g, 0.14 mmol) and 2-(methylthio)aniline (26 μL, 0.21 mmol) were were ^{1}H NMR (400 MHz, $CDCl_3$) δ 8.50-8.44 (m, 2H), 8.10 (d, J = 7.6 Hz, major 2H), 8.06 (d, J = 7.6 Hz, minor 2H), 8.04 (s, major 2H), 8.01 (s, minor 2H), 7.78-7.72 (m, 2H), 7.64-7.43 (m, 8H), 7.37 (d, J = 8.0 Hz, major 2H), 7.27 (d, J = 8.0 Hz, minor 2H), 7.07-6.87 (m, 2H), 6.65 (dd, J_1 = 7.8 Hz, J_2 = 1.2 Hz, minor 1H), 6.12 (dd, J_1 = 8.0 Hz, J_2 = 7.8 Hz, major 1H), 4.77 (s, major 2H), 4.62 (s, minor 2H), 3.89 (dd, J_1 = 8.0 Hz, J_2 = 1.2 Hz, major 1H), 2.29 (s, major 3H), 0.56 (s, minor 3H). ^{13}C NMR (100 MHz, $CDCl_3$) δ 197.3, 196.0, 173.2, 172.9, 137.7, 136.3, 134.6, 134.4, 133.9, 133.6, 131.3, 131.1, 131.1, 130.9, 130.0, 129.7, 129.5, 129.5, 129.3, 129.2, 128.5, 128.4, 128.4, 128.3, 127.9, 127.5, 127.5, 127.3, 126.7, 126.2, 126.0, 126.0, 125.9, 125.8, 125.7, 125.6, 125.5, 125.3, 124.9, 123.6, 123.4, 63.7, 45.5, 45.1, 16.2, 14.5.

A pyrene anhydride (0.070 g, 0.14 mmol) and o-anisidine (31 μL, 0.28 mmol) were used. The crude product was washed with CH_3OH, and the product was obtained as an off-white solid (0.075 g, 88%). ^{1}H NMR (400 MHz, $CDCl_3$) δ 8.53-8.46 (m, 2H), 8.11-8.06 (m, 2H), 8.03 (s, major 2H), 8.01 (s, minor 2H), 7.79-7.73 (m, 2H), 7.66-7.55

(m, 4H), 7.50-7.40 (m, 4H), 7.36 (d, J = 7.8 Hz, major 2H), 7.21 (d, J = 7.8 Hz, minor 2H), 7.05-7.01 (m, minor 1H), 6.93-6.89 (m, 1H), 6.79-6.75 (m, minor 1H), 6.67 (d, J = 8.0 Hz, major 1H), 6.22 (d, J = 8.0 Hz, minor 1H), 5.96-5.92 (m, major 1H), 4.73 (s, major 2H), 4.65 (s, minor 2H), 3.99 (dd, J_1 = 7.8 Hz, J_2 = 1.6 Hz, major 1H), 3.68 (s, major 3H), 1.42 (s, minor 3H). ^{13}C NMR (100 MHz, $CDCl_3$) δ 197.5, 196.1, 173.1, 173.0, 154.1, 134.5, 134.4, 133.8, 133.7, 131.3, 131.3, 131.1, 131.0, 130.3, 130.2, 129.5, 129.4, 129.3, 129.3, 128.5, 128.4, 128.3, 128.3, 127.5, 127.3, 127.2, 126.0, 126.0, 125.8, 125.6, 125.3, 124.9, 123.6, 123.4, 120.2, 119.9, 119.4, 111.4, 63.8, 63.7, 55.6, 52.9, 45.4, 45.1.

A pyrene anhydride (0.080 g, 0.16 mmol) and 2-(phenylthio)aniline (0.048 g, 0.24 mmol) were used. The crude product was washed with CH_3OH, and the product was obtained as an off-white solid (0.085 g, 77%). ^{1}H NMR (400 MHz, $CDCl_3$) δ 8.51 (d, J = 7.8 Hz, minor 2H), 8.41 (d, J = 7.8 Hz, major 2H), 8.09 (d, J = 7.6 Hz, major 2H), 8.03 (s, major 2H), 7.80-7.19 (m, 14H), 7.08-7.02 (m, 1H), 6.99-6.94 (m, minor 2H), 6.92-6.88 (m, minor 1H), 6.87-6.82 (m, major 1H), 6.73 (dd, J_1 = 8.0 Hz, J_2 = 7.6 Hz, minor 2H), 6.42 (dd, J_1 = 8.0 Hz, J_2 = 1.0 Hz, minor 1H), 6.21 (dd, J_1 = 8.0 Hz, , J_2 = 7.6 Hz, major 1H), 5.76 (d, J = 7.2 Hz, minor 2H), 4.74 (s, minor 2H), 4.61 (s, major 2H), 3.95 (dd, J = 7.8 Hz, major 1H). ^{13}C NMR (101 MHz, $CDCl_3$) δ 196.9, 172.8, 134.7, 134.3, 133.6, 133.5, 133.0, 131.6, 131.3, 131.0, 130.8, 129.8, 129.3, 129.3, 129.1, 128.5, 128.4, 128.1, 127.5, 127.4, 127.2, 126.8, 126.2, 125.8, 122.9, 63.4, 44.8.

A phenanthrene anhydride (0.13 g, 0.27 mmol) and 2-(methylthio)aniline (50 μL, 0.40 mmol) were used. The crude product was washed with CH_3OH, and the product was obtained as a white solid (0.15 g, 92%). ^{1}H NMR (400 MHz, $CDCl_3$) δ 8.72 (d, J =

8.4 Hz, major 2H), 8.67 (d, J = 8.4 Hz, minor 2H), 8.41-8.36 (m, 2H), 7.73-7.67 (m, 2H), 7.57-7.50 (m, 4H), 7.46-7.39 (m, 2H), 7.29-7.25 (m, 2H), 7.22-7.03 (m, 6H), 6.95 (dd, J_1 = 7.8 Hz, J_2 = 1.6 Hz, minor 1H), 6.87 (dd, J_1 = 7.8 Hz, J_2 = 1.4 Hz, minor 1H), 6.49 (dd, J_1 = 8.0 Hz, J_2 = 7.6 Hz, major 1H), 4.69 (s, major 2H), 4.65 (s, minor 2H), 4.45 (dd, J_1 = 8.0 Hz, J_1 = 1.2 Hz, major 1H), 2.35 (s, major 3H), 1.24 (s, minor 3H).

A phenanthrene anhydride (0.60 g, 1.25 mmol) and 2-(phenylthio)aniline (0.38 g, 1.89 mmol) were used. The crude product was washed with CH_3OH, and the product was obtained as an off-white solid (0.72 g, 87%). ^{1}H NMR (400 MHz, $CDCl_3$) δ 8.72 (d, J = 8.4 Hz, major 2H), 8.40 (d, J = 7.6 Hz, minor 2H), 8.32 (d, J = 7.6 Hz, major 2H), 8.08 (d, J = 8.4 Hz, minor 2H), 7.73-7.69 (m, 2H), 7.57-7.51 (m, 3H), 7.43-7.39 (m, 2H), 7.28-6.96 (m, 12H), 6.94-6.89 (m, minor 2H), 6.68-6.65 (m, minor 1H), 6.61-6.57 (dd, J_1 = 7.6 Hz, J_2 = 7.6 Hz, major 1H), 6.27-6.24 (m, minor 2H), 4.65 (s, minor 2H), 4.54 (dd, J_1 = 8.0 Hz, J_2 = 1.2 Hz, major 1H), 4.53 (s, major 2H). ^{13}C NMR (101 MHz, $CDCl_3$) δ 196.9, 172.8, 134.7, 134.3, 133.6, 133.5, 133.0, 131.6, 131.3, 131.0, 130.8, 129.8, 129.3, 129.3, 129.1, 128.5, 128.4, 128.1, 127.5, 127.4, 127.2, 126.8, 126.2, 125.8, 122.9, 63.4, 44.8. HRMS (EI) Calcd for $C_{45}H_{29}NO_3S$: 663.1868; found: 663.1878.

A phenanthrene anhydride (0.17 g, 0.35 mmol) and 2-(*p*-tolylthio)aniline (0.15 g, 0.70 mmol) were used. The crude product was washed with CH_3OH, and the product was obtained as an off-white solid (0.19 g, 79%). ^{1}H NMR (400 MHz, $CDCl_3$) δ 8.72 (d, J = 8.4 Hz, major 2H), 8.41 (d, J = 8.0 Hz, minor 2H), 8.33 (d, J = 8.0 Hz, major 2H), 8.10 (d, J = 8.4 Hz, minor 2H), 7.74-7.69 (m, 2H), 7.59-7.50 (m, 3H), 7.48-7.39 (m, 2H), 7.30-7.04 (m, 10H), 7.00-6.93 (m, 1H), 6.74 (d, J = 8.0 Hz, minor 2H), 6.60 (d, J = 7.4 Hz, minor 1H), 6.58-6.53 (m, major 1H), 6.16 (d, J = 8.0 Hz, minor 2H), 4.64 (s, minor

2H), 4.55 (s, major 2H), 4.51 (d, J = 8.0 Hz, major 1H), 2.34 (s, major 3H), 2.26 (s, minor 3H). ^{13}C NMR (101 MHz, $CDCl_3$) δ 197.0, 195.7, 173.3, 172.8, 137.9, 137.9, 137.2, 135.2, 134.0, 133.6, 133.5, 133.0, 132.1, 132.1, 131.7, 131.3, 131.0, 131.0, 130.8, 130.5, 130.4, 130.3, 130.1, 129.7, 129.3, 129.2, 129.1, 129.0, 128.5, 128.4, 128.4, 128.2, 127.7, 127.6, 127.4, 127.2, 126.8, 126.8, 126.5, 126.3, 126.2, 126.1, 125.8, 125.8, 122.9, 122.8, 63.5, 63.4, 45.4, 44.9, 21.0. HRMS (EI) calcd for $C_{46}H_{31}NO_3S$: 677.2025; found: 677.2029.

A phenanthrene anhydride (0.24 g, 0.50 mmol) and 2-((4-methoxyphenyl)thio)aniline (0.12 g, 0.52 mmol) were used. The crude product was washed with CH_3OH, and the product was obtained as a white solid (0.30 g, 86%). ^{1}H NMR (400 MHz, $CDCl_3$) δ 8.72 (d, J = 8.4 Hz, major 2H), 8.41 (d, J = 8.0 Hz, minor 2H), 8.35 (d, J = 8.0 Hz, major 2H), 8.13 (d, J = 8.4 Hz, minor 2H), 7.74-7.69 (m, 2H), 7.59-7.40 (m, 5H), 7.30-6.82 (m, 10H), 6.55-6.46 (m, 2H), 6.21 (d, J = 8.8 Hz, minor 2H), 4.67 (s, minor 2H), 4.62 (s, major 2H), 4.45 (d, J = 8.0 Hz, major 1H), 3.80 (s, major 3H), 3.76 (s, minor 3H). ^{13}C NMR (101 MHz, $CDCl_3$) δ 197.0, 172.8, 159.9, 136.5, 135.0, 133.6, 133.5, 131.0, 130.8, 130.7, 130.0, 129.6, 129.3, 129.2, 128.6, 128.4, 127.2, 126.9, 126.8, 126.2, 125.9, 125.5, 123.6, 122.9, 115.0, 63.5, 55.3, 46.1, 44.9. HRMS (EI) calcd for $C_{46}H_{31}NO_4S$: 693.1974; found: 693.1987.

A phenanthrene anhydride (0.28 g, 0.59 mmol) and 2-((4-chlorophenyl)thio)aniline (0.14 g, 0.59 mmol) were used. The crude product was washed with CH_3OH, and the product was obtained as a white solid (0.32 g, 78%). ^{1}H NMR (400 MHz, $CDCl_3$) δ 8.73 (d, J = 8.4 Hz, major 2H), 8.37 (d, J = 8.0 Hz, minor 2H), 8.31 (d, J = 8.0 Hz, major 2H), 8.10 (d, J = 8.4 Hz, minor 2H), 7.74-7.69 (m, 2H), 7.60-7.50

(m, 3H), 7.47-7.37 (m, 2H), 7.31-7.25 (m, 2H), 7.24-6.97 (m, 8H), 6.84 (d, *J* = 8.4 Hz, minor 2H), 6.71 (d, *J* = 8.0 Hz, minor 1H), 6.63-6.59 (m, major 1H), 6.13 (d, *J* = 8.4 Hz, minor 2H), 4.66 (s, minor 2H), 4.59 (s, major 2H), 4.52 (d, *J* = 8.0 Hz, major 1H). ^{13}C NMR (101 MHz, $CDCl_3$) δ ^{13}C NMR (101 MHz, $CDCl_3$) δ 196.8, 195.5, 173.4, 172.9, 136.4, 133.9, 133.8, 133.7, 133.5, 133.5, 133.3, 133.2, 133.0, 132.8, 132.4, 131.9, 131.6, 131.6, 131.0, 131.0, 130.8, 130.0, 129.4, 129.3, 129.3, 129.1, 129.1, 128.6, 128.5, 128.4, 128.3, 127.8, 127.7, 127.5, 127.2, 126.8, 126.7, 126.4, 126.2, 126.2, 125.8, 122.9, 122.7, 63.5, 63.4, 45.4, 44.9. HRMS (EI) calcd for $C_{45}H_{28}ClNO_3S$: 697.1478; found: 697.1494.

A phenanthrene anhydride (1.10 g, 2.3 mmol) and 2-((4-(trifluoromethyl)phenyl)thio)aniline (0.75 g, 2.8 mmol) were used. The crude product was washed with CH_3OH, and the product was obtained as an off-white solid (1.55 g, 92%). ^{1}H NMR (400 MHz, $CDCl_3$) δ 8.74 (d, *J* = 8.4 Hz, major 2H), 8.37 (d, *J* = 7.8 Hz, minor 2H), 8.28 (d, *J* = 7.8 Hz, major 2H), 8.05 (d, *J* = 8.4 Hz, minor 2H), 7.73-7.68 (m, 2H), 7.59-7.37 (m, 6H), 7.30-7.05 (m, 10H), 6.83 (d, *J* = 8.0 Hz, minor 1H), 6.73-6.68 (m, major 1H), 6.26 (d, *J* = 8.0 Hz, minor 2H), 4.68 (s, minor 2H), 4.58 (d, *J* = 8.0 Hz, major 1H), 4.56 (s, major 2H). ^{13}C NMR (101 MHz, $CDCl_3$) δ 196.8, 173.5, 172.9, 141.2, 135.0, 134.4, 133.7, 133.6, 133.4, 133.3, 131.9, 131.4, 131.0, 131.0, 130.8, 130.7, 130.3, 129.6, 129.3, 129.3, 129.1, 129.0, 128.6, 128.4, 128.3, 128.0, 127.8, 127.3, 126.9, 126.6, 126.5, 126.2, 126.1, 125.9, 125.9, 125.8, 124.8, 122.9, 122.6, 63.5, 63.4, 45.5, 44.9. HRMS (EI) calcd for $C_{46}H_{28}F_3NO_3S$: 731.1742; found: 731.1745.

A phenanthrene anhydride (0.11 g, 0.23 mmol) and 2-((4-nitrophenyl)thio)aniline (0.06 g, 0.24 mmol) were used. The crude product was washed with CH_3OH, and the product was obtained as an off-white solid (0.13 g, 81%). ^{1}H NMR (400 MHz, $CDCl_3$) δ

8.74 (d, J = 8.4 Hz, major 2H), 8.37 (d, J = 8.0 Hz, minor 2H), 8.28 (d, J = 8.0 Hz, major 2H), 8.09 (d, J = 8.4 Hz, minor 2H), 8.03 (d, J = 8.8 Hz, major 2H), 7.73-7.68 (m, 2H), 7.65-7.49 (m, 4H), 7.47-7.06 (m, 12H), 6.90 (d, J = 8.0 Hz, minor 1H), 6.80-6.76 (m, major 1H), 6.24 (d, J = 8.8 Hz, minor 2H), 4.72 (s, minor 2H), 4.61-4.57 (m, major 3H). ^{13}C NMR (101 MHz, $CDCl_3$) δ 196.6, 173.5, 173.0, 146.5, 145.8, 136.1, 135.3, 134.3, 133.7, 133.6, 133.4, 133.4, 131.2, 131.1, 130.9, 130.8, 130.7, 130.1, 129.9, 129.6, 129.4, 129.3, 129.0, 128.9, 128.6, 128.5, 128.4, 128.0, 127.8, 127.3, 126.9, 126.5, 126.4, 126.2, 126.0, 125.8, 124.1, 122.9, 122.9, 122.6, 63.5, 63.5, 45.5. HRMS (EI) calcd for $C_{45}H_{28}N_2O_5S$: 708.1719; found:708.1737.

A phenanthrene (0.10 g, 0.27 mmol) and 2-(phenylthio)aniline (0.10 g, 0.50 mmol) were used. The crude product was washed with CH_3OH, and the product was obtained as an off-white solid (0.10 g, 67%). ^{1}H NMR (400 MHz, $CDCl_3$) δ 8.01-7.93 (m, 4H), 7.49-7.44 (m, 4H), 7.42-7.37 (m, 2H), 7.27-7.13 (m, 9H), 7.06-6.99 (m, 3H), 6.93-6.91 (m, minor 2H), 6.77-6.74 (m, minor 2H), 5.61 (dd, J_1 = 8.0 Hz, J_2 = 1.2 Hz, major 1H), 4.29 (s, minor 2H), 4.17 (s, major 2H). ^{13}C NMR (101 MHz, $CDCl_3$) δ 172.8, 144.3, 136.2, 135.3, 134.4, 132.8, 131.7, 131.5, 130.1, 129.3, 128.6, 128.5, 128.4, 128.1, 127.9, 127.5, 127.1, 120.9, 90.4, 54.5.

1-(2-(Methylthio)phenyl)-1*H*-pyrrole-2,5-dione (0.10 g, 0.46 mmol) and 1,3-diphenylisobenzofuran (0.11 g, 0.41 mmol) were heated in toluene at 110 ˚C overnight. The crude product was washed with CH_3OH, and the product was obtained as an off-white solid (0.15 g, 75%). ^{1}H NMR (400 MHz, $CDCl_3$) δ 8.09-8.06 (m, 4H), 7.54-7.50 (m, 4H), 7.48-7.44 (m, 2H), 7.32-7.29 (m, 4H), 7.10-7.06 (m, 2H), 7.03-6.99 (m, 1H), 5.59 (d, J = 7.6 Hz, major 1H), 4.35 (s, major 2H), 4.34 (s, minor 2H), 2.40 (s, major

3H), 2.11 (s, minor 3H). ^{13}C NMR (101 MHz, $CDCl_3$) δ 172.9, 144.3, 137.2, 136.3, 130.0, 128.6, 128.5, 128.1, 127.6, 127.2, 126.0, 121.0, 90.5, 54.6, 16.1.

Preparation and NMR data of (c)

11-(2,6-Bis(phenylthio)phenyl)-9,13-diphenyl-12a,13-dihydro-9*H*-9,13-methanophenanthro[9,10-*f*]isoindole-10,12,14(9a*H*,11*H*)-trione: 1-(2,6-bis(phenylthio)phenyl)-1H-pyrrole-2,5-dione (0.15 g, 0.39 mmol) and 1,3-diphenyl-2*H*-cyclopenta[*l*]phenanthren-2-one (0.13 g, 0.35 mmol) in 5 mL toluene were heated at 110 ˚C overnight. Toluene was removed under reduced pressure and the crude product was washed with CH_3OH. The product was obtained as an off-white solid (0.26 g, 96%). ^{1}H NMR (400 MHz, $CDCl_3$) δ 8.28 (d, *J* = 7.6 Hz, 2H), 8.04 (d, *J* = 8.4 Hz, 2H), 7.66-7.61 (m, 2H), 7.45-7.41 (m, 2H), 7.35-6.72 (m, 20H), 6.39 (d, *J* = 7.6 Hz, 1H), 6.28 (d, *J* = 7.2 Hz, 2H), 4.46 (s, 2H). ^{13}C NMR (100 MHz, $CDCl_3$) δ 195.8, 172.7, 168.7, 140.0, 139.3, 135.0, 134.2, 134.1, 133.9, 133.7, 133.4, 133.0, 132.9, 131.7, 131.5, 130.9, 130.5, 130.4, 130.2, 130.0, 129.5, 129.4, 129.3, 129.2, 128.3, 128.3, 128.2, 127.7, 127.4, 126.8, 126.3, 126.1, 125.8, 122.6, 63.3, 45.2.

11-(2,6-Bis(phenylthio)phenyl)-9,13-diphenyl-12a,13-dihydro-9*H*-9,13-methanopyreno[4,5-*f*]isoindole-10,12,14(9a*H*,11*H*)-trione: 1-(2,6-Bis(phenylthio)phenyl)-1*H*-pyrrole-2,5-dione (0.075 g, 0.19 mmol) and 9,11-diphenyl-10*H*-cyclopenta[*e*]pyren-10-one (0.075 g, 0.18 mmol) in 5 mL toluene were heated at 110 ˚C overnight. Toluene was removed under reduced pressure and the crude product was washed with CH_3OH. The product was obtained as an off-white solid (0.14 g, 93%). ^{1}H NMR (400 MHz, $CDCl_3$) δ 8.36 (d, *J* = 8.0 Hz, 2H), 7.71-7.67 (m, 4H), 7.50-7.40 (m, 6H), 7.35-7.28 (m, 6H), 7.21-7.04 (m, 5H), 6.94-6.86 (m, 2H), 6.73-6.67 (m, 3H), 6.16

(d, J = 8.0 Hz, 1H), 5.76 (d, J = 7.2 Hz, 2H), 4.54 (s, 2H). ^{13}C NMR (100 MHz, $CDCl_3$) δ. HRMS (EI) calcd for $C_{53}H_{33}NO_3S_2$: 795.1902; found: 795.1907.

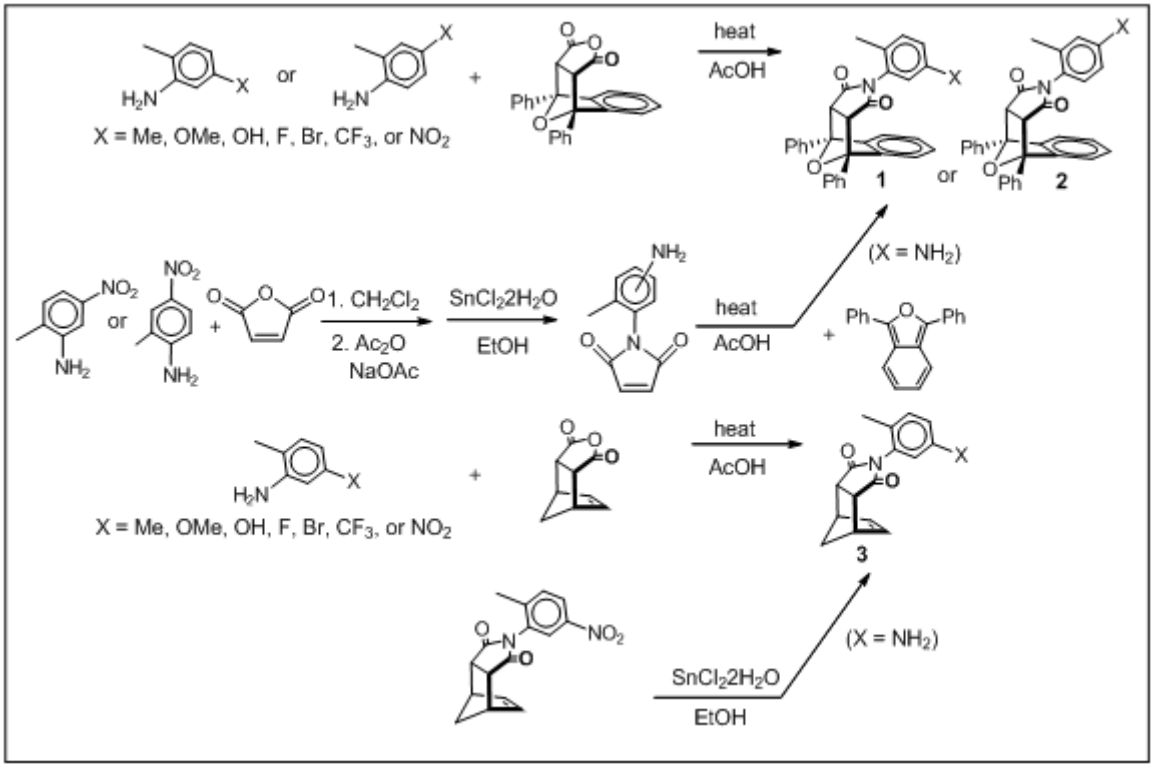

Scheme 2. Overview of synthetic procedure of the balances for the study of direct substituent-arene interactions.

2-(5-Amino-2-methylphenyl)-4,9-diphenyl-3a,4,9,9a-tetrahydro-1*H*-4,9-epoxybenzo[*f*]isoindole-1,3(2*H*)-dione ($1NH_2$). 1-(5-Amino-2-methylphenyl)-1*H*-pyrrole-2,5-dione (0.10 g, 0.49 mmol) and 1,3-diphenylisobenzofuran (0.10 g, 0.37 mmol) were used. The product was obtained as a yellow solid (0.16 g, 94%). ^{1}H NMR (400 MHz, $CDCl_3$) δ 8.09-8.02 (m, 4H), 7.56-7.50 (m, 4H), 7.49-7.43 (m, 2H), 7.33-7.29 (m, major 2H), 7.19-7.15 (m, minor 2H), 7.12-7.08 (m, major 2H), 7.05-7.01 (m, minor 2H), 6.97 (d, J = 8.0 Hz, major 1H), 6.86 (d, J = 8.0 Hz, minor 1H), 6.60 (d, J = 8.0 Hz, minor 1H), 6.55 (dd, J_1 = 8.0 Hz, J_2 = 2.4 Hz, major 1H), 6.33 (s, minor 1H), 4.83 (d, J = 2.4 Hz, major 1H), 4.29 (s, minor 2H), 4.28 (s, major 2H), 3.10 (br, 2H), 1.95 (s, major

3H), 0.95 (s, minor 3H). ^{13}C NMR (100 MHz, $CDCl_3$) δ 173.1, 144.4, 136.3, 131.3, 130.8, 128.6, 128.6, 128.0, 127.1, 121.1, 116.8, 113.9, 90.5, 54.6, 16.6. HRMS (EI) Calcd for $C_{31}H_{24}N_2O_3$: 472.1787; found: 472.1786.

2-(4-Amino-2-methylphenyl)-4,9-diphenyl-3a,4,9,9a-tetrahydro-1*H*-4,9-epoxybenzo[*f*]isoindole-1,3(2*H*)-dione ($2NH_2$). 1-(4-Amino-2-methylphenyl)-1*H*-pyrrole-2,5-dione (0.040 g, 0.20 mmol) and 1,3-diphenylisobenzofuran (0.040 g, 0.15 mmol) were used. The product was obtained as a yellow solid (0.65 g, 93%). ^{1}H NMR (400 MHz, $CDCl_3$) δ 8.10-8.04 (m, 4H), 7.56-7.50 (m, 4H), 7.49-7.43 (m, 2H), 7.30-7.26 (m, major 2H), 7.19-7.15 (m, minor 2H), 7.09-7.05 (m, major 2H), 7.05-7.01 (m, minor 2H), 6.69 (d, J = 8.4 Hz, minor 1H), 6.48-6.44 (m, 1H), 6.35 (d, J = 2.4 Hz, minor 1H), 6.27 (dd, J_1 = 8.4 Hz, J_2 = 2.4 Hz, major 1H), 5.29 (d, J = 8.4 Hz, major 1H), 4.27 (s, minor 2H), 4.25 (s, major 2H), 3.40 (br, 2H), 1.97 (s, major 3H), 0.97 (s, minor 3H). ^{13}C NMR (100 MHz, $CDCl_3$) 173.7, 147.2, 144.3, 136.5, 136.4, 128.6, 128.6, 128.2, 128.1, 128.1, 127.1, 121.1, 121.0, 116.6, 113.0, 90.5, 90.1, 54.4, 17.7, 17.0. HRMS (EI) Calcd for $C_{31}H_{24}N_2O_3$: 472.1787; found: 472.1780.

2-(2,4-Dimethylphenyl)-4,9-diphenyl-3a,4,9,9a-tetrahydro-1*H*-4,9-epoxybenzo[*f*]isoindole-1,3(2*H*)-dione (2Me). 2,4-Dimethyl aniline (80 μL, 0.65 mmol) and the anhydride (0.20 g, 0.54 mmol) were used. The product was obtained as an off-white solid (0.15 g, 59%). ^{1}H NMR (400 MHz, $CDCl_3$) δ 8.10-8.04 (m, 4H), 7.56-7.50 (m, 4H), 7.49-7.44 (m, 2H), 7.32-7.28 (m, major 2H), 7.21-7.18 (m, minor 2H), 7.11-6.98 (m, 3H), 6.91 (s, minor 1H), 6.84-6.80 (m, 1H), 5.42 (d, J = 8.0 Hz, major 1H), 4.31 (s, minor 2H), 4.28 (s, major 2H), 2.27 (s, minor 3H), 2.26 (s, major 3H), 2.05 (s, major 3H), 1.06 (s, minor 3H). ^{13}C NMR (100 MHz, $CDCl_3$) δ 173.3, 173.1, 144.8, 144.2, 139.4,

136.6, 136.4, 135.1, 131.5, 131.4, 128.6, 128.5, 128.2, 128.1, 127.6, 127.5, 127.3, 127.1, 126.9, 121.1, 120.9, 90.5, 90.1, 54.5, 54.5, 21.0, 17.5, 16.8. HRMS (EI) Calcd for $C_{32}H_{25}NO_3$: 471.1834; found: 471.1834.

2-(4-Methoxy-2-methylphenyl)-4,9-diphenyl-3a,4,9,9a-tetrahydro-1*H*-4,9-epoxybenzo[*f*]isoindole-1,3(2*H*)-dione (2OMe). 4-methoxy-2-methylphenol (84 μL, 0.65 mmol) and the anhydride (0.20 g, 0.54 mmol) were used. The product was obtained as an off-white solid (0.19 g, 70%). ^{1}H NMR (400 MHz, $CDCl_3$) δ 8.09-8.03 (m, 4H), 7.56-7.50 (m, 4H), 7.49-7.44 (m, 2H), 7.32-7.29 (m, major 2H), 7.20-7.17 (m, minor 2H), 7.10-7.03 (m, 3H), 6.85 (d, J = 8.8 Hz, minor 1H), 6.73 (d, J = 2.8 Hz, major 1H), 6.71 (d, J = 2.8 Hz, minor 1H), 6.61 (d, J = 2.8 Hz, minor 1H), 6.54 (dd, J_1 = 8.8 Hz, J_2 = 2.8 Hz, minor 1H), 5.43 (d, J = 8.8 Hz, major 1H), 4.32 (s, minor 2H), 4.28 (s, major 2H), 3.74 (s, minor 3H), 3.73 (s, major 3H), 2.05 (s, major 3H), 1.04 (s, minor 3H). ^{13}C NMR (100 MHz, $CDCl_3$) δ 173.5, 160.0, 144.9, 144.3, 136.9, 136.4, 128.7, 128.6, 128.3, 128.2, 127.1, 123.0, 121.2, 121.0, 116.0, 111.9, 90.5, 55.3, 54.5, 17.9. HRMS (EI) Calcd for $C_{32}H_{25}NO_4$: 487.1784; found: 487.1783.

2-(5-Hydroxy-2-methylphenyl)-4,9-diphenyl-3a,4,9,9a-tetrahydro-1*H*-4,9-epoxybenzo[*f*]isoindole-1,3(2*H*)-dione (1OH). 3-Amino-4-methylphenol (0.33 g, 0.27 mmol) and the anhydride (0.10 g, 0.27 mmol) were used. The product was obtained as an off-white solid (0.90 g, 69%). ^{1}H NMR (400 MHz, $CDCl_3$) δ 8.10-8.05 (m, 4H), 7.58-7.54 (m, 4H), 7.51-7.46 (m, 2H), 7.38-7.34 (m, major 2H), 7.23-7.20 (m, minor 2H), 7.15-7.05 (m, 3H), 6.97 (d, J = 8.4 Hz, minor 1H), 6.75-6.68 (m, 1H), 6.45 (d, J = 2.4 Hz, minor 1H), 5.04 (d, J = 2.4 Hz, major 1H), 4.74 (br, minor 1H), 4.52 (br, major 1H), 4.35 (s, minor 2H), 4.32 (s, major 2H), 2.02 (s, major 3H), 1.01 (s, minor 3H). ^{13}C NMR (100

MHz, $CDCl_3$) δ 173.1, 153.8, 144.8, 144.3, 139.7, 136.3, 131.5, 130.9, 128.7, 128.6, 128.2, 127.6, 127.1, 121.2, 121.0, 117.3, 116.8, 114.8, 114.3, 111.5, 90.5, 90.2, 54.6, 16.8, 16.0. HRMS (EI) Calcd for $C_{31}H_{23}NO_4$: 473.1627; found: 473.1626.

2-(4-Hydroxy-2-methylphenyl)-4,9-diphenyl-3a,4,9,9a-tetrahydro-1*H*-4,9-epoxybenzo[*f*]isoindole-1,3(2*H*)-dione (2OH). 4-Amino-3-methylphenol (0.33 g, 0.27 mmol) and the anhydride (0.10 g, 0.27 mmol) were used. The product was obtained as an off-white solid (0.060 g, 43%). ^{1}H NMR (400 MHz, $CDCl_3$) δ 8.07-8.02 (m, 4H), 7.56-7.50 (m, 4H), 7.49-7.44 (m, 2H), 7.33-7.29 (m, major 2H), 7.21-7.18 (m, minor 2H), 7.10-7.03 (m, 2H), 6.68 (d, J = 8.4 Hz, minor 1H), 6.43-6.40 (m, 1H), 6.31 (d, J = 2.4 Hz, minor 1H), 6.24 (dd, J_1 = 8.4 Hz, J_2 = 2.4 Hz, major 1H), 5.72 (br, major 1H), 5.70 (br, minor 1H), 5.25 (d, J = 8.4 Hz, major 1H), 4.32 (s, minor 2H), 4.29 (s, major 2H), 1.95 (s, major 3H), 0.93 (s, minor 3H). ^{13}C NMR (100 MHz, $CDCl_3$) δ 174.1, 173.9, 156.5, 144.9, 144.3, 136.8, 136.2, 128.8, 128.6, 128.3, 128.2, 127.1, 127.1, 122.3, 121.0, 117.4, 113.7, 90.6, 90.2, 54.4, 17.6. HRMS (EI) Calcd for $C_{31}H_{23}NO_4$: 473.1627; found: 473.1629.

2-(4-Fluoro-2-methylphenyl)-4,9-diphenyl-3a,4,9,9a-tetrahydro-1*H*-4,9-epoxybenzo[*f*]isoindole-1,3(2*H*)-dione (2F). 4-Fluoro-2-methylaniline (33 μL, 0.30 mmol) and the anhydride (0.10 g, 0.27 mmol) were used. The product was obtained as an off-white solid (0.085 g, 65%). ^{1}H NMR (400 MHz, $CDCl_3$) δ 8.08-8.03 (m, 4H), 7.56-7.51 (m, 4H), 7.50-7.46 (m, 2H), 7.34-7.29 (m, major 2H), 7.22-7.18 (m, minor 2H), 7.12-7.04 (m, 2H), 6.95-6.87 (m, 1H), 6.81 (dd, J_1 = 9.2 Hz, J_2 = 2.4 Hz, minor 1H), 6.74-6.69 (m, major 1H), 5.48 (dd, J_1 = 8.8 Hz, J_2 = 5.2 Hz, major 1H), 4.32 (s, minor 2H), 4.30 (s, major 2H), 2.08 (s, major 3H), 1.07 (s, minor 3H). ^{13}C NMR (100 MHz,

$CDCl_3$) δ 173.2, 173.0, 163.9, 161.4, 144.8, 144.2, 138.2, 138.2, 136.4, 136.2, 129.0, 129.0, 128.7, 128.7, 128.6, 128.3, 128.2, 127.1, 127.0, 126.2, 121.1, 121.0, 117.6, 117.3, 113.7, 113.5, 90.5, 90.1, 54.5, 54.5, 17.8, 17.0. HRMS (EI) Calcd for $C_{31}H_{22}FNO_3$: 475.1584; found: 475.1583.

2-(5-Bromo-2-methylphenyl)-4,9-diphenyl-3a,4,9,9a-tetrahydro-1*H*-4,9-epoxybenzo[*f*]isoindole-1,3(2*H*)-dione (1Br). 5-Bromo-2-methylaniline (0.10 g, 0.54 mmol) and the anhydride (0.20 g, 0.54 mmol) were used. An off-white solid was obtained as product (0.23 g, 78%). ^{1}H NMR (400 MHz, $CDCl_3$) δ 8.08-8.02 (m, 4H), 7.57-7.52 (m, 4H), 7.50-7.46 (m, 2H), 7.39-7.30 (m, 3H), 7.21-7.18 (m, minor 2H), 7.15-7.04 (m, 3H), 6.97 (d, *J* = 8.4 Hz, minor 1H), 5.58 (d, *J* = 2.0 Hz, major 1H), 4.31 (s, minor 2H), 4.29 (s, major 2H), 2.05 (s, major 3H), 1.04 (s, minor 3H). ^{13}C NMR (100 MHz, $CDCl_3$) δ 172.9, 172.6, 144.8, 144.2, 136.4, 136.1, 134.8, 132.4, 132.1, 131.9, 131.5, 130.8, 130.4, 128.7, 128.7, 128.6, 128.4, 128.3, 127.0, 127.0, 121.1, 121.1, 119.1, 119.0, 90.6, 90.2, 54.6, 54.5, 17.2, 16.6. HRMS (EI) Calcd for $C_{31}H_{22}BrNO_3$: 535.0783; found: 535.0787.

2-(2-Methyl-4-(trifluoromethyl)phenyl)-4,9-diphenyl-3a,4,9,9a-tetrahydro-1*H*-4,9-epoxybenzo[*f*]isoindole-1,3(2*H*)-dione (2CF3). 2-Methyl-4-(trifluoromethyl)aniline (0.11 g, 0.65 mmol) and the anhydride (0.20 g, 0.54 mmol) were used. An off-white solid was obtained as product (0.21 g, 72%). ^{1}H NMR (400 MHz, $CDCl_3$) δ 8.08-8.03 (m, 4H), 7.57-7.53 (m, 4H), 7.50-7.46 (m, 3H), 7.39-7.29 (m, 3H), 7.24-7.20 (m, minor 2H), 7.13-7.06 (m, 2H), 5.66 (d, *J* = 8.2 Hz, major 1H), 4.34 (s, minor 2H), 4.33 (s, major 2H), 2.17 (s, major 3H), 1.17 (s, minor 3H). ^{13}C NMR (100 MHz, $CDCl_3$) δ 177.3, 172.8, 172.6, 144.8, 144.2, 137.1, 136.8, 136.3, 136.0, 133.5, 131.6, 131.3, 128.7, 128.7, 128.6, 128.3,

128.2, 128.0, 127.7, 127.7, 127.0, 127.0, 124.8, 123.6, 123.6, 121.1, 121.0, 90.5, 90.2, 54.6, 20.6, 17.7, 17.1. HRMS (EI) Calcd for $C_{32}H_{22}F_3NO_3$: 525.1552; found: 525.1548.

2-(2-Methyl-5-nitrophenyl)-4,9-diphenyl-3a,4,9,9a-tetrahydro-1*H*-4,9-epoxybenzo[*f*]isoindole-1,3(2*H*)-dione (1NO_2). 2-Methyl-5-nitroaniline (0.086 g, 0.54 mmol) and the anhydride (0.20 g, 0.54 mmol) were reacted. An off-white solid was obtained as product (0.21 g, 78 %). ^{1}H NMR (400 MHz, $CDCl_3$) δ 8.12-8.00 (m, 5H), 7.91 (d, J = 2.2 Hz, minor 1H), 7.57-7.52 (m, 4H), 7.51-7.43 (m, 4H), 7.38 (d, J = 8.4 Hz, major 1H), 7.23-7.20 (m, minor 2H), 7.14-7.11 (m, major 2H), 7.08-7.05 (m, minor 2H), 6.35 (d, J = 2.2 Hz, major 1H), 4.39 (s, minor 2H), 4.35 (s, major 2H), 2.20 (s, major 3H), 1.20 (s, minor 3H). ^{13}C NMR (100 MHz, $CDCl_3$) δ 172.8, 146.5, 144.0, 143.9, 136.0, 131.5, 131.3, 128.9, 128.7, 128.6, 128.4, 127.1, 127.0, 124.2, 123.5, 121.3, 121.1, 90.8, 54.8, 54.7, 18.1. HRMS (EI) Calcd for $C_{31}H_{22}N_2O_5$: 502.1529; found: 502.1539.

2-(2-Methyl-4-nitrophenyl)-4,9-diphenyl-3a,4,9,9a-tetrahydro-1*H*-4,9-epoxybenzo[*f*]isoindole-1,3(2*H*)-dione (2NO_2). 2-Methyl-4-nitroaniline (0.045 g, 0.30 mmol) and the anhydride (0.10 g, 0.27 mmol) were reacted. A yellow solid was obtained as product (0.10, 77%). ^{1}H NMR (400 MHz, $CDCl_3$) δ 8.10 (d, J = 2.4 Hz, major 1H), 8.07-7.99 (m, 4H), 7.88 (dd, J_1 = 8.4 Hz, J_2 = 2.4 Hz, major 1H), 7.72-7.69 (m, minor 1H), 7.63-7.62 (m, minor 1H), 7.57-7.52 (m, 4H), 7.50-7.46 (m, 2H), 7.40-7.32 (m, 2H), 7.24-7.22 (m, minor 2H), 7.16 (d, J = 8.8 Hz, minor 1H), 7.13-7.06 (m, 2H), 5.69 (d, J = 8.8 Hz, major 1H), 4.38 (s, minor 2H), 4.36 (s, major 2H), 2.21 (s, major 3H), 1.21 (s, minor 3H). ^{13}C NMR (100 MHz, $CDCl_3$) δ 172.5, 172.2, 148.0, 144.8, 144.2, 138.0, 136.2, 135.9, 129.8, 128.8, 128.8, 128.7, 128.4, 128.3, 127.0, 127.0, 125.7, 121.7, 121.2,

121.1, 90.6, 90.3, 54.7, 18.0, 17.3. HRMS (EI) Calcd for $C_{31}H_{22}N_2O_5$: 502.1529; found: 502.1528.

2-(5-Amino-2-methylphenyl)-3a,4,7,7a-tetrahydro-1*H*-4,7-methanoisoindole-1,3(2*H*)-dione (3NH2). 2-(5-Amino-2-methylphenyl)-3a,4,7,7a-tetrahydro-1*H*-4,7-methanoisoindole-1,3(2*H*)-dione (3NO2) (1.2 g, 4.0 mmol) and $SnCl_2 \cdot 2H_2O$ (1.6 g, 7.1 mmol) in 5 mL EtOH were stirred overnight at rt. The reaction mixture was neutralized using 1N NaOH (aq), and was extracted using EtOAc (50 mL). The organic solution was further washed with $NaHCO_3$ (aq) and water (50 mL x 3), and the organic solvent was removed under reduced pressure. The product obtained as an off-white solid (0.030 g, 28%). ^{1}H NMR (400 MHz, $CDCl_3$) δ 7.08-7.04 (m, 1H), 6.67-6.62 (m, 1H), 6.33-6.29 (m, 2H and 1H major), 6.20 (d, J = 2.4 Hz, minor 1H), 3.54-3.45 (m, 2H), 3.18 (br, 2H), 2.00 (s, major 3H), 1.98 (s, minor 3H), 1.82-1.76 (m, 1H), 1.63-1.58 (m, 1H). ^{13}C NMR (100 MHz, $CDCl_3$) δ 176.7, 176.5, 145.1, 145.1, 135.2, 134.5, 131.7, 131.5, 125.1, 125.0, 116.6, 116.5, 114.6, 114.2, 52.6, 52.2, 46.7, 45.7, 45.4, 45.1, 17.9, 16.6. HRMS (EI) Calcd for $C_{16}H_{16}N_2O_2$: 268.1212; found: 268.1215.

2-(2,5-Dimethylphenyl)-3a,4,7,7a-tetrahydro-1*H*-4,7-methanoisoindole-1,3(2*H*)-dione (3Me). 2,5-Dimethylaniline (114 μL, 0.91 mmol) and the anhydride (0.15 g, 0.91 mmol) were reacted. The product (0.20 g, 84%) was an off-white solid. ^{1}H NMR (400 MHz, $CDCl_3$) δ 7.18-7.14 (m, 1H), 7.11-7.08 (m, 1H), 6.81 (s, minor 1H), 6.67 (s, major 1H), 6.32-6.28 (m, 2H), 3.52-3.44 (m, 4H), 2.32 (s, 3H), 2.09 (s, major 3H), 2.06 (s, minor 3H), 1.83-1.79 (m, 1H), 1.64-1.60 (m, 1H). ^{13}C NMR (100 MHz, $CDCl_3$) δ 176.8, 176.5, 136.6, 136.5, 135.2, 134.6, 132.5, 132.3, 130.9, 130.8, 130.2, 130.2, 128.6, 128.1,

52.6, 52.3, 46.7, 45.7, 45.4, 45.1, 20.7, 20.7, 18.4, 17.1. HRMS (EI) Calcd for $C_{17}H_{17}NO_2$: 267.1259; found: 267.1260.

2-(5-Methoxy-2-methylphenyl)-3a,4,7,7a-tetrahydro-1*H*-4,7-methanoisoindole-1,3(2*H*)-dione (3MeO). 5-Methoxy-2-methylaniline (0.13 g, 0.91 mmol) and the anhydride (0.15 g, 0.91 mmol) were reacted. The product (0.23 g, 87%) was a white solid. ^{1}H NMR (400 MHz, $CDCl_3$) δ. 7.19-7.14 (m, 1H), 6.84 (dd, J_1 = 8.6 Hz, J_2 = 2.6 Hz, 1H), 6.52 (d, J = 2.6 Hz, minor 1H), 6.39 (d, J = 2.6 Hz, major 1H), 6.31-6.27 (m, 2H), 3.75 (s, minor 3H), 3.74 (s, major 3H), 3.50-3.43 (m, 4H), 2.03 (s, major 3H), 2.00 (s, minor 3H), 1.82-1.77 (m, 1H), 1.63-1.58 (m, 1H). ^{13}C NMR (100 MHz, $CDCl_3$) δ 176.6, 176.3, 158.1, 158.0, 135.1, 134.5, 131.7, 131.6, 131.6, 131.4, 127.5, 127.4, 115.2, 114.6, 113.7, 113.4, 55.3, 52.6, 52.2, 46.7, 45.7, 45.3, 45.0, 17.9, 16.7. HRMS (EI) Calcd for $C_{17}H_{17}NO_3$: 283.1208; Found: 283.1212.

2-(5-Hydroxy-2-methylphenyl)-3a,4,7,7a-tetrahydro-1*H*-4,7-methanoisoindole-1,3(2*H*)-dione (3OH). 3-Amino-4-methylphenol (0.12 g, 1.01 mmol) and the anhydride (0.15 g, 0.91 mmol) were reacted. A light brown solid was obtained as product (0.21 g, 84%). ^{1}H NMR (400 MHz, $CDCl_3$) δ 7.09 (d, J = 8.4 Hz, major 1H), 7.08 (d, J = 8.4 Hz, major 1H), 6.71 (dd, J_1 = 8.4 Hz, J_2 = 2.4 Hz, 1H), 6.40 (d, J = 2.4 Hz, minor 1H), 6.32 (d, J = 2.4 Hz, major 1H), 6.30-6.26 (m, 2H), 5.57 (br, minor 1H), 5.44 (br, major 1H), 3.53-3.42 (m, 4H), 2.02 (s, major 3H), 1.99 (s, minor 3H), 1.84-1.76 (m, 1H), 1.66-1.58 (m, 1H). ^{13}C NMR (100 MHz, $CDCl_3$) δ 177.0, 154.4, 135.2, 134.6, 131.9, 131.7, 127.3, 116.8, 115.1, 114.8, 52.7, 52.3, 46.7, 45.8, 45.4, 45.1, 18.0, 16.7. HRMS (EI) Calcd for $C_{16}H_{15}NO_3$: 269.1052; found: 269.1053.

2-(5-Fluoro-2-methylphenyl)-3a,4,7,7a-tetrahydro-1*H*-4,7-methanoisoindole-1,3(2*H*)-dione (3F). 5-Flouro-2-methylaniline (0.11 g, 0.91 mmol) and the anhydride (0.15 g, 0.91 mmol) were reacted. The product (0.22 g, 89%) was a white solid. ^{1}H NMR (400 MHz, $CDCl_3$) δ 7.24-7.19 (m, 1H), 7.03-6.97 (m, 1H), 6.75 (dd, J_1 = 8.8 Hz, J_2 = 2.8 Hz minor 1H), 6.59 (dd, J_1 = 8.8 Hz, J_2 = 2.8 Hz major 1H), 6.30-6.26 (m, 2H), 3.51-3.42 (m, 4H), 2.07 (s, major 3H), 2.04 (s, minor 3H), 1.81-1.76 (m, 1H), 1.62-1.57 (m, 1H). ^{13}C NMR (100 MHz, $CDCl_3$) δ 176.3, 176.0, 162.0, 161.9, 159.5, 159.4, 135.2, 134.5, 132.0, 132.0, 131.9, 131.8, 131.6, 131.5, 131.5, 131.5, 116.4, 116.3, 116.2, 116.1, 115.5, 115.3, 115.1, 114.9, 52.7, 52.3, 46.7, 45.7, 45.4, 45.1, 18.2, 17.0. HRMS (EI) Calcd for $C_{16}H_{14}FNO_2$: 271.1009; found: 271.1010.

2-(5-Bromo-2-methylphenyl)-3a,4,7,7a-tetrahydro-1*H*-4,7-methanoisoindole-1,3(2*H*)-dione (3Br). 5-Bromo-2-methylaniline (0.18 g, 0.91 mmol) and the anhydride (0.15 g, 0.91 mmol) were reacted. The product (0.29 g, 98%) was a white solid. ^{1}H NMR (400 MHz, $CDCl_3$) δ 7.43-7.39 (m, 1H), 7.17-7.13 (m, 1H and minor 1H), 6.98 (d, J = 2.0 Hz, major 1H), 6.33-6.28 (m, 2H), 3.52-3.45 (m, 4H), 2.06 (s, major 3H), 2.03 (s, minor 3H), 1.84-1.79 (m, 1H), 1.65-1.60 (m, 1H). ^{13}C NMR (100 MHz, $CDCl_3$) δ 176.3, 176.0, 135.2, 135.0, 134.9, 134.6, 132.4, 132.3, 132.2, 131.1, 130.6, 119.2, 119.2, 52.7, 52.3, 46.7, 45.8, 45.4, 45.1, 18.4, 17.3. HRMS (EI) Calcd for $C_{16}H_{14}BrNO_2$: 331.0208; Found: 331.0202.

2-(2-Methyl-5-(trifluoromethyl)phenyl)-3a,4,7,7a-tetrahydro-1*H*-4,7-methanoisoindole-1,3(2*H*)-dione (3CF3). 3-Amino-4-methylbenzotrifluoride (0.16 g, 0.91 mmol) and the anhydride (0.15 g, 0.91 mmol) were reacted. The product (0.28 g, 95%) was an off-white solid. ^{1}H NMR (400 MHz, $CDCl_3$) δ 7.54 (d, J = 8.0 Hz, 1H),

7.42-7.38 (m, 1H), 7.28 (s, major 1H), 7.08 (s, minor 1H), 6.34-6.29 (m, 2H), 3.54-3.46 (m, 4H), 2.17 (s, minor 3H), 2.14 (s, major 3H), 1.84-1.79 (m, 1H), 1.65-1.60 (m, 1H). ^{13}C NMR (100 MHz, $CDCl_3$) δ 176.3, 176.1, 140.3, 140.2, 135.3, 134.7, 131.7, 131.6, 129.5, 129.2, 126.1, 126.1, 125.6, 125.0, 125.0, 52.8, 52.4, 46.8, 45.9, 45.5, 45.2, 19.0, 17.8. HRMS (EI) Calcd for $C_{17}H_{14}F_3NO_2$: 321.0977; found: 321.0975.

2-(2-Methyl-5-Nitrophenyl)-3a,4,7,7a-tetrahydro-1*H*-4,7-methanoisoindole-1,3(2*H*)-dione (3NO2). 2-Methyl-5-nitroaniline (0.15 g, 0.91 mmol) and the anhydride (0.15 g, 0.91 mmol) were reacted. The product (0.24 g, 89%) was a yellow solid. ^{1}H NMR (400 MHz, $CDCl_3$) δ 8.21-8.16 (m, 1H), 7.94 (d, J = 2.0 Hz, minor 1H), 7.75 (d, J = 2.0 Hz, major 1H), 7.49-7.45 (m, 1H), 6.40-6.33 (m, 2H), 3.57-3.52 (m, 4H), 2.25 (s, major 3H), 2.22 (s, minor 3H), 1.89-1.84 (m, 1H), 1.69-1.64 (m, 1H). ^{13}C NMR (100 MHz, $CDCl_3$) δ 176.1, 175.8, 146.6, 144.1, 135.3, 134.7, 131.8, 131.7, 124.1, 124.1, 124.0, 123.6, 52.8, 52.4, 46.9, 46.0, 45.5, 45.2, 19.2, 18.2. HRMS (EI) Calcd for $C_{16}H_{14}N_2O_4$: 298.0954; Found: 298.0952.

APPENDIX B - COPYRIGHT PERMISSIONS

Chapter 2

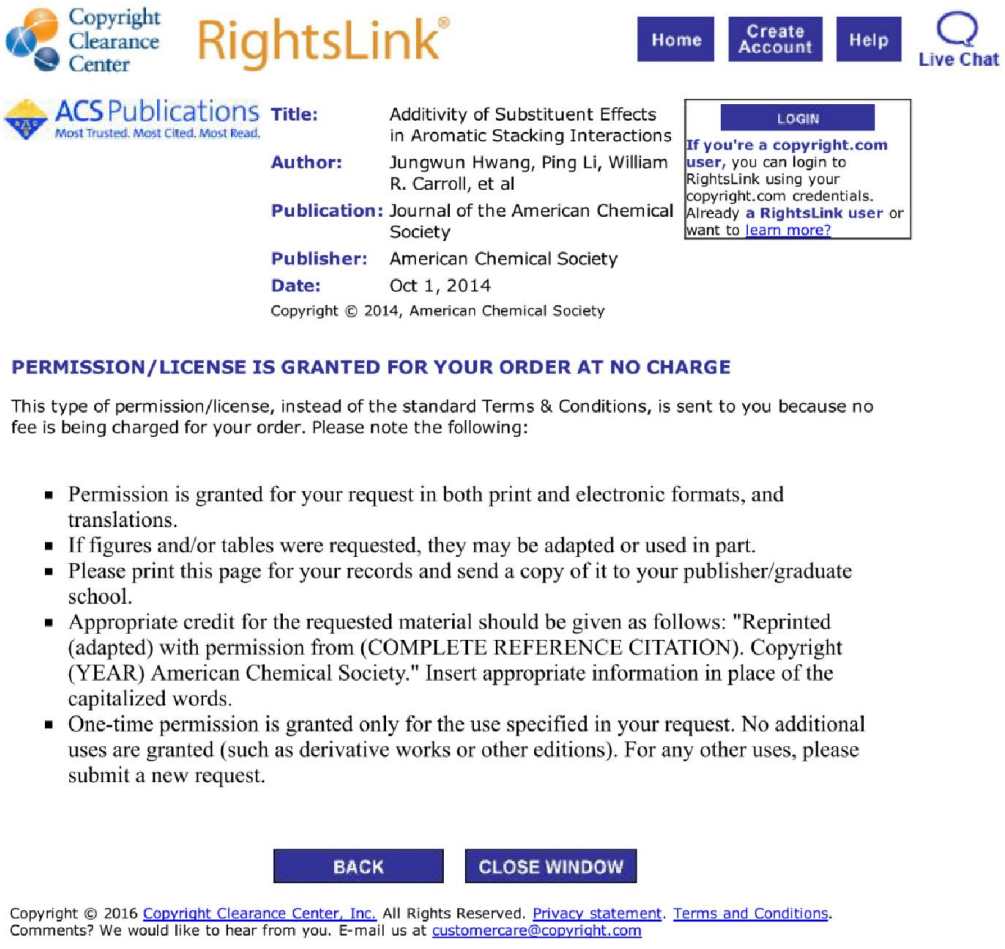

Copyright Clearance Center RightsLink®

Home | Create Account | Help | Live Chat

ACS Publications
Most Trusted. Most Cited. Most Read.

Title:	Additivity of Substituent Effects in Aromatic Stacking Interactions
Author:	Jungwun Hwang, Ping Li, William R. Carroll, et al
Publication:	Journal of the American Chemical Society
Publisher:	American Chemical Society
Date:	Oct 1, 2014

Copyright © 2014, American Chemical Society

LOGIN

If you're a copyright.com user, you can login to RightsLink using your copyright.com credentials. Already **a RightsLink user** or want to learn more?

PERMISSION/LICENSE IS GRANTED FOR YOUR ORDER AT NO CHARGE

This type of permission/license, instead of the standard Terms & Conditions, is sent to you because no fee is being charged for your order. Please note the following:

- Permission is granted for your request in both print and electronic formats, and translations.
- If figures and/or tables were requested, they may be adapted or used in part.
- Please print this page for your records and send a copy of it to your publisher/graduate school.
- Appropriate credit for the requested material should be given as follows: "Reprinted (adapted) with permission from (COMPLETE REFERENCE CITATION). Copyright (YEAR) American Chemical Society." Insert appropriate information in place of the capitalized words.
- One-time permission is granted only for the use specified in your request. No additional uses are granted (such as derivative works or other editions). For any other uses, please submit a new request.

BACK | CLOSE WINDOW

Copyright © 2016 Copyright Clearance Center, Inc. All Rights Reserved. Privacy statement. Terms and Conditions.
Comments? We would like to hear from you. E-mail us at customercare@copyright.com

Chapter 3

How important are dispersion interactions to the strength of aromatic stacking interactions in solution?

J. Hwang, B. E. Dial, P. Li, M. E. Kozik, M. D. Smith and K. D. Shimizu, *Chem. Sci.*, 2015, **6**, 4358
DOI: 10.1039/C5SC01370D

Chapter 4

JOHN WILEY AND SONS LICENSE TERMS AND CONDITIONS

Jul 06, 2016

This Agreement between Jung wun Hwang ("You") and John Wiley and Sons ("John Wiley and Sons") consists of your license details and the terms and conditions provided by John Wiley and Sons and Copyright Clearance Center.

License Number	3903220814409
License date	Jul 06, 2016
Licensed Content Publisher	John Wiley and Sons
Licensed Content Publication	Angewandte Chemie
Licensed Content Title	Distance-Dependent Attractive and Repulsive Interactions of Bulky Alkyl Groups
Licensed Content Author	Jungwun Hwang,Ping Li,Mark D. Smith,Ken D. Shimizu
Licensed Content Date	May 9, 2016
Licensed Content Pages	4
Type of use	Dissertation/Thesis
Requestor type	Author of this Wiley article
Format	Print and electronic
Portion	Full article
Will you be translating?	No
Title of your thesis / dissertation	MEASUREMENT OF NON-COVALENT AROMATIC INTERACTIONS USING MOLECULAR BALANCES
Expected completion date	Aug 2016
Expected size (number of pages)	10